

2019

Functional Characterization of Glutamate Carboxypeptidase II in *Caenorhabditis elegans*

Hashni Epa Vidana Gamage

Thesis Maintenance and Reproduction Certificate

FOR: Graduate Candidates Completing Theses in Partial Fulfillment of the Degree
 Graduate Faculty Advisors Directing the Theses

RE: Preservation, Reproduction, and Distribution of Thesis Research

Preserving, reproducing, and distributing thesis research is an important part of Booth Library's responsibility to provide access to scholarship. In order to further this goal, Booth Library makes all graduate theses completed as part of a degree program at Eastern Illinois University available for personal study, research, and other not-for-profit educational purposes. Under 17 U.S.C. § 108, the library may reproduce and distribute a copy without infringing on copyright; however, professional courtesy dictates that permission be requested from the author before doing so.

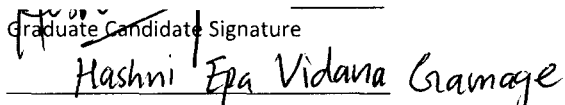
Your signatures affirm the following:

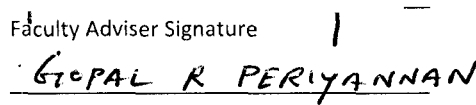
- The graduate candidate is the author of this thesis.
- The graduate candidate retains the copyright and intellectual property rights associated with the original research, creative activity, and intellectual or artistic content of the thesis.
- The graduate candidate certifies her/his compliance with federal copyright law (Title 17 of the U. S. Code) and her/his right to authorize reproduction and distribution of all copyrighted materials included in this thesis.
- The graduate candidate in consultation with the faculty advisor grants Booth Library the nonexclusive, perpetual right to make copies of the thesis freely and publicly available without restriction, by means of any current or successive technology, including but not limited to photocopying, microfilm, digitization, or internet.
- The graduate candidate acknowledges that by depositing her/his thesis with Booth Library, her/his work is available for viewing by the public and may be borrowed through the library's circulation and interlibrary loan departments, or accessed electronically. The graduate candidate acknowledges this policy by indicating in the following manner:

Yes, I wish to make accessible this thesis for viewing by the public

No, I wish to quarantine the thesis temporarily and have included the **Thesis Withholding Request Form**

• The graduate candidate waives the confidentiality provisions of the Family Educational Rights and Privacy Act (FERPA) (20 U. S. C. § 1232g; 34 CFR Part 99) with respect to the contents of the thesis and with respect to information concerning authorship of the thesis, including name and status as a student at Eastern Illinois University. I have conferred with my graduate faculty advisor. My signature below indicates that I have read and agree with the above statements, and hereby give my permission to allow Booth Library to reproduce and distribute my thesis. My adviser's signature indicates concurrence to reproduce and distribute the thesis.

Graduate Candidate Signature _____

 Printed Name
MS. Biological Sciences
 Graduate Degree Program

Faculty Adviser Signature _____

 Printed Name
5/17/2019
 Date

Please submit in duplicate.

Functional Characterization of Glutamate Carboxypeptidase II

in Caenorhabditis elegans

(TITLE)

BY

Hashni Epa Vidana Gamage

THESIS

SUBMITTED IN PARTIAL FULFILLMENT OF THE REQUIREMENTS
FOR THE DEGREE OF

Master of Science

IN THE GRADUATE SCHOOL, EASTERN ILLINOIS UNIVERSITY
CHARLESTON, ILLINOIS

2019

YEAR

I HEREBY RECOMMEND THAT THIS THESIS BE ACCEPTED AS FULFILLING
THIS PART OF THE GRADUATE DEGREE CITED ABOVE

5/17/19
THESIS COMMITTEE CHAIR DATE

5/17/19
DEPARTMENT/SCHOOL CHAIR
OR CHAIR'S DESIGNEE DATE

5/17/19
THESIS COMMITTEE MEMBER DATE

THESIS COMMITTEE MEMBER DATE

THESIS COMMITTEE MEMBER DATE

THESIS COMMITTEE MEMBER DATE

**Functional Characterization of Glutamate
Carboxypeptidase II in *Caenorhabditis elegans***

Hashni Epa Vidana Gamage

Department of Biological Sciences

Department of Chemistry and Biochemistry

Eastern Illinois University

COMMITTEE IN CHARGE OF CANDIDACY

Gopal R. Periyannan, Ph.D., Advisor

Britto Nathan, Ph.D., Co-Advisor

Gary A Bulla, Ph.D., Committee Member

Abstract

Glutamate carboxypeptidase II (GCPII) is a transmembrane zinc metalloprotease expressed in a number of organisms: from yeast to worm to humans. In humans, GCPII has been observed as a multifunctional protein and expressed in prostate, intestine, kidney, brain, tumor-associated neovasculature and other tissues as five paralogs. In the human small intestine, hGCPII is proposed to facilitate the folate absorption by cleaving terminal glutamate residues in dietary folates. Folates act as a cofactor in one-carbon metabolic pathways such as nucleotide synthesis, amino acid synthesis, DNA repair, and consequently involved in cell division and growth. The hGCPII homolog is found in the nematode *Caenorhabditis elegans* (cGCPII) as three paralogs and shares a high structural similarity with hGCPII. In this study, the *C. elegans* strains: wild-type (N2), and *gcp-2* deletion mutant strains: RB1055 (*gcp-2.1*), TM6632 (*gcp-2.2*) and TM5414 (*gcp-2.3*) were used to investigate the role of *gcp-2* in folate metabolism. This study shows that the *gcp-2.1* and *gcp-2.2* paralogs play a significant role in folate metabolism, reproduction, and embryonic and post-embryonic development in *C. elegans*. When the *gcp-2* mutant worms were fed with a folate-deficient diet, it showed folate deficient phenotypes, infertility and growth retardation, as observed in mice and humans. This work establishes, for the first time, the relationship between GCPII and folate metabolism in *C. elegans* as proposed for human folate metabolism. This study demonstrates that *C. elegans* can be used as a genetically tractable model organism to investigate the tissue-specific multifunctional roles of GCPII in development and reproduction of a multicellular organism.

Acknowledgements

I would like to express my sincere gratitude to,

- My advisor, Dr. Gopal Periyannan for his support and encouragement at every stage of this research over the past 2 years.
- My co-advisor and graduate coordinator, Dr. Britto Nathan for his guidance, encouragement and giving me this opportunity.
- My committee members, Dr Tomas Cannam and Dr. Gary Bulla, for their time, willingness support and valuable input.
- My fellow lab members, Theresa, Viet, Jessica and Hannah, who has being with me through the best and the worst experiment days for their wonderful friendship and collaboration.
- Viet Bui, for his useful discussions and guidance with regard to HPLC.
- EIU Graduate school for Research and Creative Activity Grants and materials from the Department of Chemistry and Biochemistry, and Biological Sciences.
- Last but not least, the wonderful faculty in the Department of Biological Sciences and the Department of Chemistry/Biochemistry, for giving me the necessary tools and knowledge to succeed!

Declaration

I confirm that the work presented in this thesis is my original research work. Wherever contributions of others are involved, every effort is made to indicate this clearly, with due reference to the literature.

.....

Hashni Epa Vidana Gamage

Copyright

The copyright of this thesis rests with the author. No quotation from it should be published without the author's prior consent and information derived from it should be acknowledged.

Table of Contents

Abstract	1
Acknowledgements	2
Declaration	3
Copyright	3
Table of Contents	4
List of Figures	9
List of Tables	13
List of Abbreviations	14

CHAPTER 1: INTRODUCTION

1.1 Proteases	17
1.2 M28 Family of Metalloproteases.....	19
1.3 Glutamate Carboxypeptidase (GCPII).....	20
1.3.1 Localization and Physiological Role	21
1.3.2 Structure	23
1.3.3 Splice Variants.....	26
1.3.4 Paralogs, Homologs and Orthologs	30
1.3.5 GCPII in <i>C. elegans</i>	31
1.3.6 Inhibitors	33
1.4 Model Organism: <i>Caenorhabditis elegans</i>	36
1.4.1 Genetics.....	36

1.4.2 The Use of RNA Interference (RNAi).....	38
1.4.3 Anatomy.....	39
1.4.4 The Alimentary System	42
1.4.5 Development and Life Cycle	45
1.4.6 The Use of RNA Interference (RNAi).....	

**CHAPTER 2: INVESTIGATION OF THE BIOLOGICAL SIGNIFICANCE OF
GCPII IN *C. ELEGANS***

2.1 General Introduction	49
2.2 Hypothesis and Objectives	49
2.3 Material and Methods	49
2.3.1 <i>C. elegans</i> and <i>E. coli</i> Strains	49
2.3.2 Preparation of Nematode Growth Media (NGM)	52
Bacterial Food Source	52
Preparation of NGM Plates	52
Seeding Plates with <i>E. Coli</i>	53
2.3.3 <i>C. elegans</i> Strain Maintenance	53
General Maintenance	53
Preparation of <i>C. elegans</i> Stocks	54
2.3.4 Obtaining an Age Synchronized Population of <i>C. elegans</i>	55
2.3.5 Brood Size Assay	55
2.3.6 Longevity Assay in Solid Media.....	56
2.3.7 Longevity Assay in Liquid Media	56
2.3.8 Body Length Measurement.....	57

2.3.9 Investigation of The Effect of RNAi	58
RNAi Feeding Strains	61
Plasmid Isolation.....	61
Gel Electrophoresis	62
Restriction Digestion	62
RNAi Primers.....	62
RNAi Plasmid Sequencing	63
RNAi Feeding Protocol.....	64
2.4 Results.....	65
2.4.1 Establish the role of GCPII in <i>C. elegans</i> reproduction.....	65
2.4.2 Establish the role of GCPII in <i>C. elegans</i> ageing	67
2.4.3 Establish the role of GCPII in <i>C. elegans</i> development	70
2.4.4 Establish the role temperature on <i>C. elegans</i> aging and reproduction.....	73
2.4.5 Investigation of The Effect of RNAi	76
Gel Electrophoresis.....	76
RNAi Sequence Alignment.....	77
Brood Size Assay	78
2.5 Discussion.....	80
2.5 Conclusions.....	83

**CHAPTER 3: INVESTIGATION OF THE ROLE OF GCPII IN FOLATE
METABOLISM**

3.1 General Introduction	84
--------------------------------	----

3.2	Chemistry and Stability.....	84
3.3	Biosynthesis in Bacteria	87
3.4	Intestinal Absorption.....	90
3.5	Metabolism (Human, <i>C. elegans</i> And Bacteria; <i>E. coli</i>).....	95
3.6	Deficiency	97
3.7	The Mechanism of Sulfamethoxazole Action	97
3.8	Hypothesis and Objectives	98
3.9	Material and Methods	99
3.9.1	Preparation of NGM Assay Plates	99
	Bacterial Food Source: SMX treated <i>E. coli</i> OP50.....	99
	Preparation of NGM Plates.....	99
3.9.2	Brood Size Assay	99
3.9.3	Body Length Assay	100
3.9.4	Bacterial Folate Extraction	100
3.9.5	Bacterial Folate Extract Purification.....	101
3.9.6	Folate Standard Preparation.....	102
3.9.7	Nuclear Magnetic Resonance Spectroscopy (NMR) Based Folate Analysis	102
3.9.8	High Performance Liquid Chromatography (HPLC) Based Folate Analysis	102
3.10	Results.....	104
3.10.1	The Effect of Reduced Dietary Foliates on Reproduction.....	104
3.10.2	The Effect of Reduced Dietary Foliates on Development	112

3.10.3 The Effect of Folinic Acid (5-Formyl-THF) Supplementation	122
3.10.4 Identification and Quantitation of Folate Derivative in <i>E. coli</i> OP50	128
3.10.5 HPLC Based Folate Analysis.....	128
3.11 Discussion	136
CHAPTER 4: CONCLUSIONS AND FUTURE PERSPECTIVES.....	145
BIBLIOGRAPHY	147
APPENDICES.....	163
Appendix 1: Stock Solutions	163
Appendix 2: Preparation of Liquid Growth Medium	164
Appendix 3: RNAi Sequence Alignment Data	165
Appendix 4: Extraction Buffer Components	171
Appendix 5: NMR Spectral Parameters and Conditions	172
Appendix 6: <i>E. coli</i> OP50 Growth Curve	174

List of Figures

Figure 1. Catalytic Mechanisms of Proteases.	18
Figure 2. The mechanism of GCPII action in the brain.	22
Figure 3. The structure of human GCPII homodimer (35).	24
Figure 4. The 3D Structure of human GCPII.	27
Figure 5. Splice variants of GCPII gene (41).	28
Figure 6. Homology modeling of the extracellular domains of published hGCPII (38) compared to cGCPII crystal structure.	32
Figure 7. Complete mRNA transcript of cGCPII paralogs.	32
Figure 8. Structures of GCPII inhibitors. (24)	35
Figure 9. The mechanism of RNAi. (72)	39
Figure 10. Anatomy of an adult hermaphrodite and male.	40
Figure 11. C. elegans cross sections from head to tail.	41
Figure 12. The intestine of an adult hermaphrodite.	44
Figure 13. Life cycle of C. elegans at 22 °C.	46
Figure 14. Body length measurement steps (98).	57
Figure 15. Full Sequence Map of L4440 RNAi Feeding Vector (100).	59
Figure 16. The Map of L4440 RNAi Feeding Vector (100).	60
Figure 17. The brood size of wild-type (N2) and gcp-2 mutants.	66
Figure 18. The longevity of wild-type and gcp-2 mutants.	69
Figure 19. The body length of wild-type and gcp-2 mutants.	71
Figure 20. The images of the body length of wild-type and gcp-2 mutants.	72

Figure 21. The effect of temperature on longevity of the wild-type and gcp-2.1 mutant <i>C. elegans</i>	74
Figure 22. The effect of temperature on brood size of the wild-type and gcp-2.1 mutant <i>C. elegans</i>	75
Figure 23. The gel electrophoresis images of RNAi plasmids.	77
Figure 24. The effect of RNAi induced GCP-2 inhibition on brood size of wild-type <i>C. elegans</i>	79
Figure 25. Chemical structure of Folates.	86
Figure 26. Pathway of de novo bacterial biosynthesis of folate.	89
Figure 27. Hydrolysis of dietary folates by GCPII in the jejunal brush border membrane.	91
Figure 28. Folate absorption from intestinal lumen, metabolism in enterocytes, and transportation out into the hepatic portal vein as 5-Methyl-THF.	94
Figure 29. Folate-mediated one-carbon metabolism.	96
Figure 30. Sulfamethoxazole (SMX) is a structural analogue for PABA and inhibits bacterial folate biosynthesis.....	98
Figure 31. Bacterial Folate Purification Steps.	101
Figure 32. The effect of SMX dependent folate inhibition on brood size of wild-type <i>C. elegans</i>	105
Figure 33. The effect of SMX dependent folate inhibition on brood size of gcp-2.1 mutant <i>C. elegans</i>	107
Figure 34. The effect of SMX dependent folate inhibition on brood size of gcp-2.2 mutant <i>C. elegans</i>	108

Figure 35. The effect of SMX dependent folate inhibition on brood size of <i>gcp-2.3</i> mutant <i>C. elegans</i>	110
Figure 36. Growth assay showing growth phenotype of the wild-type and <i>gcp-2</i> mutants. <i>C. elegans</i> were maintained on 1000 µg/mL SMX treated <i>E. coli</i> OP50.	111
Figure 37. The effect of SMX dependent folate inhibition on body length of wild-type <i>C. elegans</i>	113
Figure 38. The images of wild-type worms at different concentrations of SMX.	114
Figure 39. The effect of SMX dependent folate inhibition on body length of <i>gcp-2.1</i> mutant <i>C. elegans</i>	116
Figure 40. The images of <i>gcp-2.1</i> mutants at different concentrations of SMX.	117
Figure 41. The effect of SMX dependent folate inhibition on body length of <i>gcp-2.2</i> mutant <i>C. elegans</i>	119
Figure 42. The images of <i>gcp-2.2</i> mutants at different concentrations of SMX	120
Figure 43. The effect of SMX dependent folate inhibition on body length of <i>gcp-2.3</i> mutant <i>C. elegans</i>	121
Figure 44. The effect of Folinic Acid supplementation on brood size of <i>C. elegans</i> that were supplied with 1000 µg/mL SMX treated OP50 as food.....	123
Figure 45. The effect of folinic acid supplementation on the body length untreated controls.....	125
Figure 46. The effect of folinic acid supplementation on the body length of worms maintained on <i>E. coli</i> treated with 100 µg/mL SMX.....	126
Figure 47. The effect of folinic acid supplementation on the body length of worms maintained on <i>E. coli</i> treated with 1000 µg/mL SMX.....	127

Figure 48. Chromatogram with florescence intensity of Extraction buffer without folates.	129
Figure 49. Chromatogram with florescence intensity of DHF standards.	130
Figure 50. Chromatogram with florescence intensity of THF standard.	130
Figure 51. Chromatogram with florescence intensity of 5-Methyl-THF standard.	131
Figure 52. Chromatogram with florescence intensity of 5-Formyl-THF standard.	131
Figure 53. Chromatogram with florescence intensity of Folic Acid standard.	132
Figure 54. Chromatogram with florescence intensity of L-Glutamic Acid standard.	132
Figure 55. Chromatogram with florescence intensity of a mixture of different folate forms.	133
Figure 56. Comparative chromatogram of different folate forms.	133
Figure 57. Overlaid Chromatograms with florescence intensity of E. coli OP50 folate extracts with varying concentrations of SMX.	134
Figure 58. Comparative plot of the effect of SMX dependent folate inhibition on brood size of wild-type and gcp-2 mutant C. elegans.	140
Figure 59. Comparative plot of the effect of SMX dependent folate inhibition on body length of wild-type and gcp-2 C. elegans mutants.	144
Figure 60. Graphical representation of proposed GCPII function in folate mediated reproductive and developmental biology of C. elegans.	146

List of Tables

Table 1. Description of splice variants derived from GCPII gene (41).....	29
Table 2. Sequences details of <i>cGCPII</i> . (46–48).....	33
Table 3. <i>C. elegans</i> and <i>E. coli</i> strains used in this study.....	50
Table 4. The Gene-Pairs primer sequences (99, 103).....	63
Table 5. Substituents carried by a THF molecule.....	87
Table 6. Fluorescence Detection of Folate Standard. ^a	135

List of Abbreviations

2-MPPA: 2-(3-mercaptopropyl) pentanedioic acid

2-PMPA: 2-(phosphonomethyl)pentanedioic acid

5-Formyl-THF, 5-Formyl-Tetrahydrofolate

5-Methyl-THF, 5-Methyl-Tetrahydrofolate

Aa, amino acid residues

ATP, Adenosine triphosphate

B12, vitamin B12

C. elegans, *Caenorhabditis elegans*

cGCPII, *C. elegans* Glutamate Carboxypeptidase II

CRISPR, clustered regularly interspaced short palindromic repeats

DHF, dihydrofolate

DHFR, dihydrofolate reductase

DHP, 7,8-dihydropteroate

DHPPP, 6-hydroxymethyl-7,8-dihydropterin pyrophosphate

dsRNA double stranded RNA

dTMP, deoxythymidine monophosphate; Glu_n,

dUMP, deoxyuridine monophosphate

E. coli, *Escherichia coli*

EPSP, 3-enolpyruvylshikimic acid 3-phosphate

Folates-Glu₁, monoglutamated folates

Folates-Glu_n, polyglutamated folates

FOLH1, folate hydrolase

FOLT, folate transporter

FPGS, Folate polyglutamate synthetase

GCPII, Glutamate Carboxypeptidase II

GTP, guanosine triphosphate

hGCPII, human Glutamate Carboxypeptidase II

mGluR-1, metabotropic glutamate receptor-1

MRP3, multidrug resistance protein-3.

MTHFD1, methylenetetrahydrofolate dehydrogenase

MTHFD1L, monofunctional tetrahydrofolate synthase

MTHFR, methylenetetrahydrofolate reductase

NAAG, *N-acetyl-l-aspartyl-l-glutamate*

NAALADase, *N-acetylated-alpha-linked acidic dipeptidase*

NADPH, Nicotinamide Adenide Dinucleotide Phosphate

NTDs, neural tube defects

*p*ABA, para-aminobenzoic acid

PCTF, proton-coupled folate transporter

PSMA, prostate specific membrane antigen

PSMAL, Prostate specific membrane antigen-like

RFC, reduced folate carriers

RISC, RNAi inducing silencing complex

RNAi, RNA Interference

SAH, S-adenosyl homocysteine

SAM, S-adenosylmethionine

SEM, Standard Error of Mean

SHMT1/2, serine hydroxymethyl transferase, cytosolic (1)/ mitochondrial (2);

MTHFD2/L, methylenetetrahydrofolate dehydrogenase 2/ 2-like

siRNAs, short interfering RNAs

SMX, Sulfamethoxazole

SSZ, Sulfasalazine

THF, tetrahydrofolate

TYMS, thymidylate synthetase

Chapter 1: Introduction

1.1 Proteases

Proteases, also known as proteolytic enzymes, peptidases or proteinases, are enzymes that catalyze the cleavage of peptide bonds between amino acid residues in a polypeptide chain or molecules containing peptide bonds (1). These enzymes were believed to appear at the initial stages of protein evolution in primitive organisms as a destructive enzyme for protein catabolism and amino acids production. Proteases play an essential role in metabolism such as regulation of protein degradation, localization, and activity, modulation of protein-protein interactions, production of bioactive molecules, and signal generation, transduction and amplification. Thus, involved in replication and transcription of DNA, cellular proliferation and differentiation, tissue morphogenesis and remodeling, heat shock and unfolded protein responses, angiogenesis, neurogenesis, ovulation, fertilization, wound repair, stem cell mobilization, hemostasis, blood coagulation, inflammation, immunity, autophagy, senescence, necrosis, and apoptosis (2).

Based on the catalytic mechanisms, proteases fall into six classes: aspartic, glutamic, metalloproteases, cysteine, serine, and threonine proteases. Glutamic proteases are not present in mammals. The first three classes attack the peptide bond of the substrate by activating a water molecule to serve as the nucleophile, while the rest attack the peptide bond of the substrate by utilizing a catalytic amino acid residue (cysteine, serine, and threonine respectively) located in the active site as the nucleophile (Figure 1). These protease classes can be further branched based on the amino acid sequence and characteristics of their three-dimensional folding (2, 3). According to the Mammalian Degradome Database (4, 4), there are 588, 658, 658 total number of protease genes present

in human, rat and mouse genomes respectively. Human catalytic classes; aspartic, cysteine, metallo, serine and threonine proteases has 21, 164, 192, 184 and 27 different members respectively (4). The protein Glutamate Carboxypeptidase II (GCPII), the subject of this thesis, is a metalloprotease.

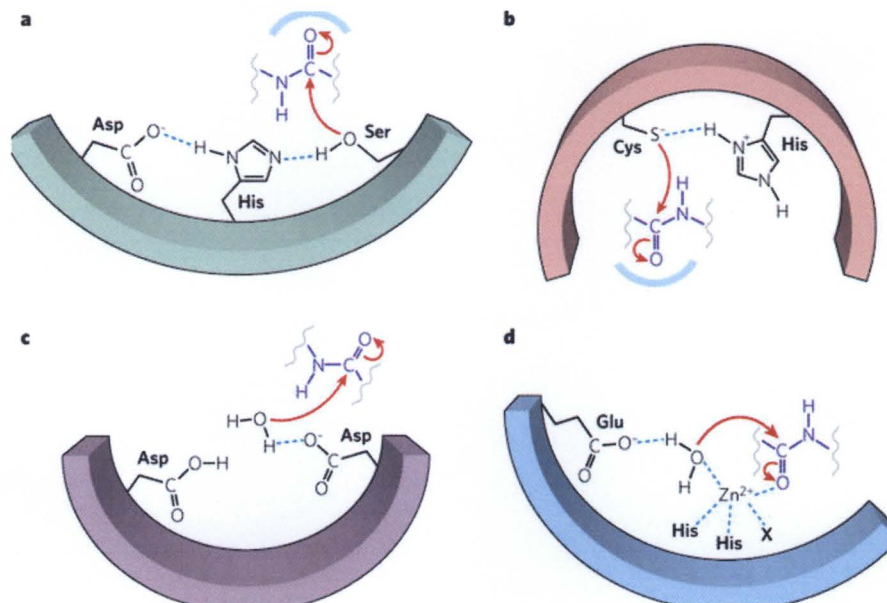


Figure 1. Catalytic Mechanisms of Proteases.

(a) serine proteases; (b) cysteine proteases; (c) aspartyl proteases; and (d) metalloproteases (5).

1.2 Metalloprotease and M28 family

Metalloproteases are the largest subclass of proteases with 192 members in humans (4). This is a vastly diverse group of proteases distributed across families M1 through M91, each family represents a set of homologous proteases (6). The active site of metalloproteases consists one or two divalent metal ions to catalyze the hydrolytic cleavage of the peptide bonds as shown in Figure 1b (7, 8). These metal ions are bound in an approximate tetrahedral conformation at the active site. The catalytic metal ion coordinates with three amino acid residues of the substrate polypeptide chain and a water molecule. These amino acid residues are usually charged (9). Metalloproteases usually employ Zinc ion (Zn^{2+}) (10). Other transition metals such as Co^{2+} and Mn^{2+} have been found at active sites. GCPII is a Zn-metalloprotease.

Based on the cleavage site of the hydrolysis-targeted protein there are two subgroups of metalloproteases: metalloendopeptidase and metalloexopeptidase. Metalloendopeptidase cleave a terminal peptide bond, while metalloendopeptidases cleave an internal peptide bond (11). Metalloendopeptidases can be further divided as aminopeptidases and carboxypeptidases which hydrolyzes the first peptide at the amino terminal (N-terminus) and carboxyl terminal (C-terminal) end of protein substrates respectively (12, 13).

Peptidases in M28 family have co-catalytic zinc ions, meaning that two Zn^{2+} ions act together in the active site, and such active sites are found in aminopeptidases and carboxypeptidases. Each Zn^{2+} is coordinated in tetrahedral conformation with three amino acid residues and a catalytic water molecule. An aspartate residue binds Zn^{2+} . The Zn^{2+} ligands (with the bound metal ion indicated by Roman Figures) occur in the sequence in

the order His (II), Asp (I and II), Glu (I), Asp or Glu (II) and His (I). Two additional residues, an Asp and a Glu, are believed to be important for catalysis. Four of these residues appear in the motifs His-Xaa-Asp and Glu-Glu (14–16).

1.3 Glutamate Carboxypeptidase (GCPII)

In 1985, Koller and Coyle (17, 18) discovered a novel enzyme that cleaves the peptide neurotransmitter *N-acetyl-l-aspartyl-l-glutamate* (NAAG) and consequently termed as *N-acetylated-alpha-linked acidic dipeptidase* (NAALADase). In 1987 (19), a novel monoclonal antibody was found upon immunizing isolated LNCaP cells of human prostate malignant. The antigen of this antibody was believed to be prostate specific. Hence, termed as prostate specific membrane antigen (PSMA). In 1996 (20), it was discovered that PSMA has similar NAAG hydrolytic activity, pharmacologic properties and high sequence identity to NAALADase. Therefore, NAALADase and PSMA refer to one protein. In the same year Pinto *et al* (21) found that PSMA possess folate hydrolase activity or acts as a pteroyl poly-gamma-glutamyl carboxypeptidase (21, 22). NAALADase, PSMA and folate hydrolase are now known with the unified name Glutamate Carboxypeptidase II (GCPII; EC 3.4.17.21) approved by the International Union of Biochemistry and Molecular Biology (23). This is a transmembrane, zinc-dependent metalloprotease belonging to M28 family (described above in Chapter 1.2) (23, 24). GCPII is identified in many different organisms including *Homo sapiens* (human), *Caenorhabditis elegans* (soil nematode) and *Mus musculus* (mouse). Human GCPII (hGCPII) is encoded by folate hydrolase (FOLH1) gene (24). GCPII has been extensively

studied over the last three decades as a therapeutic target for various neurological and oncological diseases.

1.3.1 Localization and Physiological Role

hGCPII is expressed in the central and peripheral nervous system, small intestine, kidney and tumor-associated neovasculature with the highest expression levels present in astrocytes and testis (24, 25). In astrocytes and Schwann cells, it modulates excitatory neurotransmission by hydrolyzing the neuropeptide NAAG into N-acetyl-l-aspartate and glutamate, which is the major excitatory neurotransmitter in the brain (Figure 2). Then released glutamate binds to metabotropic glutamate receptor-1 (mGluR-1) on astrocytes to initiate Ca^{2+} waves, which increases neuron excitability (26, 27). Therefore, over-expression of hGCPII in the central nervous system instigates glutamate excitotoxicity (28–30). Glutamate is the major excitatory neurotransmitter in the mammalian brain. Therefore, prolonged exposure to glutamate leads excessive influx of ions into the neuronal cells resulting calcium overload which is toxic to neurons. This results in activation of enzymes that degrade proteins, membranes and nucleic acids leading to the damage and death of neurons. This is known as glutamate excitotoxicity (31). This can lead to stroke, traumatic brain injury and neurodegenerative diseases such as Alzheimer's disease, Parkinson's disease, Huntington's disease and amyotrophic lateral sclerosis (28–30). Pharmacological inhibition and genetic knock down of GCPII in tissue culture and animal models was shown to be neuroprotective. Thus, GCPII is a putative therapeutic target (32, 33).

In the jejunum, GCPII aids absorptions of dietary folates by cleaving folly-poly- γ -glutamate into folate and glutamate (Figure 27) (32). Then folate is absorbed by enterocytes

via reduced folate carriers and folate binding proteins. Mutations in GCPII is associated with folate malabsorption resulting depression, anemia, infertility, Crohn's disease and inflammatory bowels disease. Folate deficiency during pregnancy can lead to infants with severe birth defects of spine and skull, termed neural tube defects (NTDs) and child developmental delay (34). The role GCPII in folate metabolism is further discussed in the Chapter 3 under section 4.

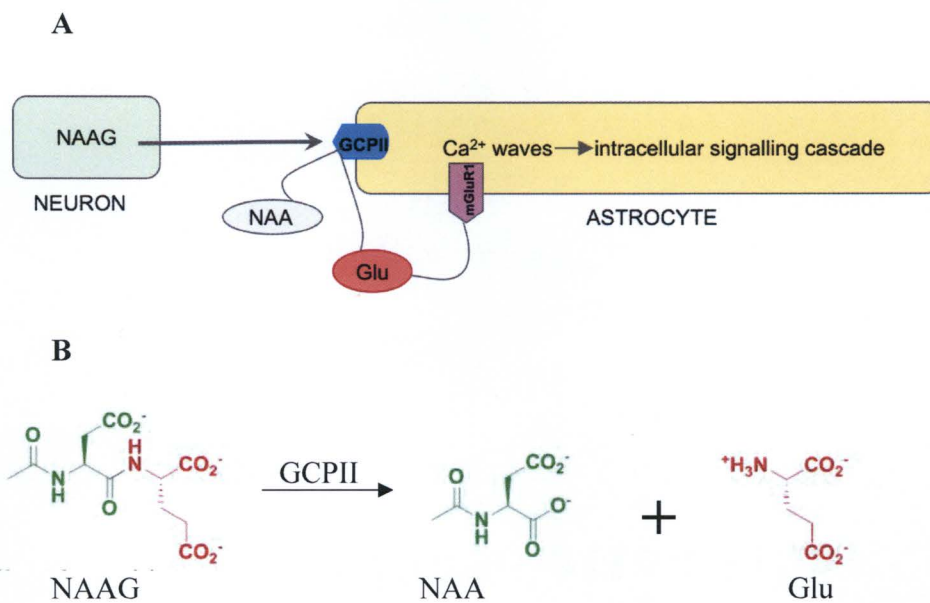


Figure 2. The mechanism of GCPII action in the brain.

(A) Pathway of NAAG hydrolysis and excitatory neurotransmission in astrocytes. (B) Hydrolysis of NAAG by GCPII. NAAG, N-acetyl-L-aspartyl-L-glutamate; NAA, N-acetylaspartate; Glu, glutamate; mGluR1, metabotropic glutamate receptor-1.

GCPII is highly expressed in prostate carcinoma cells. Therefore, GCPII is an established cancer marker as the expression is correlated with the progression of prostate cancer. Although the role in prostate cancer progression is unknown, several studies have linked its role to tumor progression (35). It is also expressed in the neovasculature of including glioblastomas, breast, bladder and lung cancers (35, 36). Thus, GCPII is a potential target for anti-tumor therapy. The roles of GCPII in prostate, kidney and many other tissues remain unknown.

1.3.2 Structure

GCPII is encoded by FOLH1 gene which has 19 exons spanning 60 Kilobases (Kb) of genomic DNA. The GCPII cDNA is 2.65 Kb long, which is mapped to chromosome 11 and translates into a 750 amino acid protein (35, 37). As shown in Figure 3, GCPII is type II transmembrane protein with a short cytoplasmic N-terminal sequence of 1-18 amino acid residues (aa), a single transmembrane helix of 19-43 aa and a large extracellular C-terminal sequence of 44-750 aa. The N-terminal portion modulates GCPII endocytosis by interacting with membrane scaffold proteins such as clathrin, clathrin adaptor protein-2, caveolin-1 and filamin-A (24, 35). Thus, N-terminal sequence is pivotal to recycle and internalize GCPII. The large C-terminal portion is a single subunit; however, it can be subdivided into three structurally distinct domains: protease domain consists of 57-116 aa and 352-590 aa, apical domain consist of 117-351 aa and dimerization or C-terminal domain consist of 591-750 aa. Substrate recognition, binding and processing demands combined action of all three domains (24, 35).

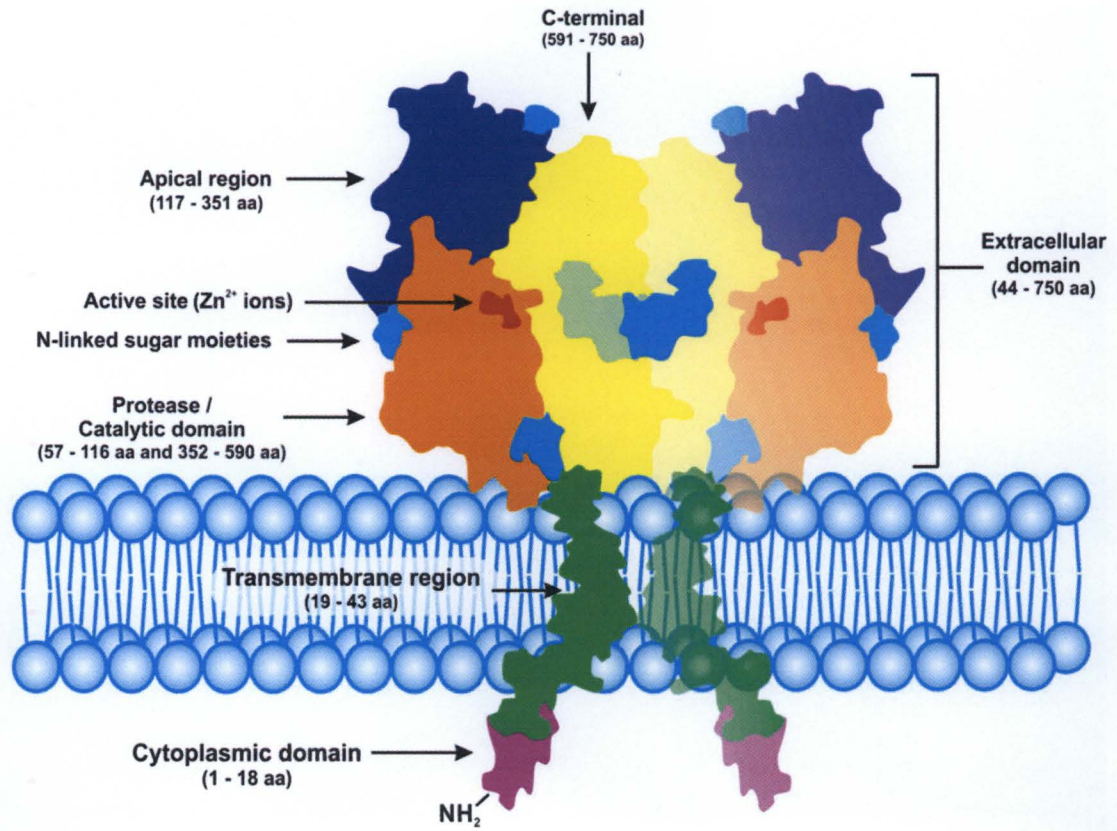


Figure 3. The structure of human GCPII homodimer (35).

The secondary structure of GCPII is organized into α -helices and β -sheets (Figure 4). Protease domain has a central 7 stranded mixed β -sheet with 10 flanking α -helices. The β 1 and its antiparallel strands links protease and apical domains. Apical domain is inserted between the central β 1 and β 2 strands. C-terminal domain consists 4 α -helices and two of these α -helix loops that interacts with the protease domain via hydrogen bonding, which contributes to the tertiary structure (24, 38).

GCPII exhibits C-terminal homodimerization via crystallographic two-fold symmetry which is fundamental for its catalytic activity. However, these dimers consist structurally distinct active sites. The C-terminal domain of each monomer is linked by two salt bridges between arginine662 and asparagine663. Dimerization is stabilized by a single Ca^{2+} that is coordinated by Glu432, Glu436, Thr269 and Tyr272 residues. However, the Ca^{2+} do not contribute to the enzymatic activity as it is located away from the active sites (38).

The active site of GCPII can be divided into two binding pockets: S1' and S1. There is a Zn^{2+} in each binding pocket (total of 2 Zinc ions) linked by a water molecule. Glu424 in the binuclear Zinc active site acts as the catalytic residue of GCPII. Glu424 accepts a proton from $\text{Zn}^{2+}:\text{H}_2\text{O}$ during substrate cleavage and donate it to the leaving peptide (38). For example, a proton is transferred to glutamate after attacking the aspartyl carbonyl group of NAAG to complete hydrolysis (38, 39). S1' pocket prefers glutamate and glutamate like moieties binding via H-bonds and ionic interactions. However, the amphipathic nature of S1' allows formation of polar and non-polar interactions like H-bonds, ionic bonds and hydrophobic and van-der-waals interactions, respectively. S1 pocket is optimized for

glutamate and aspartate binding. Therefore, NAAG and folate naturally become substrates for GCPII (24).

The molecular weight of the primary GCPII structure is ~79 kDa, however, the molecular weight of folded GCPII complex is 110 kDa (40). This is due to the post-translational glycosylation modifications. Barinka *et al* (25) revealed the presence of heavy N- and O-glycosylation accounting 10-25% of the total molecular weight of the enzyme. N-glycosylation is required for proper protein folding and translocation, therefore, indispensable for its catalytic functions (25). In addition, glycosylation contributes to C-terminal dimerization of the protein. The role of O-glycosylation is not clear yet (38).

1.3.3 Splice Variants

Several alternative splice variants have been identified in GCPII. These splice variants were extensively studied in prostate cancer epithelium, thus referred as PSMA variants. Most alternative splicing occurs at the 5' end. They are PSM-D, PSM-F, PSM-E, PSM-C, PSMA+68 and PSM' (Figure 5 and Table 1). The wild-type GCPII/PSMA mRNA contains of 750 aa with 19 exons and 18 introns. PSM' is the first identified splice variant with 693 aa. This variant lack bases 114-379 in the first exon at 3' end and deletions include the initiation codon. PSM' is abundantly expressed in prostate cancer cells compared to non-cancerous cells. PSMC and PSMA+68 encodes for a protein with 693 aa. PSM-D and PSM-F encodes for a protein with 735 by addition of novel 24 aa and deletion of 39 aa. PSM-E is similar to PSM-F but lacks exon 18 (41).

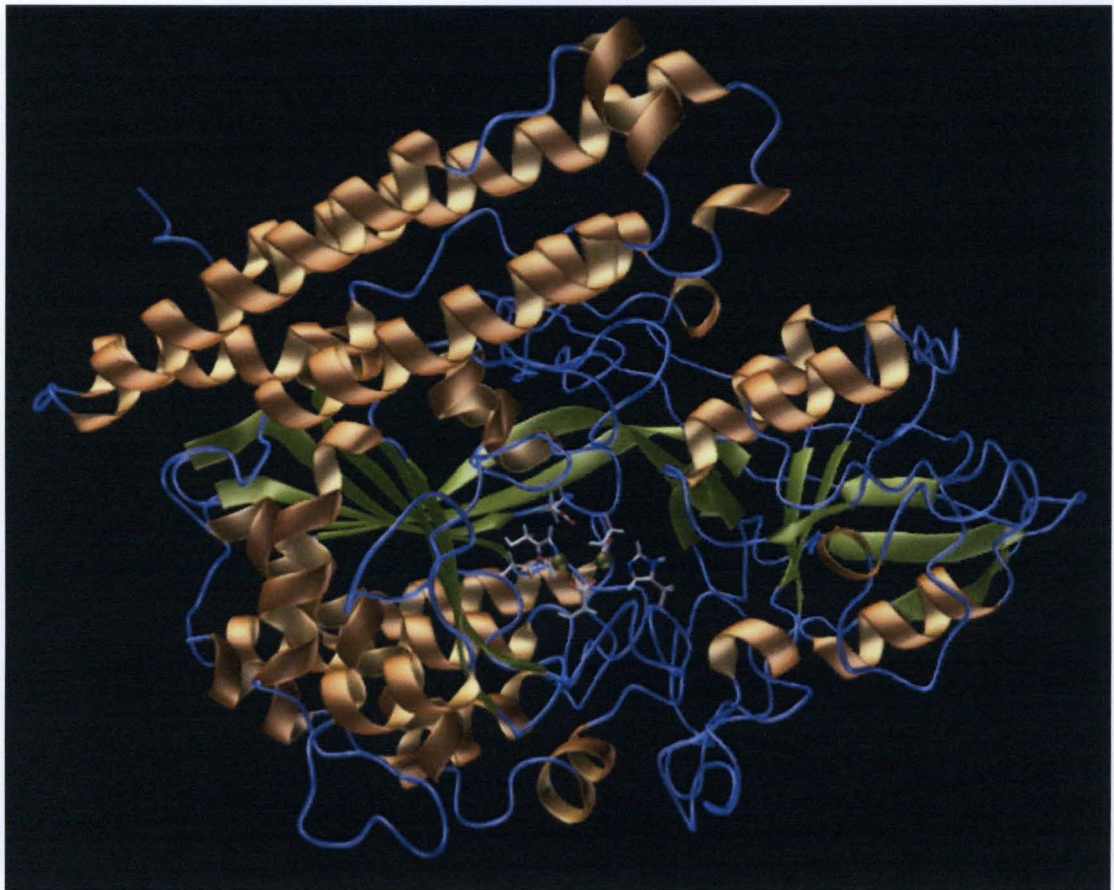


Figure 4. The 3D Structure of human GCPII.

Two Zn ligands in the active site are shown as golden spheres. Brown ribbon, β -sheets; green ribbon, α -helices; light gray, carbons; cyan, hydrogen; red, oxygen; blue, nitrogen; yellow, sulfurs. (4)

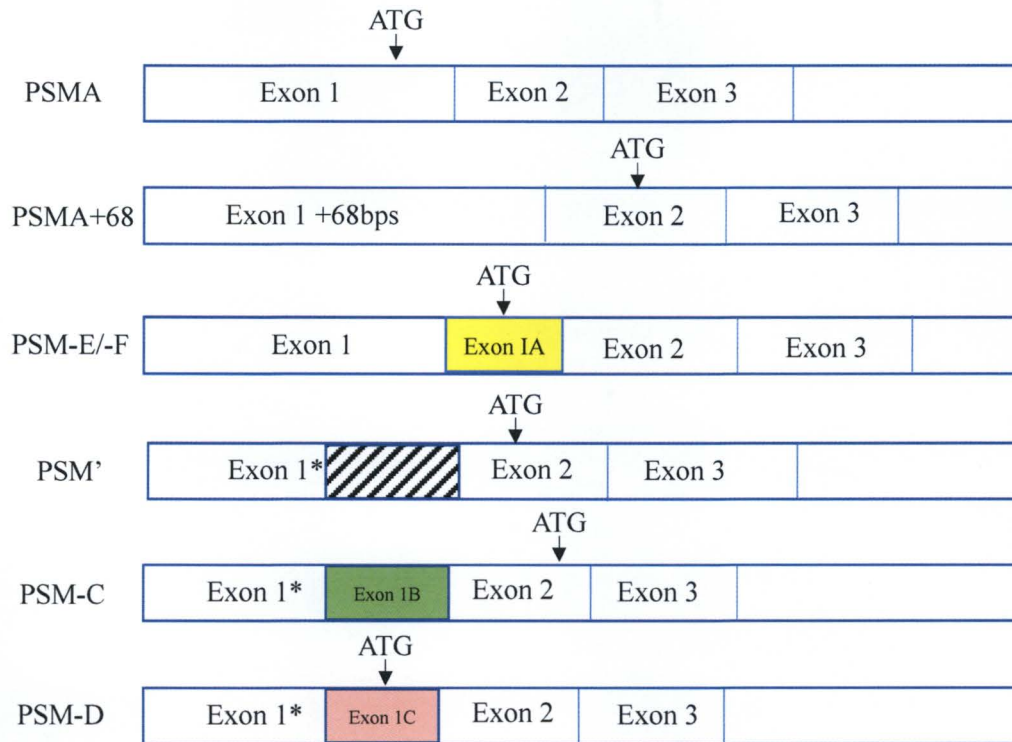


Figure 5. Splice variants of *GCPII* gene (41).

ATG is the translation start codon; PSMA is the 'wild-type' GCPII mRNA consisting of 19 exons and 750 aa. Most alternative splicing occurs at the 5' end (i.e. N-terminus of the protein) and the first three constitutive exons of PSMA: PSMA+68, PSM-E/-F, PSM', PSM-C, and PSM-D are shown. Yellow, green and red shows alternative exons 1A, 1B and 1C. PSM', PSM-C and PSMA+68 encodes for a protein with 693 aa. PSM-D and PSM-F encodes for a protein with 735. PSM-E is similar to PSM-F but lacks exon 18. Crosshatched rectangle indicates the missing region in PSM' compared to PSMA.

Table 1. Description of splice variants derived from <i>GCPII</i> gene (41).		
Exon ^a	Nucleotides ^b	<i>FOLHI</i> gene ^c
1	379	1-379
1+68	447	1-447
1*	113	1-113
1A	97	1797-1893
1B	113	776-908
1C	101	1794-1894
2	106	2499-2604
3	187	8230-8416

^a Exon number as indicated in the Figure 5

^b Number of nucleotides

^c the size of putative protein products; Sequence of *FOLHI* gene stored as “NC_000011” at NCBI server

1.3.4 Paralogs, Homologs and Orthologs

Homologs are genes that have a common ancestor inherited into two species. Homologous genes can have similar sequences, but, all similar sequences are not homologous (42, 43). There are two types of homologous genes: orthologs and paralogs. Paralogs are products of gene duplication followed by mutations. This is a mechanism of neofunctionalization in which genes acquire functional divergence. In other words, paralogs may or may not have the same function after a gene duplication event (44). Orthologs are products of speciation event followed by gene divergence, in which genes' main function is conserved (42).

Many paralogs and structural homologs of GCPII have been identified in the human proteome and they are predominantly type II transmembrane glycoproteins. Although these homologs are structurally related, the function remains unknown. However, it is possible to have non-proteolytic functions. The closest GCPII relative is Prostate specific membrane antigen-like (PSMAL) with 98% sequence similarity and present only in primates. But it lacks the entire first exon and a part of the first intron. PSMAL is proteolytically inactive and this could be due to extensive N-terminal deletion. PSMAL mRNA has been identified in human liver, kidney and associated with hearing loss. The second GCPII homolog is Glutamate Carboxypeptidase III (GCPIII) with 68% sequence similarity and shows NAAALDase activity. Other homologs are NAALADase L and NAALADase L2 with 37% and 20% sequence similarity, respectively (41).

Identifying GCPII orthologs is important for researchers when selecting suitable model organisms for research. GCPII is present in many animal species, often in several paralogs. Murine, rat and porcine GCPII shares >90% sequence similarity with hGCPII.

However, the tissue specific expression varies. GCPII is absent in mouse, rat, pig, dog or monkey prostate tissue, where it is largely present in humans. The expression levels in testis, brain and kidneys of mouse, rat and pig is similar to humans. GCPII is highly expressed in human and pig intestine, however, absent in mouse and rat intestines (41).. *C. elegans* have three paralogs of GCPII; *gcp-2.1*, *gcp-2.2* and *gcp-2.3*. A homologous gene of GCPII is found in plants known as AMP1 which is functionally divergent (45). Furthermore, this protein is not found in yeasts (41).

1.3.5 GCPII in *C. elegans*

hGCPII and *C. elegans* GCPII (hereafter identified as cGCPII) shows high structural similarity when the homology modeling of the extracellular domains of published human GCPII (hGCPII) was compared the extracellular domains of cGCPII (unpublished data from Periyannan lab) crystal structure using Modeller program as shown in the Figure 6. This indicates that both proteins may possess similar functions. Therefore, used as the model organism for this study. As shown in Figure 7, cGCPII encodes as 3 paralogs compared to 5 paralogs in humans (Chapter 1.3.4): *gcp-2.1*, *gcp-2.2* and *gcp-2.3*. The *gcp-2.1* gene is encoded as 3 isoforms: isoform *a*, isoform *b* and isoform *c* (Table 2) (46–48).

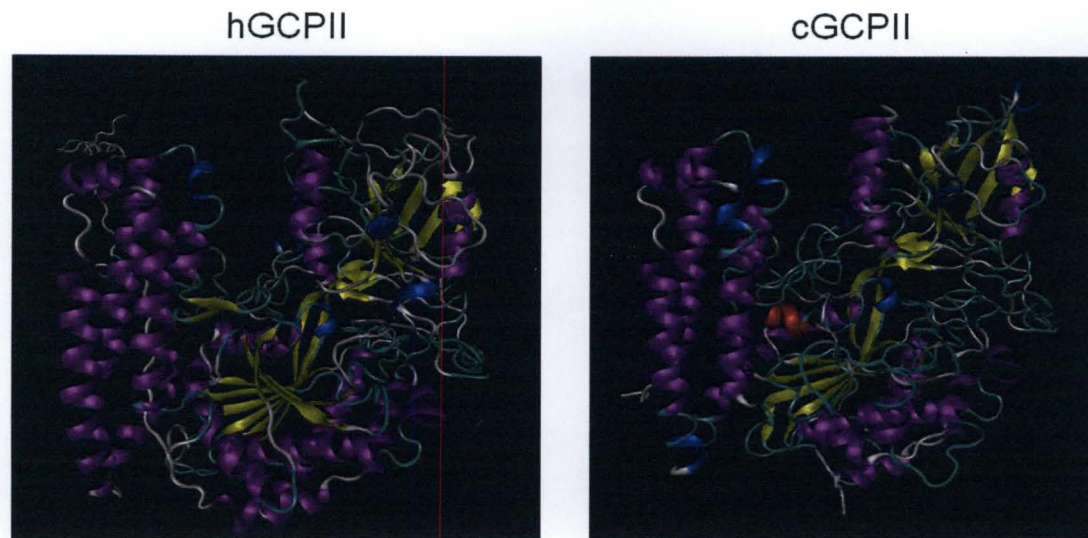


Figure 6. Homology modeling of the extracellular domains of published hGCPII (38) compared to cGCPII crystal structure.

Unpublished cGCPII model generated using Modeller Software and published hGCPII ectodomain structural data by Periyannan lab).

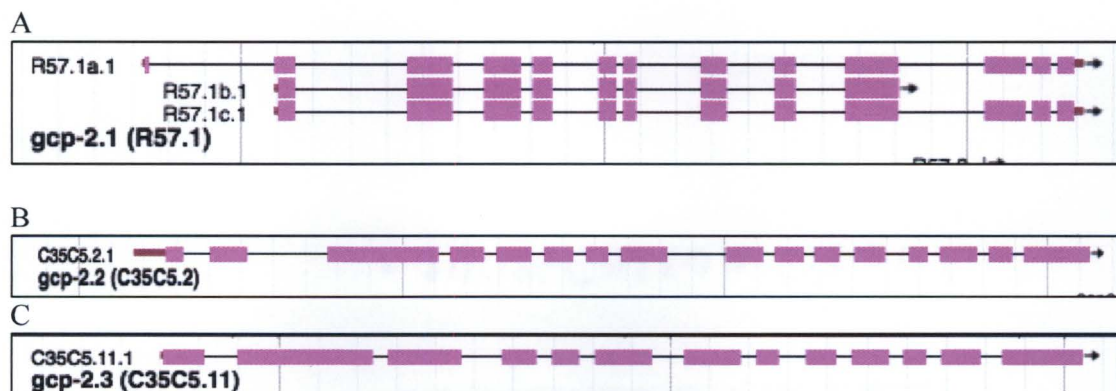


Figure 7. Complete mRNA transcript of cGCPII paralogs.

Introns are indicated by the dense pink boxes. (A) *gcp-2.1* paralog encodes as 3 isoforms: isoform a, isoform b and isoform c. (B) *gcp-2.2* paralog. (C) *gcp-2.3* paralog. (46–48)

Table 2. Sequences details of cGCPII . (46–48)		
Protein ^a	Transcript ^b	Protein length ^c
cGCP-2.1 Isoform a	R57.1a.1 ^d	770
cGCP-2.1 Isoform b	R57.1b.1 ^d	576
cGCP-2.1 Isoform c	R57.1c.1 ^d	751
cGCP-2.2	C35C5.2.1 ^e	779
cGCP-2.3	C35C5.11.1 ^f	700
^a cGCPII paralog/isoform ^b Coding transcript ^c Number of amino acids ^d Shown in Figure 7 (A) ^e Shown in Figure 7 (B) ^f Shown in Figure 7 (C)		

1.3.5 Inhibitors

As discussed above, the involvement of GCPII over-expression in certain neurological and oncological diseases elevated the interest for the development of GCPII inhibitors. These inhibitors must meet two conditions to be effective; presence of glutamate-like moiety to bind to the C-terminal glutamate recognition site and zinc chelating group to coordinate the divalent zinc atoms at the active sites. There are three classes of GCPII inhibitors that has been extensively studied. They are phosphonate-based, urea-based and thiol-based inhibitors (24).

2-(phosphonomethyl)pentanedioic acid (2-PMPA) (Figure 8) is a phosphonate-based, potent, competitive inhibitor, which was first discovered in 1996 (49). The glutamate moiety (pentanedioic acid) portion of the inhibitor was designed to interact with the glutamate recognition site of GCPII, whereas the phosphonate group strongly chelate the active site zinc ions that contributes to the high potency with a IC_{50} value of 300 pM (24, 50). However, 2-PMPA showed poor pharmacokinetic properties; low oral bioavailability. This directed researchers towards development of small molecule inhibitors such as 2-(3-mercaptopropyl) pentanedioic acid (2-MPPA) using 2-PMPA as template (50).

2-MPPA (Figure 8) is a thiol-based, selective, competitive inhibitor with a IC_{50} value of 90 nM (50). This showed higher oral bioavailability compared to 2-PMPA in several animal models. However, research discontinued due to its' low potency and potential immune reactivity in humans (24, 50).

ZJ-43 (Figure 8) is a urea-based inhibitor, which consists NAAG-like analogs. These analogs have two amino acids joined by their NH_2 groups with a urea bond and employ both the aspartate binding site and glutamate moiety in GCPII. Although, ZJ-43 had shown GCPII inhibition in animal models, like 2-PMPA and 2-MPPA, ZJ-43 also showed poor pharmacokinetic properties and limited bioavailability (24).

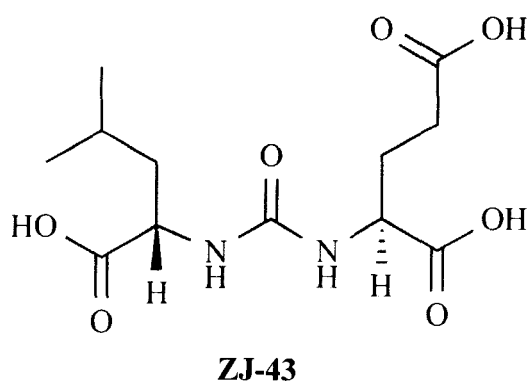
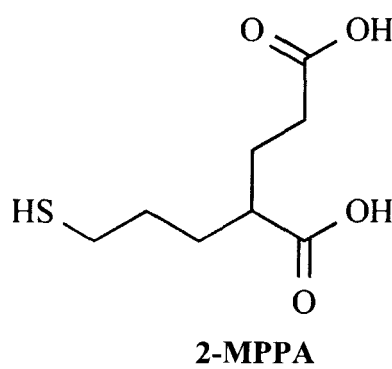
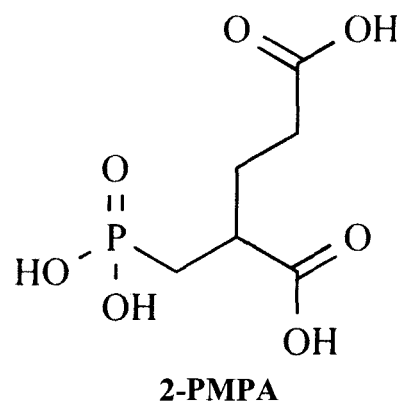


Figure 8. Structures of GCPII inhibitors. (24)

1.4 Model Organism: *Caenorhabditis elegans*

Model organisms are non-human species that helps scientists understand biological processes, traits or diseases. Therefore, for basic biological and clinical research model organisms such as *C. elegans*, *Drosophila*, *Arabidopsis*, zebrafish and rodents are essential tools (51). Typically, model organisms, share several characteristics such as short generation time, characterized genome, inexpensive cultivation, easy physical manipulation, availability of genetic/molecular tools and similarity to humans (51, 52). There are several distinct advantages of *C. elegans* makes it an ideal *in vivo* model organism to investigate the biological roles of GCPII.

C. elegans, which is commonly known as roundworms, is a multicellular, eukaryotic, non-hazardous, non-infectious, non-pathogenic, non-parasitic, bacterivore organism belonging to the phylum Nematoda (53, 54). In the wild, it is often found in soil, compost and rotting fruits (55). In the laboratory environment, *C. elegans* are maintained in petri dishes with agar or liquid culture and usually fed on lawns of the *Escherichia coli* strain OP50. However, other bacterial strains can also be used (56). The ability of *C. elegans* to grow from egg to egg laying adults in a short generation time (~3 days) in high densities, shorter life span and smaller size (~1 mm) allows efficient, inexpensive and easy growth in petri dishes. This model organism has been extensively used for research in developmental biology, cell biology and neurobiology.

1.4.1 Genetics

C. elegans have two sexes: self-fertilizing hermaphrodites with two copies of the X chromosome (XX) and males with one copy of the X chromosome (XO) (56, 57).

Hermaphrodites (Figure 10) are basically females that are capable of producing and storing sperms for self-fertilization at one stage in their life cycle before they begin the production of oocytes. (52). Hermaphrodites are also capable of mating with males. However, they are not able to cross-fertilize with other hermaphrodites. If hermaphrodites self-fertilize, males appear rarely with a frequency of ~0.1% by spontaneous non-disjunction in the hermaphrodite germ line. Self-fertilization allows homozygous worms to generate genetically identical progeny (56, 57). However, if a hermaphrodite mate with a male, males appear at higher frequency of ~50% in which 50% of the offspring does not receive a copy of the X chromosome from sperm. This is beneficial for breeding with different worm strains: generate a wild-type sibling of a mutant worm or generate a double mutant (56).

The *C. elegans* genome was fully sequenced by the *C. elegans* Genome Mapping and Sequencing Consortium and published in 1998 (58). *C. elegans* genome is 100,291,840 base pair long with six chromosomes and a mitochondrial genome (59, 60). There are about 20,470 protein-coding genes in the genome (*cf* human genome is estimated to code for 19,000-22,000 genes) (61, 62). Mutations can be induced by a wide range of mutagens: chemical mutagenesis or exposure to ionizing radiation (57, 63, 64). This makes *C. elegans* a powerful genetic model organism to study genes responsible for a particular biological trait. The central *C. elegans* worm stock center, Caenorhabditis Genetics Center at the University of Minnesota has over 3000 *C. elegans* mutant strains (<https://cbs.umn.edu/cgc/home>). Deletion mutant strains can also be purchased through the National Bio-Resource Project (<https://shigen.nig.ac.jp/c.elegans/>) at the Tokyo Women's Medical University School of Medicine in Japan. RNA interference (RNAi) is also an

extensively used technique to regulate gene expression of *C. elegans* to assess gene function which is discussed in the Section 1.4.5. Furthermore, recently researchers focused genome editing tools to generate gene deletions in *C. elegans* by clustered regularly interspaced short palindromic repeats (CRISPR)-Cas9 system to induce DNA Double-Strand Breaks (65, 66). CRISPR Plasmids can be purchased from Addgene plasmid repository (<https://www.addgene.org/crispr/worm/>).

1.4.2 RNA Interference (RNAi)

RNAi is a rapid and simple molecular biological method to understand the loss-of-function phenotypes by silencing the gene expression in organisms. Andrew Fire and Craig Mello received the Nobel Prize for Physiology and Medicine in 2006 for their discovery of RNAi (67). RNAi stops the gene expression using double stranded, gene specific RNA (dsRNA) sequences (Figure 9). This dsRNA is then cleaved into short interfering RNAs (siRNAs) by RNase III type endonuclease called “Dicer”. These siRNAs are (about 21-25 nucleotides in length) then incorporated into a large nuclease complex known as RNAi inducing silencing complex (RISC). An enzyme within RISC cleaves mRNA targeted by siRNAs, thus initiates mRNA degradation as shown in Figure 9 (68–70).

In *C. elegans*, gene silencing can be induced by introducing siRNA or miRNA (micro RNA) through microinjection, feeding and soaking. Microinjection involves mechanical delivery of dsRNA by a needle in which dsRNA is injected directly into the gonad or the body cavity (69, 71). Soaking involves delivery of dsRNA passively through soaking worms in a solution with dsRNA. Feeding involves transcribing dsRNA into *E. coli* and ingesting by *C. elegans* (71).

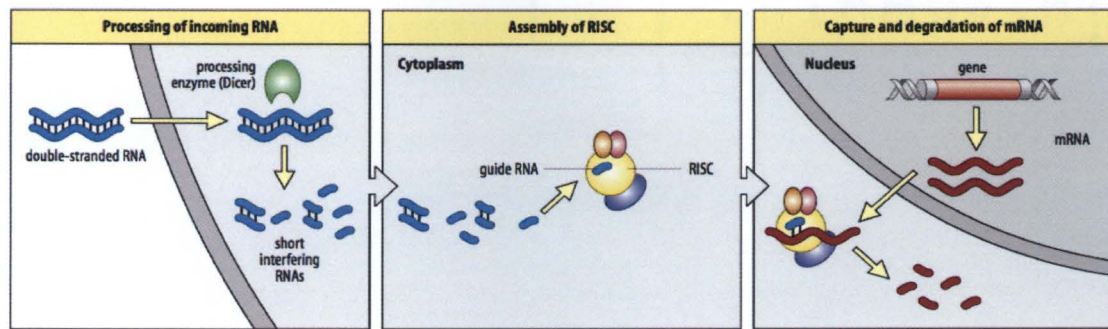


Figure 9. The mechanism of RNAi. (72)

1.4.3 Anatomy

Adult hermaphrodites have 959 somatic cells with 302 neurons while adult males have 1031 somatic cells (Figure 10) (52). The anatomy of an adult hermaphrodite is shown in Figure 10. *C. elegans* has an unsegmented, cylindrical body shape that is narrowed at the ends (57). Their body consists two concentric “tubes”: outer tube and inner tube. These tubes are separated by a fluid filled pseudocoelomic space as shown in Figure 11. The outer tube (body wall) comprises the cuticle, the hypodermis (“worm skin”), the body-wall muscles, excretory system and the nervous system (52, 57). Cuticle is a sturdy but malleable collagenous structure secreted by the underlying epithelium. Cuticle not only surrounds the outside of worm but also it lines the pharynx and rectum. There are several pores in the cuticle that open tissues to outside: excretory pore, vulva, anus, lateral lips for sensilla, and two papillae for anterior deirids. The inner tube consists digestive system with anterior pharynx which helps in grinding food followed by the intestine that extends along the body length and ends at the anal pore where waste is passed from the body. In adult hermaphrodites, the gonad is also found in the pseudocoelomic space (Figure 11E) (52).

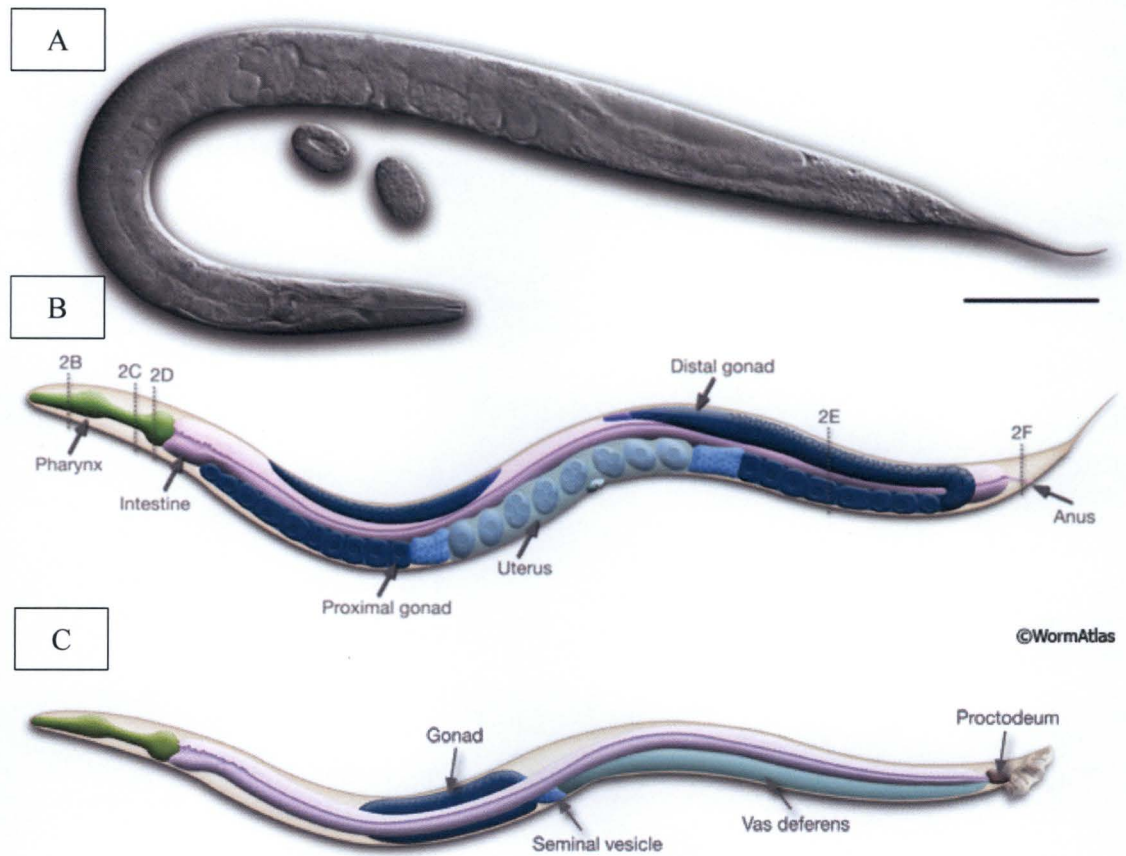


Figure 10. Anatomy of an adult hermaphrodite and male.

(A) Differential interference contrast image of an adult hermaphrodite. (B) Schematic illustration of anatomical structures of the left lateral side of an adult hermaphrodite. See Figure 11 for cross sections at the levels 2B, 2C, 2D, 2E and 2F. (C) Schematic illustration of anatomical structures of a male (57)

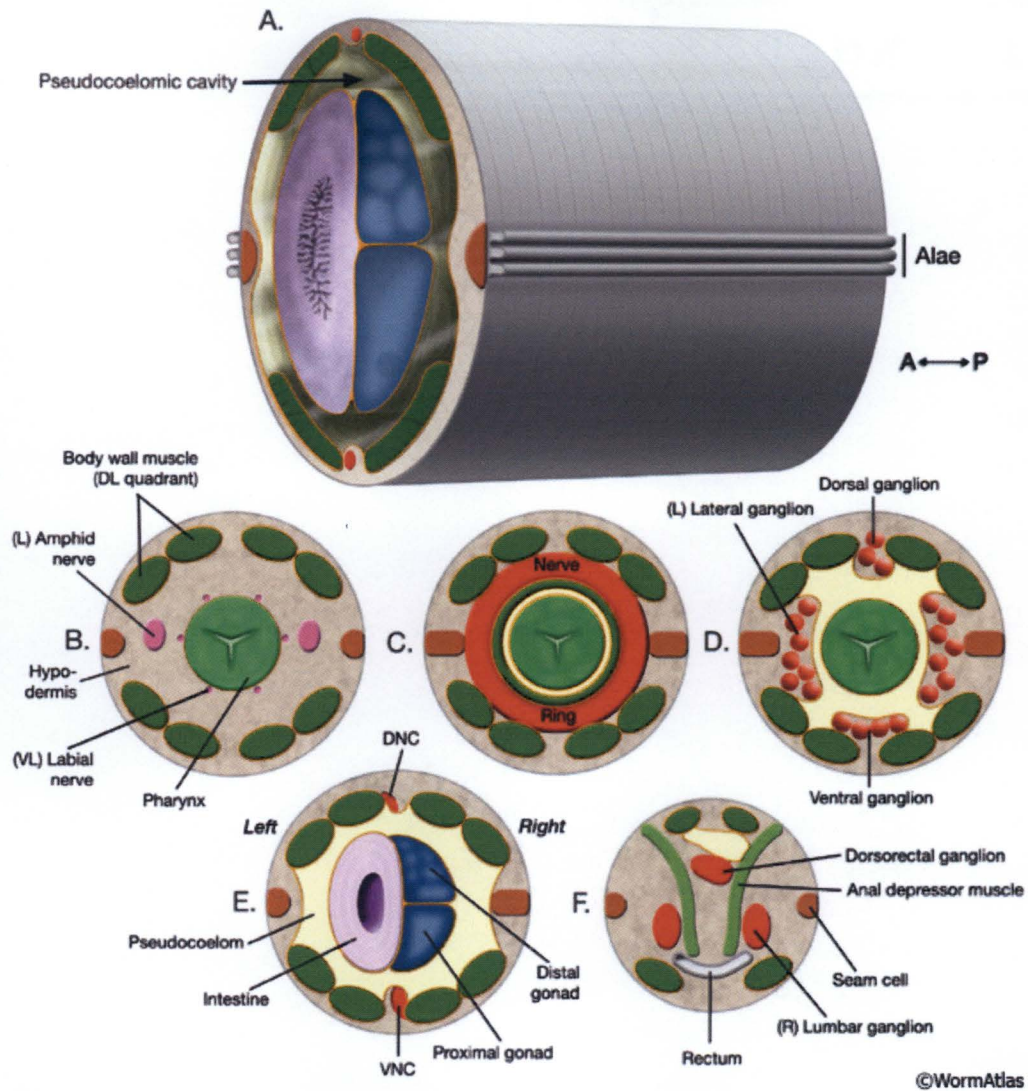


Figure 11. *C. elegans* cross sections from head to tail.

The level of each cross section is labeled in Figure 10 (2B-2F). (A) Cross-section at level 2A in Figure 10. Posterior body. (B) Cross-section at level 2B in Figure 10. Section through anterior head. (C) Cross-section at level 2C in Figure 10. Section through the middle of head. (D) Cross-section at level 2D in Figure 10. Section through posterior head. (E) Cross-section at level 2E in Figure 10. Section through posterior body. DNC, Dorsal nerve cord; VNC ventral nerve cord. (F) Cross-section at level 2F in Figure 10. Section through tail, rectum area. (57)

1.4.4 The Alimentary System

The alimentary system of an adult hermaphrodite is shown in Figure 12. The alimentary system can be divided into three sections: foregut (contains the pharynx), midgut (contains the intestine), and hindgut (contains the rectum and anus) as shown in Figure 12A. Like in higher eukaryotes, *C. elegans* alimentary system carries out several functions such as food digestion, nutrient absorption, macromolecule synthesis and storage and immune response initiation. Furthermore, the intestine also nurtures germ cells through yolk production (57). When food is consumed via mouth, pharynx pump food into the intestinal lumen, which runs through the body from the pharynx to the anus (73).

Firstly, when *C. elegans* ingest bacteria (food) through their mouth, a tube-like muscular pump known as the pharynx is involved in concentrating, grinding and transporting food to the intestine. Pharynx comprises 9 epithelial, 20 muscle, 9 marginal, 4 gland, 20 neuronal and 6 valve cells. This connects buccal cavity to the intestine (Figure 12A/B) (57, 74).

Secondly, food is transported across the intestine. *C. elegans* intestine contains 20 large epithelial cells. These cells are arranged in bilaterally symmetric pairs (ring-like) to form a long tube around a lumen (Figure 11E and 12). Intestinal lumen is not is firmly associated with the body wall, but tightly attached to the pharyngeal and rectal valves at either end. Two intestinal cells are sealed through adherens junctions (Figure 12D). These cells contain several microvilli extending into the lumen forming a brush border (57, 75).

The main function of intestinal cells is to secrete digestive enzymes into the lumen and absorb processed nutrients. These cells contain assorted storage granules, therefore,

act as storage units. In hermaphrodites, the intestinal cells synthesize and secrete yolk material into the body cavity (57, 75). Then gonads take up the yolk from the body cavity and transport to the oocytes (76). Yolk material contain essential nutrients such as vitellogenin proteins and phospholipids, support embryonic development (77, 78). Nutrients may also be transported out into non-intestinal cells (57, 75).

Thirdly, after absorption food through the intestine food is transported into hindgut for excretion. Hindgut contains rectal valve, rectal gland and rectal muscles. Rectal valve that connects the gut to the rectum and anus in order to excrete intestinal waste to outside. There are three rectal glands that may secrete digestive enzymes. There are four specialized rectal muscles in the hindgut that are innervated by motor neurons to generate contractions in order defecate (57, 79).

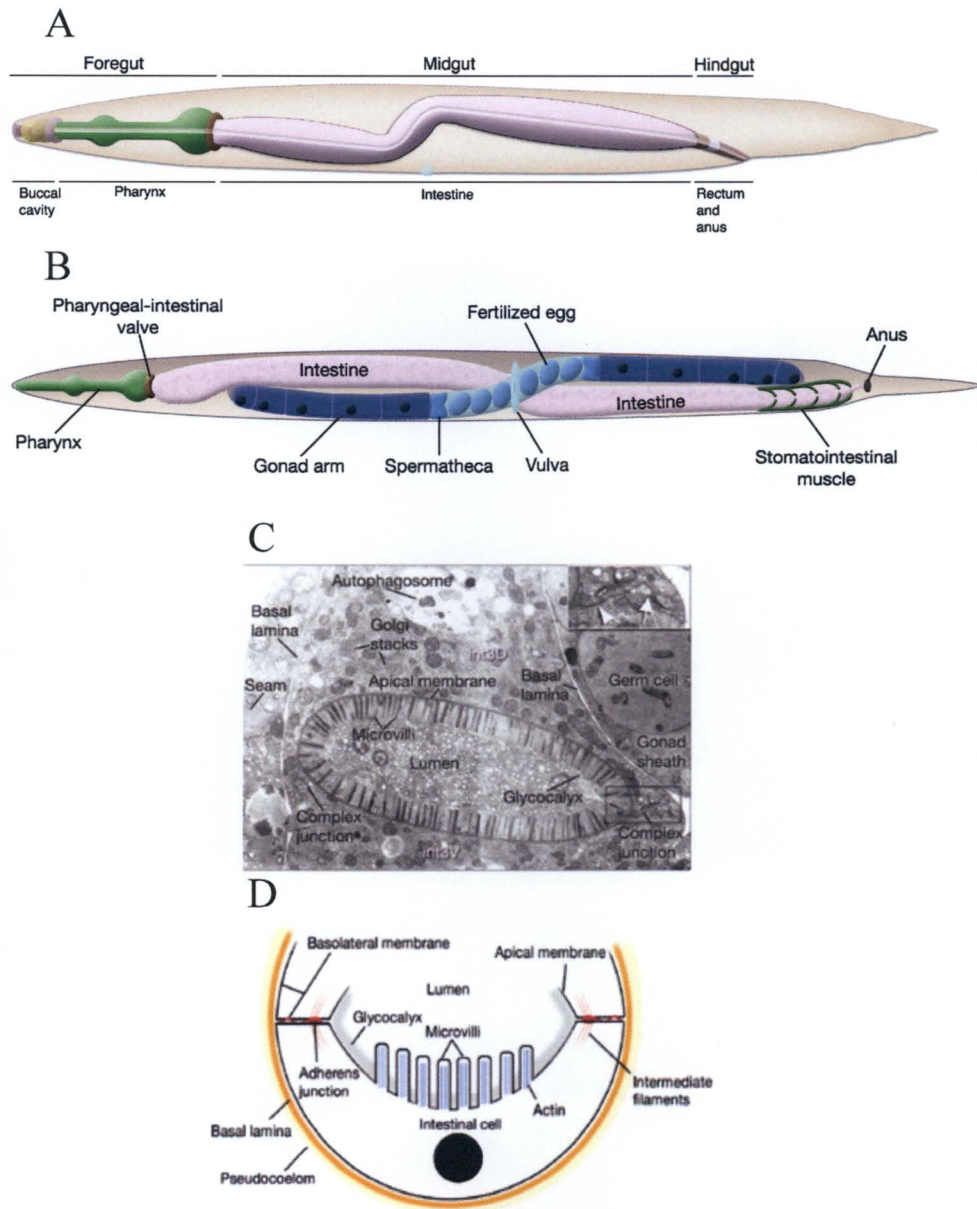


Figure 12. The intestine of an adult hermaphrodite.

(A) Schematic illustration the alimentary system (B) Schematic illustration of intestinal anatomical structures. Ventral view. (C) Magnified transverse TEM image of the intestinal lumen. Complex junctions to next to an adherens junction seal two intestinal cells. (D) Diagram of an intestinal cell cross section showing microvilli. (57)

1.4.5 Development and Life Cycle

The *C. elegans* has a rapid life cycle as shown in Figure 13 and starts with the embryonic stage. The embryonic development can be allocated into two stages: proliferation and organogenesis. During proliferation, a single cell is divided into ~550 undifferentiated cells. Embryo is released to the environment through vulva opening when the embryo is 28–30 cells and then embryonic development is completed outside the hermaphrodite (52, 80). At the end of proliferation, cells are arranged into three germ layers: ectoderm, mesoderm and endoderm. Ectoderm produces hypodermis and neurons; mesoderm gives rise to pharynx and muscle whereas endoderm generates germline and intestine. During organogenesis, cells are terminally differentiated without further cell division and embryo extends its length to form as an animal with fully differentiated tissues and organs. At the end of embryonic development, embryos are capable of pharyngeal pumping and have the general body plan which does not alter during postembryonic development (80).

After hatching, feeding through pharyngeal pumping stimulates postembryonic development, in which under favorable conditions, *C. elegans* go through four larval stages (named L1, L2, L3 and L4) followed by adulthood as shown in Figure 12. During the larval stages cells further divide and animals substantially grow (81). At the end of each larval stage worms molt, in which the collagen cuticle is shed and replaced by newly synthesized cuticle. This allows cuticle to accommodate body growth (80). Additionally, during larval stages, blast cells divide, sexually dimorphic characteristics such as the hermaphrodite vulva and male tail arise (52).

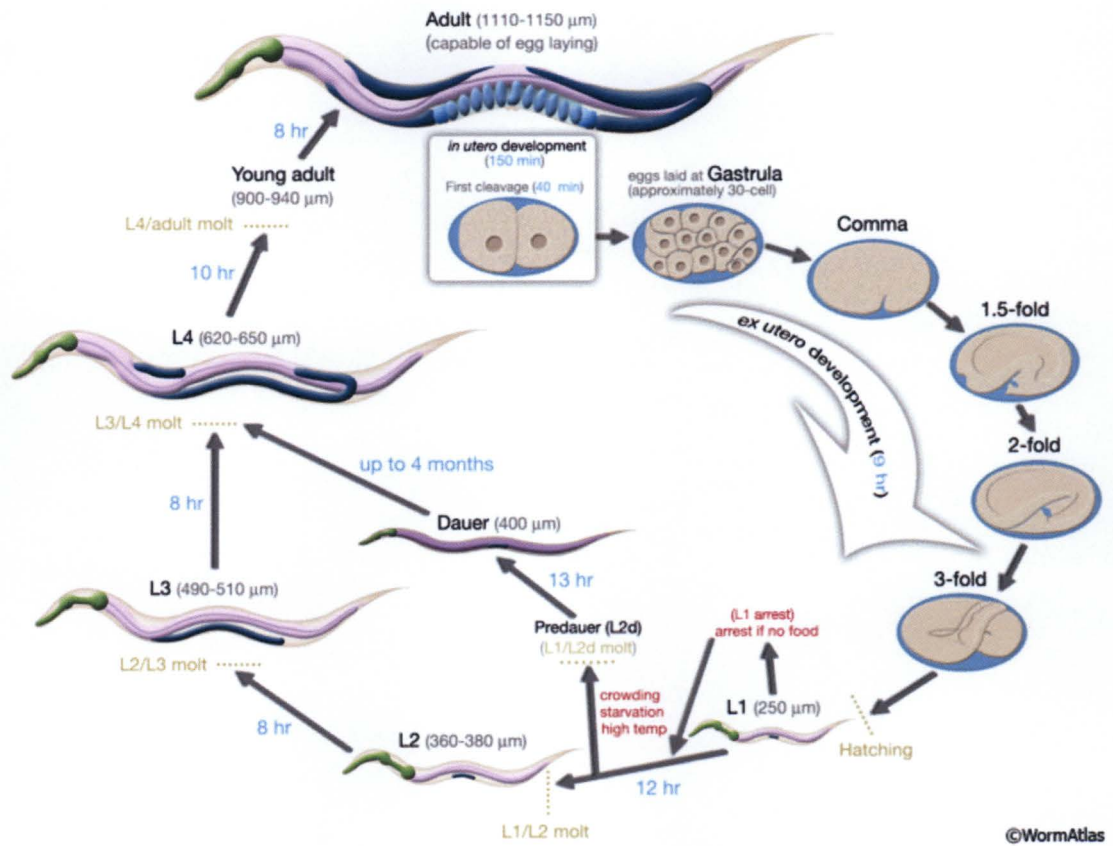


Figure 13. Life cycle of *C. elegans* at 22 °C.

Life cycle from egg through four larval stages (L1-L4) to egg laying adult (57, 80).

However, if *C. elegans* encounter unfavorable conditions for growth such as high temperature, limited food or high population density, L1 larva will arrest in development and progress into an alternative third stage, known as the Dauer stage. Dauer means “to endure” in German. This stage plays an essential role in long-term survival and *C. elegans* can remain in Dauer state for up to 4 months, as they have high lipid stores (stored in intestinal and skin-like epidermal cells), are non-feeding and highly resistant to stress (52, 82–84). If conditions improve, worms exit the Dauer stage and develop into adulthood as normal. Post-Dauer stage lifespan is not affected by Dauer stage, therefore, considered as non-ageing (80, 85).

C. elegans develop from egg to egg laying adult in ~3 days at 22°C. The average brood size of *C. elegans* is ~ 300. Recently, Pickett *et al* (86) have shown that the brood size can vary with the mode of fertilization. When a hermaphrodite was self-fertilized, the progeny size was ~330 with a reproductive span of ~5 days. When a hermaphrodite was mated with males, the progeny size increased to ~710 with a reproductive span of ~9 days (86).

Under standard laboratory conditions, the average lifespan is ~2-3 weeks. Reproduction rate decreases after the initial 3-5 days of adulthood. As aging progresses, movement declines, neuronal signaling decreases, muscles cell breakdown and mechanical defense ability deteriorates (87). The lifespan can be influenced by several factors: temperature, oxygen and diet. For example, previous study (88) showed that mean life span at 16 °C was ~ 23 days while 9 days at 25 °C. In addition, *C. elegans* cultured in media with high levels of oxygen showed reduced life span and extended life span at low levels

of oxygen (89). Furthermore, inducing caloric restriction by growing *C. elegans* in liquid media with a low concentration of bacteria increased life span by ~50% (88, 90).

The overall goal of our lab is to understand the catalytic mechanisms and cellular signaling properties of GCPII. The goal this project is to characterize the functions of cGCPII in *C. elegans*. As mentioned in the Section 1.3.5, cGCPII shares high structural similarity which indicates that it is likely to have similar functions. This encouraged us to use *C. elegans*, as a powerful model organism to explore structure-function relationships, hydrolytic mechanisms, cellular signaling properties, GCPII function and associated diseases to extrapolate findings to humans.

Chapter 2: Investigation of the Biological Significance of GCPII in *C. elegans*

2.1 General Introduction

In this chapter, I intend to characterize the biological functions of cGCPII and provide a comparative analysis of the phenotypes of *C. elegans gcp-2* gene and its paralogs (*gcp-2.1*, *gcp-2.2* and *gcp-2.3*). This will provide a deeper understating of the role of cGCPII in reproductive, developmental and physiological characteristics of *C. elegans*

2.2 Hypothesis and Objectives

The hypothesis that governs this study is that cGCPII plays an essential role in reproduction, ageing and development of *C. elegans*. The objectives of this study were to:

1. Establish the role or identify the effect of cGCPII in *C. elegans* reproduction
2. Establish the role or identify the effect of cGCPII in *C. elegans* lifespan
3. Establish the role or identify the effect of cGCPII in *C. elegans* development
4. Establish the role or identify the effect of each *gcp-2* paralog in *C. elegans* reproduction, lifespan and development
5. The investigate the effect of complete cGCPII knock-down by RNAi

2.3 Materials and Methods

2.3.1 *C. elegans* and *E. coli* Strains

Five *C. elegans* strains used in this study were: N2, RB1055, TM6632, TM5414 and TM5710 is shown in the Table 3. The N2 and RB1055 were obtained from the Caenorhabditis Genetics Center; and TM6632, TM5414 and TM5710 were obtained from the National Bio-Resource Project.

Table 3. *C. elegans* and *E. coli* strains used in this study.

Strain	Genotype	Origin ^d	Mutation site ^e	Reference
N2	Wild-type	CGC	NA	(91)
RB1055	<i>gcp-2.1</i> mutant (<i>ok1004</i>) ^c	CGC	Outer Left Sequence: GACCCCAACCAATATCATG C. Outer Right Sequence: TGGATACGTGTCCCATGTT G. Inner Left Sequence: CGTTTCGGTTTCAAAGTGG T. Inner Right Sequence: TGAAGTTGATCACCGGAAC A. Deletion size: 1523 bp.	(92)
TM6632 ^a (FX06632) ^b	<i>gcp-2.2</i> mutant (C35C5.2)	NBRP	10442/10443- CAAGGTACATACAA- 10875/10876 (433 bp deletion and 14 bp insertion)	(93)
TM5414 (FX05414)	<i>gcp-2.3</i> mutant (C35C5.11)	NBRP	13527/13528-13873/13874 (346 bp deletion)	(93)
TM5710 (FX05710)	<i>gcp-2.3</i> mutant (C35C5.11)	NBRP	13913/13914-TCA-14311/14312 (398 bp deletion and 3 bp insertion)	(93)

<i>E. coli</i>	uracil	CGC	NA	(94)
OP50	auxotroph			
^a <i>C. elegans</i> allele name ^b <i>C. elegans</i> strain name ^c Sequence name ^d CGC, Caenorhabditis Genetics Center, University of Minnesota; NBRP, National Bio-Resource Project, Japan ^e In chromosome X; NA, Not Applicable; bp, base pair				

2.3.2 Preparation of Nematode Growth Media (NGM)

Bacterial Food Source

C. elegans are typically fed on *E. coli* strain OP50 in the laboratory. This bacterial strain is an uracil auxotroph (i.e. impaired uracil biosynthetic pathway), therefore, the growth in NGM plates is restricted (56). Stock culture of *E. coli* strain OP50 was stored in -80 °C. A frozen (-80 °C) stock of 50 µL OP50 Bacteria was used for the inoculation of into 100 mL Luria Bertani (LB) broth (Fisher BioReagents). Then the culture was incubated overnight at 35 °C and 250 rpm using an incubating orbital shaker (New Brunswick Scientific E24). Bacterial pellet was obtained by centrifuging (Thermo Scientific Sorvall ST8R) at 3500 rpm for 5 minutes. The bacterial pellet was weighed, and sterile water was added to normalize the bacterial cell concentration to 200 mg/mL.

LB broth was prepared by adding 25 g LB powder (Casein Peptone 10 g/L, Yeast extract 5 g/L, Sodium Chloride 10 g/L) into 1 L Millipore water. The media was sterilized by autoclaving at 120 °C for 45 min.

Preparation of NGM Plates

NGM plates was prepared as described (56) with slight modifications. Briefly, for 1 L NGM medium, 3 g NaCl (Fisher), 2.5 g bacto-peptone (BD™ Difco™), 17 g technical agar (BD™ Difco™) and 975 mL Millipore water were mixed with a magnetic stir bar until the solution is uniform. This mixture was sterilized by autoclaving at 120 °C for 45 min (Tuttnauer 2540 EP). Media was cooled down to ~55 °C using a water bath (Fisher Scientific Isotemp 205). Once NGM reached ~55 °C, 25 mL 1 M potassium phosphate Buffer (pH 6.0), 1 mL 1M CaCl₂, 1 mL 1 M MgSO₄, 1 mL 5 mg/mL cholesterol (in

ethanol), 100 mg/mL streptomycin and 1 mL 10 mg/mL nystatin was added and swirled to mix. 5 mL of the NGM solution was aseptically dispensed into petri dishes (60 x 15 mm) (Fisherbrand™) using a peristaltic pump (Drummond Scientific) in a sterile hood. Once medium solidified then the plates were stored at 4 °C in inverted position to preserve moisture until seeded with OP50. Preparation of stock solutions and liquid growth medium used in experiments are given in the Appendix 1.

Seeding Plates with *E. coli* OP50

100 µL of 200 mg/ml *E. coli* OP50 culture was pipetted onto the center of solidified NGM plates and swirled plates gently to spread out bacteria culture to cover ~1-inch diameter circle under sterile conditions.

2.3.3 *C. elegans* Strain Maintenance

General Maintenance

All strains of *C. elegans* were maintained on NGM plates seeded with *E. coli* OP50 in order to ensure that they were available for research when necessary. In order to maintain a healthy population, worms were transferred onto new plates every two weeks. This can be done by several methods. The quickest and most convenient method is "chunking" and mostly used during this study. Chunking involves cutting off an agar section (~0.5 cm²) with abundant worms using a sterile spatula and placing onto a new seeded plate. The spatula was sterilized by passing through flame of the ethanol burner and allowed to cool down before transferring. The other method is picking single worms with a worm picker and transferring to new seeded NGM plates. The worm picker was sterilized by passing through flame of the ethanol burner and allowed to cool down before transferring. Worm

were maintained at 20 °C in an incubator at all times. Worms can be maintained at room temperature but that produce slightly different brood size.

The worm picker was made by mounting a ~1.5-inch platinum wire into the tip of a glass Pasteur pipette. In order to ensure that wire is attached to the pipette, tip was heated by the Bunsen burner. The end of the wire was slightly bended making it easy to pick them.

Preparation of frozen *C. elegans* Stocks

Frozen stocks of *C. elegans* can be stored at -80 °C. First worms were grown for 4 days in 10 cm NGM plates with 500 µL bacteria at 20 °C. Washed worms off the plates by adding 10 mL M-9 solution. Worms and M-9 was collected by a Pasteur pipette into a 15 mL conical tube, centrifuged at 2000 rpm for 1 min to pellet worms. Much of the supernatant was aspirated without disturbing the pellet, 10 mL M-9 solution was added and resuspended the pellet. Repeated centrifugation – wash cycle twice to ensure there is no bacteria. To the final aspirated step ~ 3 mL M9 supernatant containing worm was as mixed with equal amount of freezing solution (see Appendix 1). Resuspended the pellet and transferred 1 mL of the solution (worms) to 1.5 mL sterile microfuge tubes. The tubes with worms were froze with liquid nitrogen prior to storage at -80 °C.

It is essential to ensure that plates are ready for successful preparation of stocks. Well-fed worms, adults, eggs and Dauers do not survive well. Worms are ready to freeze if: (i) there is little or no food (just starved), (ii) plenty of worms at L1-L2 stages, (iii) some eggs on the plate and no signs of contamination. If worms starved too long and enter to Dauer stage, then these worms will not survive the freeze process. Therefore, the plate needs to have some eggs, which indicate that the plate has not been without food for a long

time. The worms at early larval (L1-L2) stages will only survive after freezing, hence, it is essential to have plenty of L1-L2s. If the plates are contaminated with other bacteria, then the worms will continue to eat and grow, thus there will be no stalling at the L1 stage.

2.3.4 Preparation of Age Synchronized Population of *C. elegans*

This is also known as the worm bleaching protocol. This method was used to obtain eggs from gravid (egg carrying) adults. In addition, this protocol was used in events of contamination, as the eggs are free from *E. coli*. Worms were grown for 3 days and 5 plates per strain per treatment were used for each experiment. Plates are ready to bleach if: (i) there are plenty of eggs and egg laying adults, (ii) there is sufficient food and not starved.

Age-synchronized worms were obtained as previously described with slight modification (95). Synchronized eggs in M9 buffer in a 50 mL conical tube was incubated overnight at the room temperature with gentle rocking (rocker type). Then 200 μ L of L1 larvae in M-9 solution was transferred to seeded NGM plates and placed at 20 °C. If controlled number of worms required, then multiple 10 μ L solution was used to count the worms under microscope and the stock solution is either diluted or concentrated (by pelleting and adding fresh M9) to obtained desired number of worms per milliliter volume.

2.3.5 Brood Size Assay

Brood size was determined by counting the total number progeny from a single hermaphrodite, as described before (96) using 10 worms per strain. Two replicates were performed for each experiment. Before counting worms, petri dishes containing progenies were stored at the 4 °C for at least 30 minutes to inhibit movement to accurately count the

worms as the worms constantly move across the petri dish if counted at room temperature. Additionally, drawing a grid on the bottom of petri dish allows counting the number of worms in each small square, making it easier to keep track of which worms were already counted. Statistical Analysis was conducted using two-sample t-test assuming equal variances. p value < 0.001 considered significant. Error bars represent \pm standard error of mean (SEM).

2.3.6 Longevity Assay in Solid Media

5-fluoro-2'-deoxyuridine-5'-phosphate (FuDR) containing NGM plates were prepared by adding 33 μ L of 150 mM FuDR stock to 100 mL NGM media that has been autoclaved, cooled down to 55 °C, mixed well and poured. After overnight hatching of a synchronized worm population, L1 worms were transferred onto seeded NGM plates. These plates were incubated at 20 °C and allowed worms to grow for 24 hrs. Then 10 worms were transferred onto each seeded FuDR containing NGM plates and return to 20 °C. The worms were transferred to a new plate every 5 days to prevent the bacteria from being depleted. The number of worms alive were recorded every 2 days. Dead worms were confirmed by gently tapping the worm's head with platinum worm transfer pick. The worms that failed to respond by moving its head considered as dead and removed from the plate. Two replicates were performed for each experiment.

2.3.7 Longevity Assay in Liquid Media

The longevity assay in liquid media was determined the number of worms alive every 2 days, as described before (97).

2.3.8 Body Length Measurement

After overnight hatching of a synchronized worm population, L1 worms were transferred onto seeded NGM plates. After 48 hours of incubation at 20 °C, L4 worms were mounted on 2% agarose pads and paralyzed with a drop of 1 mM levamisole and examined with a dissecting microscope (Olympus Model LMS-225R Microscope.). The body length measurement procedure is shown in Figure 14. Measurements were made from 10 worms per strain. Two replicates were performed for each experiment. Statistical Analysis was conducted using two-sample t-test assuming equal variances. p value < 0.001 considered significant. Error bars represent \pm SEM.

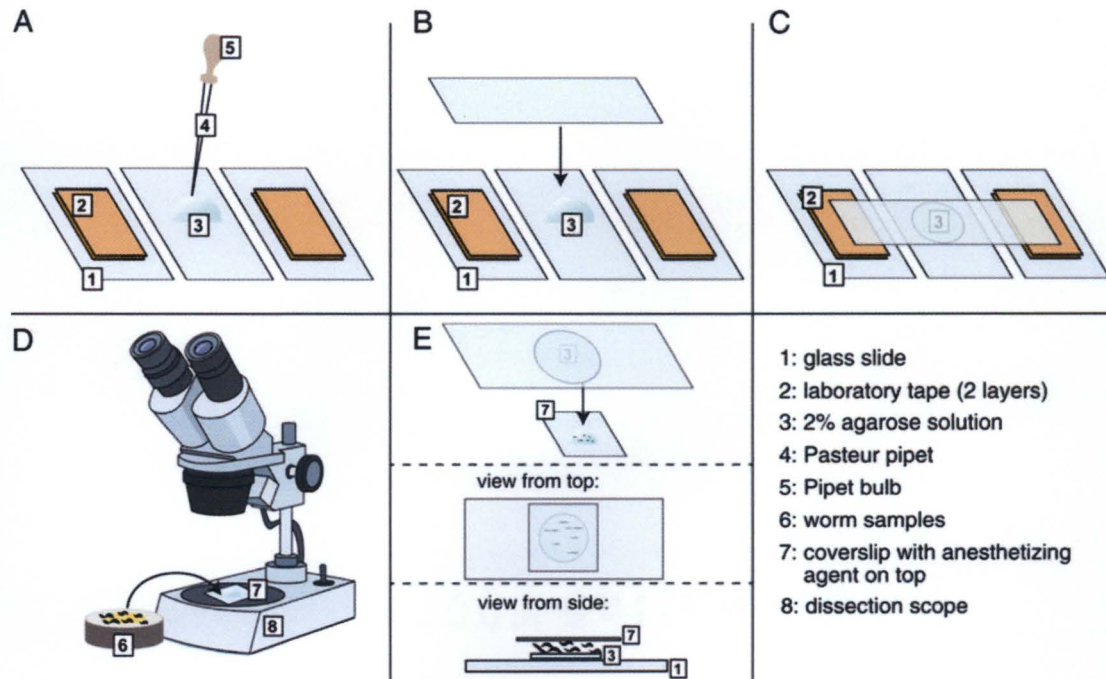


Figure 14. Body length measurement steps (98).

A drop of 1 mM levamisole used as the anesthetizing agent.

2.3.9 Investigation of the Effect of RNAi

RNAi Feeding Vector

The feeding method of RNAi based gene silencing experiment was followed to study the expression of *gcp-2* genes in *C. elegans*. *C. elegans* RNAi feeding vectors were purchased from Addgene (<https://www.addgene.org/1654/>). These vectors contained *gcp-2* genes cloned into the Timmons and Fire feeding plasmid vector (L4440) (Figure 15). The plasmid L4440 backbone vector was converted by inserting *gcp-2* gene-specific DNA fragments between inverted T7 promoter sites (Figure 16). The backbone of L4440 plasmid is 2790 bp and ampicillin resistant (99, 100). Four RNAi harboring bacterial strains were obtained as gift from the University of Texas Health Science Center at Houston: *gcp-2.1* - strain 1A03; *gcp-2.2* - strain 5D09; *gcp-2.3* - strain 8D23; Vector Control (contains only the backbone L4440).

RNAi Feeding Strain

L4440 constructs for *gcp-2.1*, *gcp-2.2* and *gcp-2.3* were transformed into an RNaseIII-deficient *E. coli* strain HT115 (DE3). This strain is also referred to as RNAi feeding strain. HT115 was engineered to express T7 RNA polymerase under an isopropyl- β -D-thiogalactopyranoside- (IPTG-) inducible *lac* promoter (99). In other words, when IPTG is added to HT115 cells, T7 RNA polymerase is expressed resulting in the transcription of the inserted *gcp-2* genes.

The genotype of *E. coli* strain HT115 is as follows: F-, *mcrA*, *mcrB*, IN(*rrnD*-*rrnE*)1, λ -, *rnc14::Tn10*(DE3 lysogen: *lavUV5* promoter -T7 polymerase) (IPTG-inducible T7 polymerase) (RNase III minus) (99).

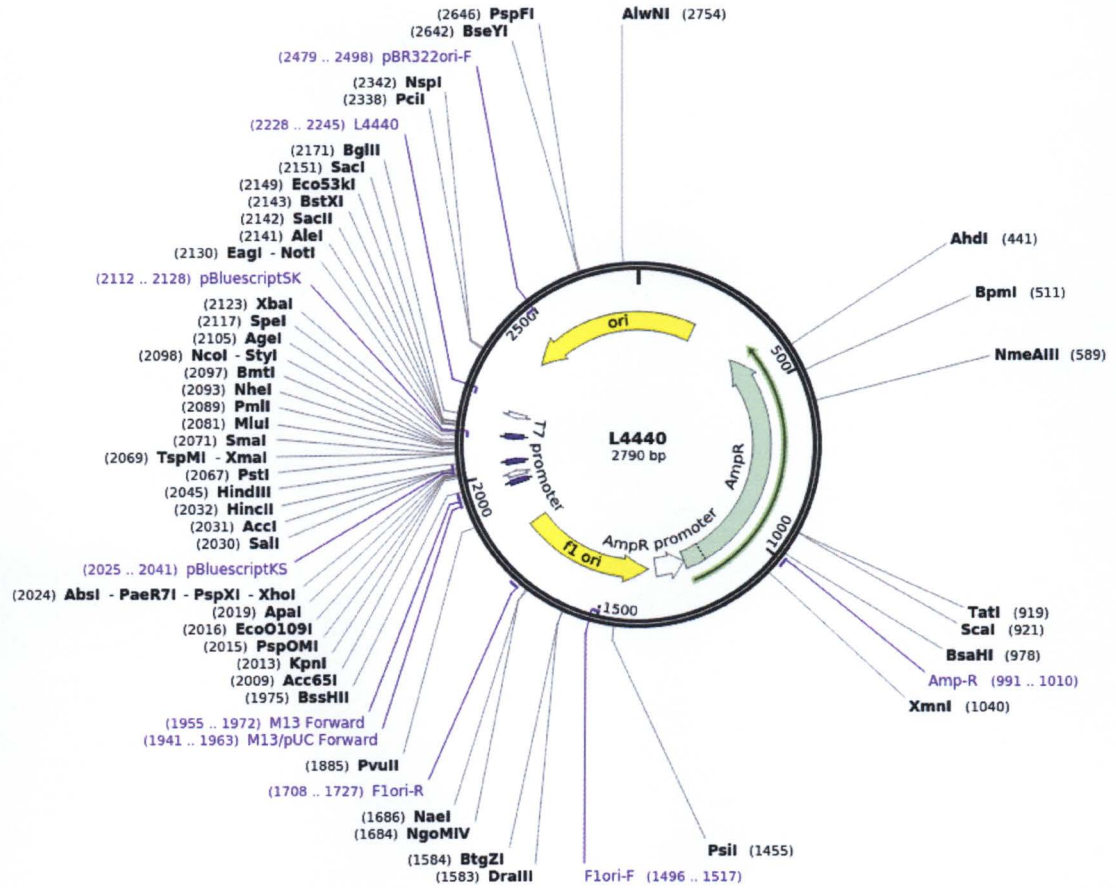


Figure 15. Full Sequence Map of L4440 RNAi Feeding Vector (100).

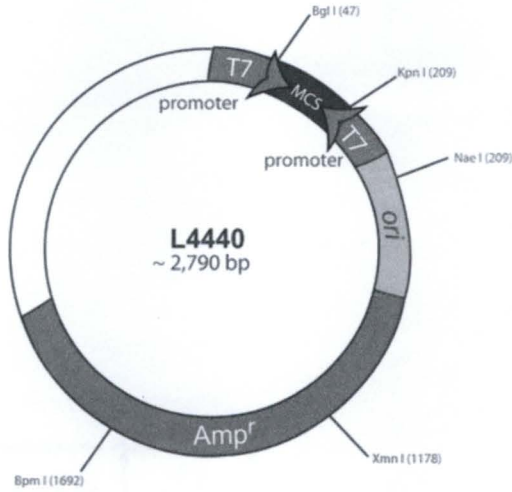


Figure 16. The Map of L4440 RNAi Feeding Vector (100).

Verification of RNAi Feeding Stains

Plasmid Isolation: Plasmids were isolated from all four RNAi plasmid harboring bacteria using IBI Scientific Plasmid Extraction Kit. Followed manufactures guidelines (101). Briefly, **Harvesting Step:** transferred 1.5 ml of cultured RNAi harboring bacterial cells to a microcentrifuge tube and centrifuge (Thermo Sorvall Legend Micro 17) at 14000 rpm for 1 minute then discarded the supernatant. **Re-Suspension Step:** Added 200 μ l of PD1 Buffer to the tube and re-suspended the cell pellet by vortex (Thermolyne). **Lysis Step:** Added 200 μ l of PD2 Buffer and mix by inverting the tube \sim 10 times. Then left it at room temperature 2 minutes. **Neutralization Step:** Added 300 μ l of PD3 Buffer and mixed by inverting the tubes for \sim 10 times. Centrifuged at 14000 rpm for 3 minutes. **DNA Binding Step:** Placed a PD Column in a 2 ml collection tube and the supernatant from the neutralization step was added. Centrifuged at 14000 rpm for 30 seconds and discarded the flow-through. Placed the PD Column back in the 2 ml collection tube. **Sequencing Step:** Added 400 μ L of W1 buffer into the PD Column. Centrifuged at 14000 rpm for 30 seconds then discarded the flow-through and place the PD Column back in the 2 ml collection tube. **Wash Step:** Added 600 μ l of Wash Buffer (with ethanol) into the PD Column then centrifuged at 14000 rpm for 30 seconds and discarded the flow through. Placed the PD Column back in the 2 ml collection tube. Centrifuged at 14000 rpm for 3 minutes to dry the column matrix. Placed the PD Column in a new 1.5 ml microcentrifuge tube. **DNA Elution Step:** Added 50 μ l of Elution Buffer into the center of the PD Column matrix. Left it for 2 minutes to allow the Elution Buffer to be completely absorbed. Centrifuged at 14000 rpm for 2 minutes to elute the purified DNA. Repeated the elution step.

Gel Electrophoresis: In order to confirm the plasmid isolation Gel Electrophoresis was used. Prepared 0.8% agarose gel by adding 0.4 g of agarose (Fisher) to 50 mL 1X Tris-acetate-EDTA (TAE) buffer. Microwaved for ~1 min until agarose melts and allowed to cool down 5 mins. Then added 4 μ L ethidium bromide, poured to gel plate and allowed to solidify for 20 mins. Wells were loaded with extracted plasmids for each strain: *gcp-2.1*-strain 1A03; *gcp-2.2*- strain 5D09; *gcp-2.3*-strain 8D23; and vector control. Connected to the electrophoresis unit set to ~100-110 V until the dye line is approximately 80% of the way down the gel. This took around 1.5 hours.

Restriction Digestion: Added 1 μ L of enzymes: SacI HF (Bio-Rad) or Hind II lambda (NEB) was added to 5 μ L of 10X NEB Buffer, 5 μ L of Extracted Plasmid and 39 μ L of nuclease free water. Incubated in water bath set to 37 °C for 2 hours. Prepared the agarose gel as mentioned in above. Loaded the wells with 10 μ L digested plasmids and 10 μ L of EZ Load 100 bp Molecular Ruler (Bio-Rad). For storage, enzymes in digested plasmid samples were inactivated by 60 °C heat for 20 mins. Stored at -20 °C. SacI HF recognition site is GAGCTC and Hind II recognition site is GTCGAC as shown in Figure 16 (102).

Gene – Specific RNAi Primers: RNAi primers specific for *gcp-2.1*, *gcp-2.2* and *gcp-2.3* were obtained from the University of Texas Health Science Center at Houston and given in the Table 4.

Table 4. The Gene-Pairs primer sequences (99, 103)				
Strain	Primer sequences		Product (bases)	cDNA Length
	Left	Right		
<i>gcp-2.1</i> (R57.1)	ctcgctcgagtgaaatcatactt	aaaacctcaataaacatcacg	1630	2256
<i>gcp-2.2</i> (C35C5.2)	gtggccggaacagaaaataa	actgtttggatcaacagccc	1165	-
<i>gcp-2.2</i> (C35C5.1)	ttgaattttctgccgagctt	ttcctgctcgtcttgtttcc	1173	-

RNAi Plasmid Sequencing

RNAi plasmids sequencing was used to determine the proper insertion of the *gcp-2* gene into the L4440 vector and to verify *gcp-2.1*, *gcp-2.2* and *gcp-2.3* gene sequence using the RNAi primers obtained from the University of Texas Health Science Center at Houston as mentioned before. DNA sequencing was performed at the Core Sequencing Facility at the University of Illinois at Urbana-Champaign.

Data analysis was done using the sequence nucleotide alignment tool “BLAST engine” provided by NCBI, which produces the alignment of two given sequences. (visit: https://blast.ncbi.nlm.nih.gov/Blast.cgi?PAGE_TYPE=BlastSearch&BLAST_SPEC=blast2seq&LINK_LOC=align2seq).

RNAi Feeding Protocol

NGM Feeding Plates: NGM agar plates were prepared as mentioned earlier with slight modifications. When the autoclaved media was cool down to ~55 °C, 1 mM IPTG (final concentration) and 25 µg/ml Carbenicillin (final concentration) was added but neither nystatin nor streptomycin was added, to reduce the possibility of these compounds interfering with the efficacy of RNAi. Poured plates 5 days before the experiment and dried at room temperature. It is important that the plates are dried well as if the plates are too wet, the bacteria may not dry well after seeding and RNAi phenotypes can be weaker (99).

Bacterial Feeding Culture: Frozen –80 °C stock feeding strains that contained the desired construct **were** Streaked onto LB agar plates containing 50 µg/mL tetracycline. Streaked plates were incubated at 37 °C overnight to grow feeding bacterial strains. Tetracycline will select for feeding competent bacteria (104). A bacterial colony was picked from the streaked plates with a sterile inoculating loop using sterile technique and placed in 2 mL of LB broth with 50 µg/mL ampicillin. Incubated overnight at 37 °C and 250 rpm using the orbital shaker. Ampicillin will select for the cloned gene of interest (104). Did not add tetracycline as inclusion of it during feeding can reduce the efficiency of RNAi (71, 99). Repeated the previous step in order to get rid of any tetracycline by inoculating 20 µL of bacterial culture to 2 mL of LB broth with 50 µg/mL ampicillin and incubated for 3 h at 37 °C and 250 rpm until the optical density is between 0.35 and 0.40. Seeded 100 µL of culture onto NGM agar plates with Carbenicillin and IPTG (above) and induced overnight. IPTG should only be added to the NGM plates as addition of IPTG to overnight culture can reduce efficacy for RNAi (99).

Transferring *C. elegans* to RNAi Plates: On the following day, transferred an L4 hermaphrodite onto the first RNAi plate. In order to minimize the amount of *E. coli* OP50 being transferred, worms were washed with M9 buffer prior to transferring onto RNAi plates. Plates (with worms) were incubated at 20 °C for 72 hours for RNAi to take effect. Then transferred adults onto another plate. After 24 hours, removed the adults. Transferred worms every 24 hours and after three transfers, *C. elegans* progeny were used for brood size and longevity assay.

2.4 Results

2.4.1 Establish the role of GCPII in *C. elegans* reproduction

In order to determine the effect of cGCPII in *C. elegans* reproduction, the brood size assay was conducted in wild-type and *gcp-2* mutants as shown in Figure 17. Quantification of reproduction was measured by the brood size. The data of this experiment was representative of two biological replicates of five animals each. Data showed that the progeny size of *gcp-2* mutants were decreased compared the wild-type ($P < 0.001$). The average brood size of wild-type was 283.1 whereas *gcp-2.1* mutant, 242.5 ($p= 1.3471E-06$); *gcp-2.2* mutant, 238.6 ($p= 3.24641E-06$); *gcp-2.3* mutant, 249.8 ($p=0.000106744$). Therefore, *gcp-2.1* mutants showed 14.3% and *gcp-2.2* mutants showed 15.7 % decline in brood size when compared with the wild-type hermaphrodites. However, *gcp-2.3* mutants showed relatively lower reduction in progeny size compared to other two mutants, which is a 11.7% drop compared to the wild-type *C. elegans*. Hence, data indicate that the reproduction in *C. elegans* is partially affected by absence of *gcp-2* paralogs, but not

completely. Furthermore, it appears that *gcp-2* paralogs affect reproduction in *C. elegans* at different levels.

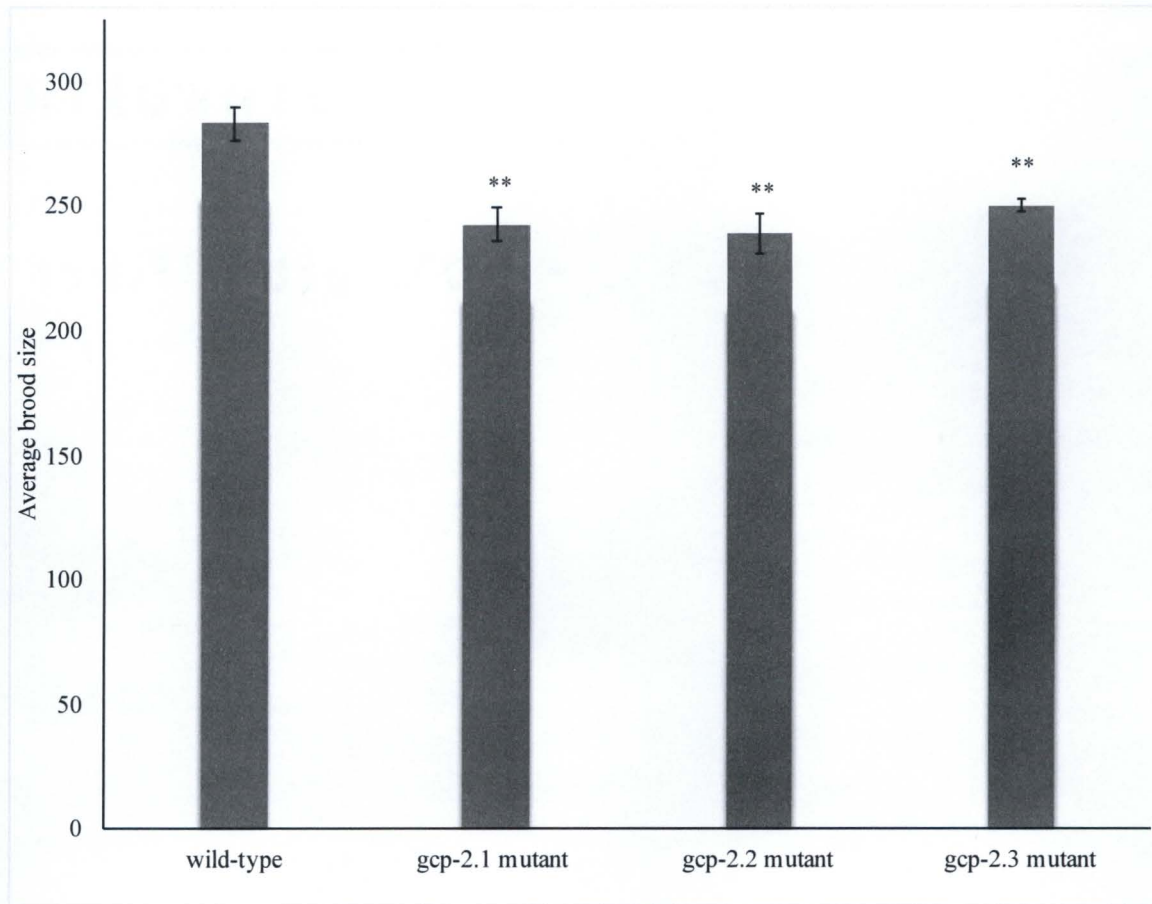
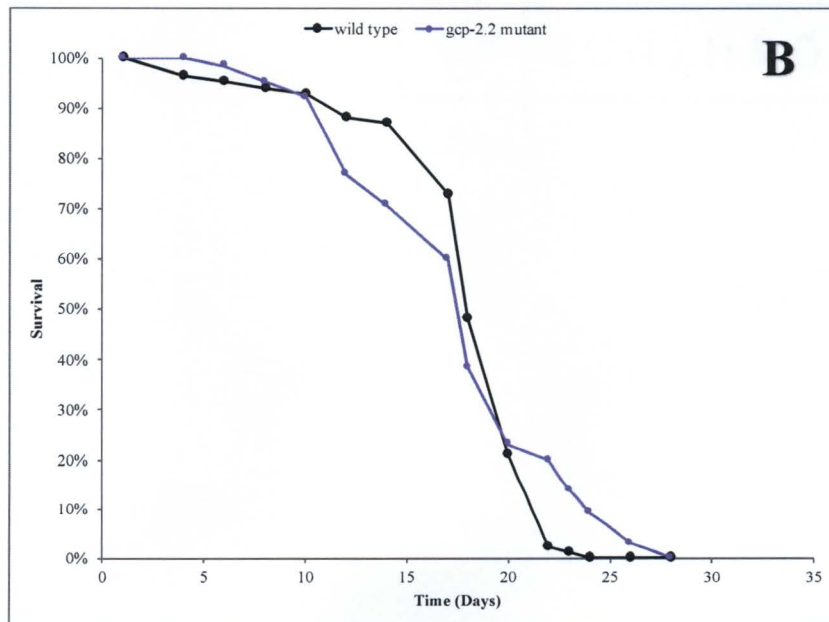
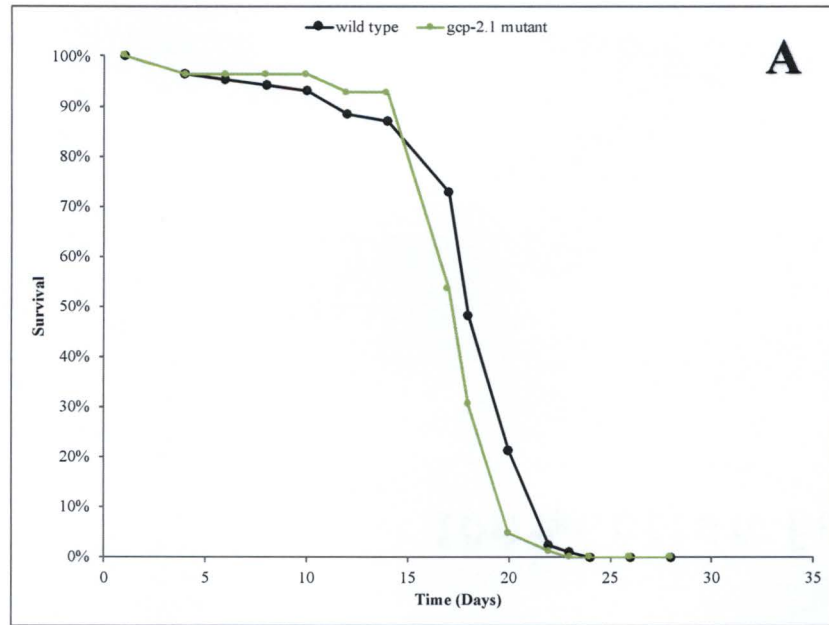


Figure 17. The brood size of wild-type (N2) and *gcp-2* mutants.

Mean brood size of wild-type (N2), 283.1; *gcp-2.1* mutant, 242.5 ($p= 1.3471E-06$); *gcp-2.2* mutant, 238.6 ($p= 3.24641E-06$); *gcp-2.3* mutant, 249.8 ($p=0.000106744$). Statistical significance was determined using two sample T-test ($*p > 0.001$, $**p < 0.001$). $**p < 0.001$ considered significant. The error bars represent \pm standard deviation. Data shown are of two biological replicates of five animals each.

2.4.2 Establish the role of GCPII in *C. elegans* aging

In order to determine the effect of GCPII in *C. elegans* aging, the longevity assay was conducted in wild-type and *gcp-2* mutants. Quantification of the aging was measured by the longevity and shown in Figure 18. The data of this experiment was representative of two biological replicates of five animals each. Data showed that the lifespans of *gcp-2.1* and *gcp-2.2* mutants are similar to that of the wild-type. However, the survival curve of *gcp-2.3* mutants was slightly shifted towards the left indicating faster death rate. The observed maximum lifespan for all strains were 25-28 days. The number of worms alive decreased significantly from 90% to 0% after 14th day in wild-type and *gcp-2.1* mutants. However, in *gcp-2.2* and *gcp-2.3* mutants, the number of worms alive significantly reduced after 10th and 6th day respectively. On the 24th day all worms were dead in wild-type and *gcp-2.1* mutants whereas small percentage of *gcp-2.2* and *gcp-2.3* mutants were alive until the 28th and the 26th day. Hence, data indicates that the longevity is slightly increased by the absence of *gcp-2.1* or *gcp-2.2* and absence of *gcp-2.3* does not show such increase in longevity. Collectively, these results indicate that *gcp-2* mutants differently affect the longevity of *C. elegans*. However, the change in the longevities do not appear very significant.



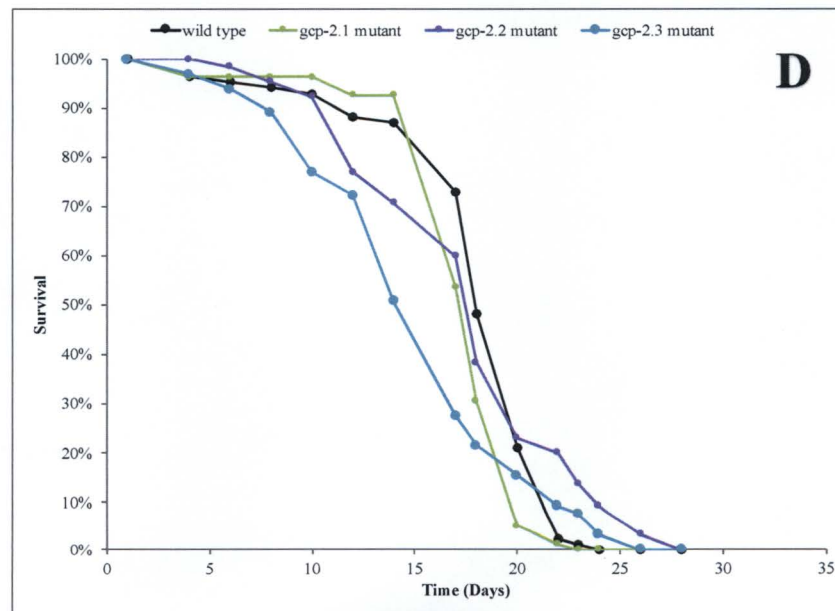
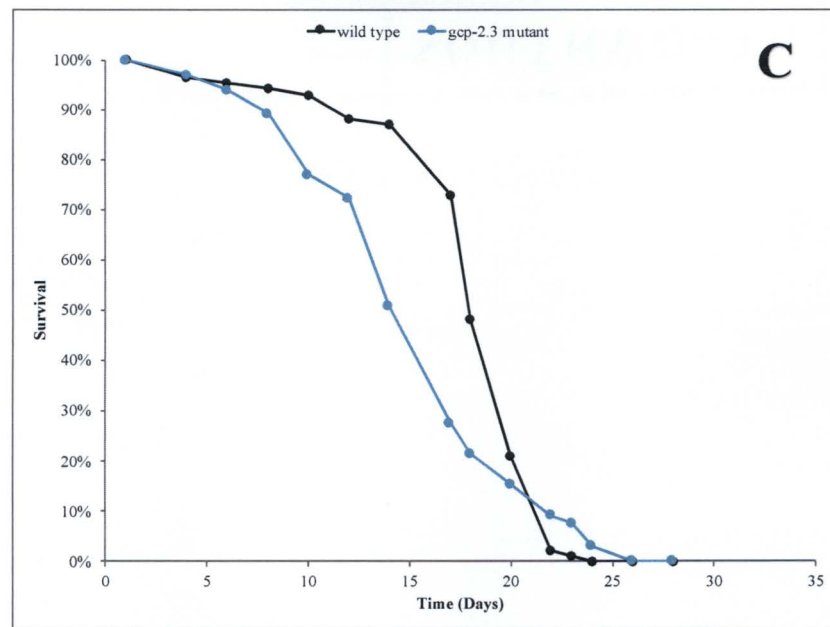


Figure 18. The longevity of wild-type and *gcp-2* mutants.

Data shown are representative of two biological replicates of five animals each. (A) The longevity of *gcp-2.1* compared to wild-type *C. elegans*. (B) The longevity of *gcp-2.2* compared to wild-type *C. elegans*. (C) The longevity of *gcp-2.3* compared to wild-type *C. elegans*. (D) Comparative longevity plot of wild-type and *gcp-2* mutants.

2.4.3 Establish the role of GCPII in *C. elegans* development

In order to determine the effect of GCPII in *C. elegans* growth, the body length assay was conducted in wild-type and *gcp-2* mutants. Quantification of the development was measured by the body length and shown in Figure 19. Previous studies have reported *C. elegans* body length as a physiological measurement of development (105, 106). The images of body length are shown in Figure 20. The data of this experiment was representative of three biological replicates of five animals each. Data showed that the body length of *gcp-2.1* and *gcp-2.2* mutants were higher compared to the wild-type ($P < 0.001$) whereas the body length of *gcp-2.3* mutant was lower compared to the wild-type ($P < 0.001$). The average body length of wild-type was 31.1 whereas *gcp-2.1* mutant, 37.4 ($p=2.96702E-07$); *gcp-2.2* mutant, 43.1 ($p=9.33288E-13$); *gcp-2.3* mutant, 28.2 ($p=4.82118E-06$). Therefore, *gcp-2.1* mutants showed 16.8% and *gcp-2.2* mutants showed 27.8% increase in body length when compared with the wild-type worms. However, *gcp-2.3* mutants showed relatively lower body length which is a 10.2% drop compared to the wild-type *C. elegans*. Hence, data indicates that the development was affected by absence of *gcp-2* paralogs.

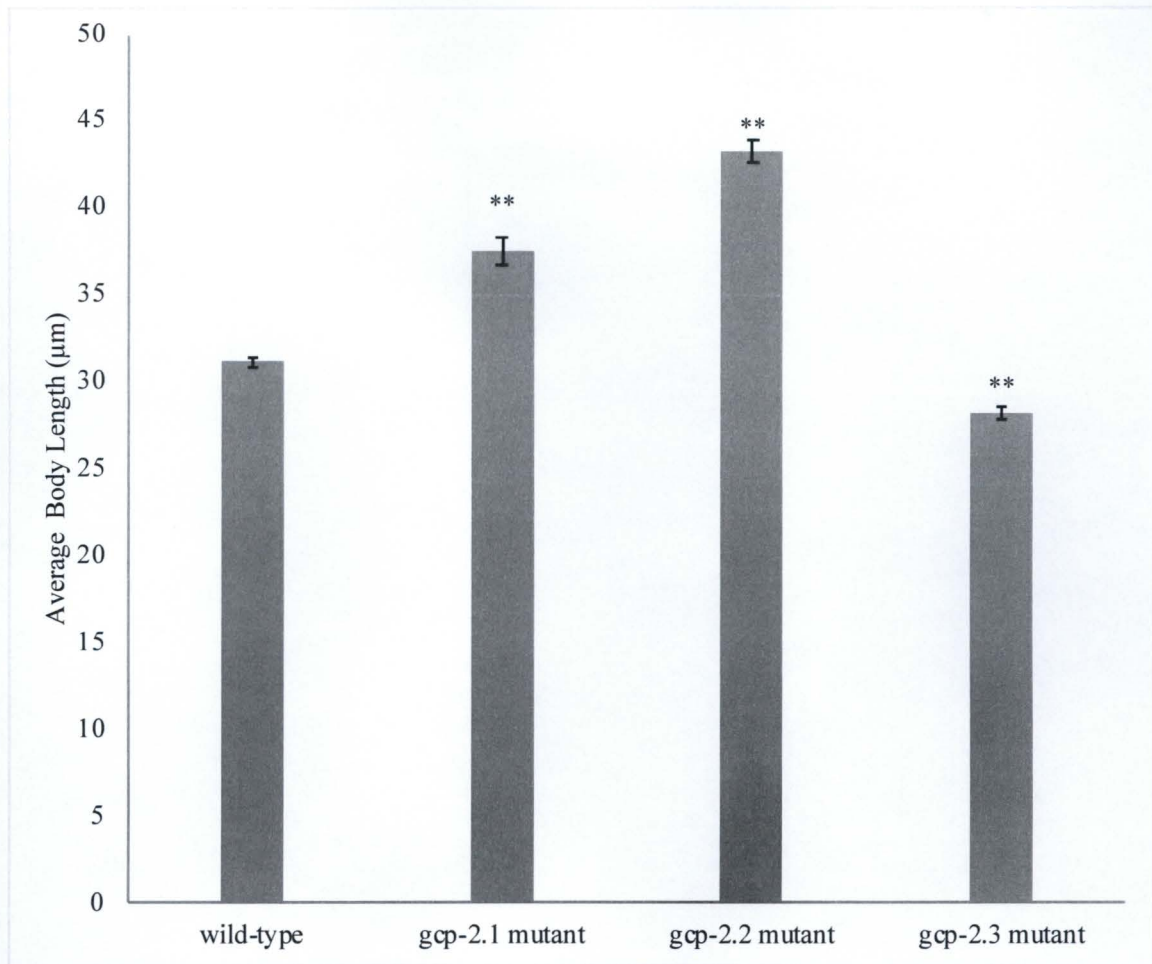


Figure 19. The body length of wild-type and *gcp-2* mutants.

Mean body length of wild-type, 31.1 µm; *gcp-2.1* mutant, 37.4 (p=2.96702E-07); *gcp-2.2* mutant, 43.1 (p=9.33288E-13); *gcp-2.3* mutant, 28.2 (p=4.82118E-06). Data shown are representative of three biological replicates of five animals each. Statistical significance was determined using two sample T-test (*p > 0.001, **p < 0.001). **p < 0.001 considered significant. The error bars represent ± standard deviation.

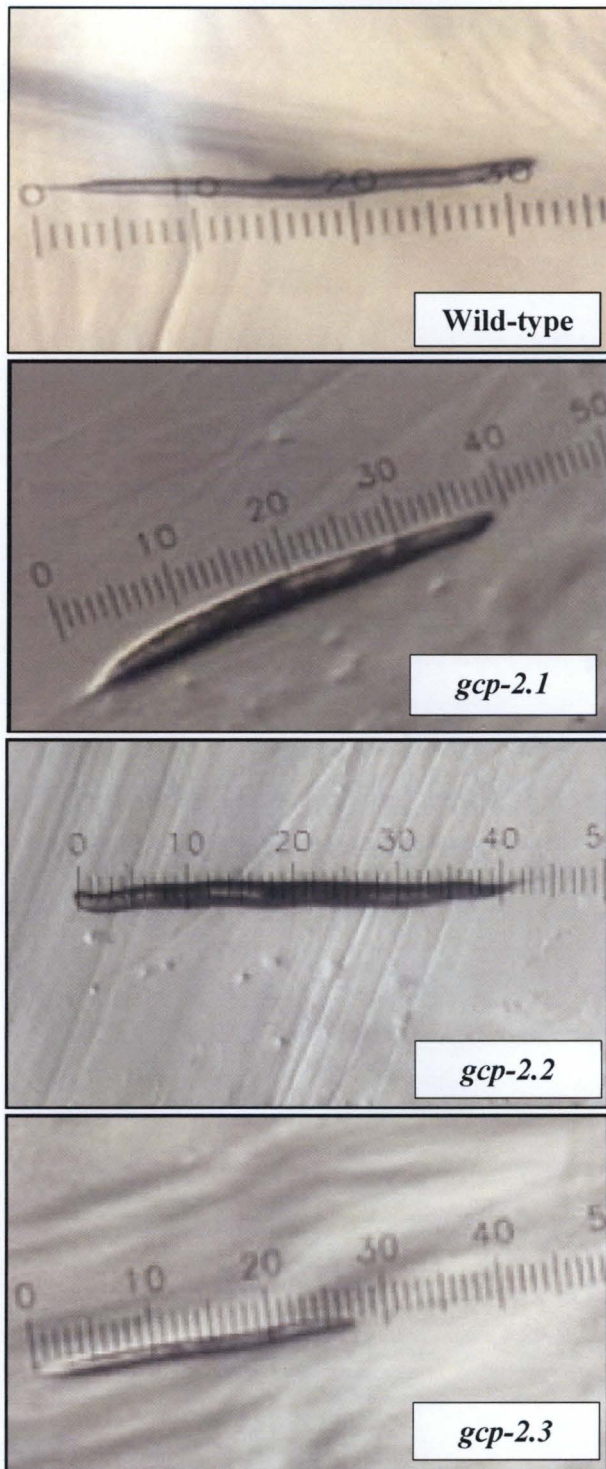


Figure 20. The images of the body length of wild-type and *gcp-2* mutants.

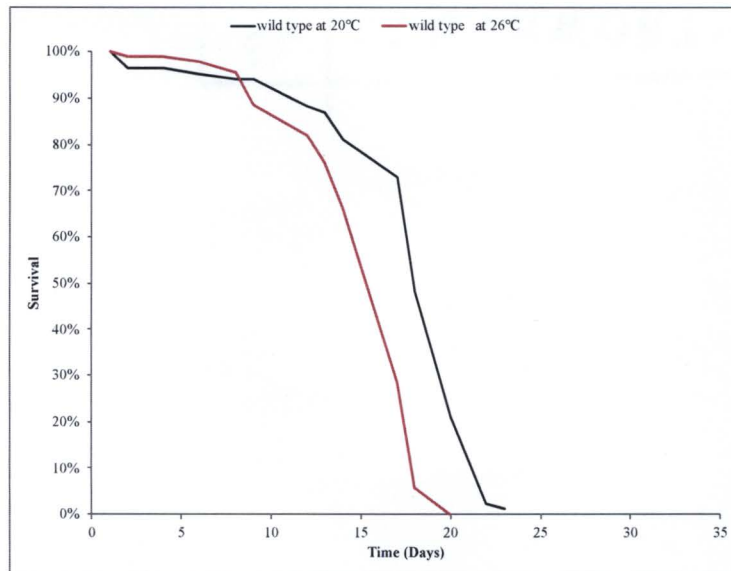
Images taken on day 2 at 20 °C using an Olympus Model LMS-225R Microscope.

2.4.4 Establish the role temperature on *C. elegans* aging and reproduction

In order to determine the effect of temperature and GCPII in *C. elegans* aging and reproduction, the longevity and brood size assays were conducted at 26 °C and 20 °C in wild-type and *gcp-2.1* mutant worms as shown in Figure 21 and Figure 22. Quantification of the aging was measured by the longevity and reproduction was measured by progeny size. The data of this experiments were representative of 2 biological replicates of five animals each.

The lifespan of wild-type and *gcp-2.1* mutants at 20 °C were similar. The survival curves of both strains were shifted towards the left at 26 °C in a parallel pattern. Therefore, wild-type and *gcp-2.1* mutant worms showed reduced lifespan as the temperature increases. The data also indicates that the mutation in *gcp-2.1* paralog does not play a role in the ability of worms to respond increased temperature as both wild-type and *gcp-2.1* mutant worms were similarly affected. The average brood size of wild-type at 20 °C was 247.5 whereas at 26 °C it was reduced to 197.5 ($p= 9.91E-06$). This is a 20.2% decrease in progeny size. The average brood size of *gcp-2.1* mutant at 20 °C was 221.6 whereas at 26 °C it was reduced to 172.7 ($p= 0.00357$). This is a 22% decrease in progeny size. Therefore, both wild-type and *gcp-2.1* mutant hermaphrodites showed decrease in progeny production as the temperature increases in a parallel pattern. This indicates that *gcp-2* paralog does not play a role in temperature dependent reduction in brood size and lifespan. Furthermore, data indicates that the lifespan and reproduction was inversely correlated with the increasing temperature.

A



B

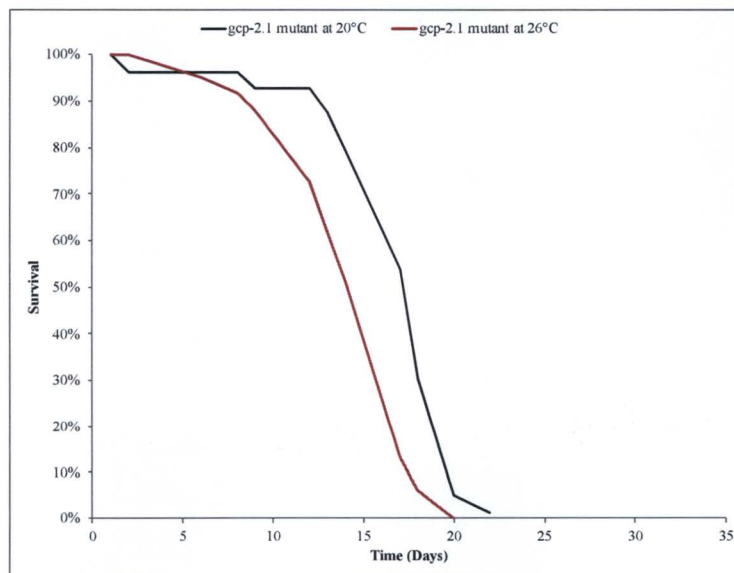


Figure 21. The effect of temperature on longevity of the wild-type and gcp-2.1 mutant *C. elegans*.

(A) The longevity of wild-type worms at 20 °C and 26 °C (RT). (B) The longevity of gcp-2.1 mutant worms at 20 °C and 26 °C (RT).

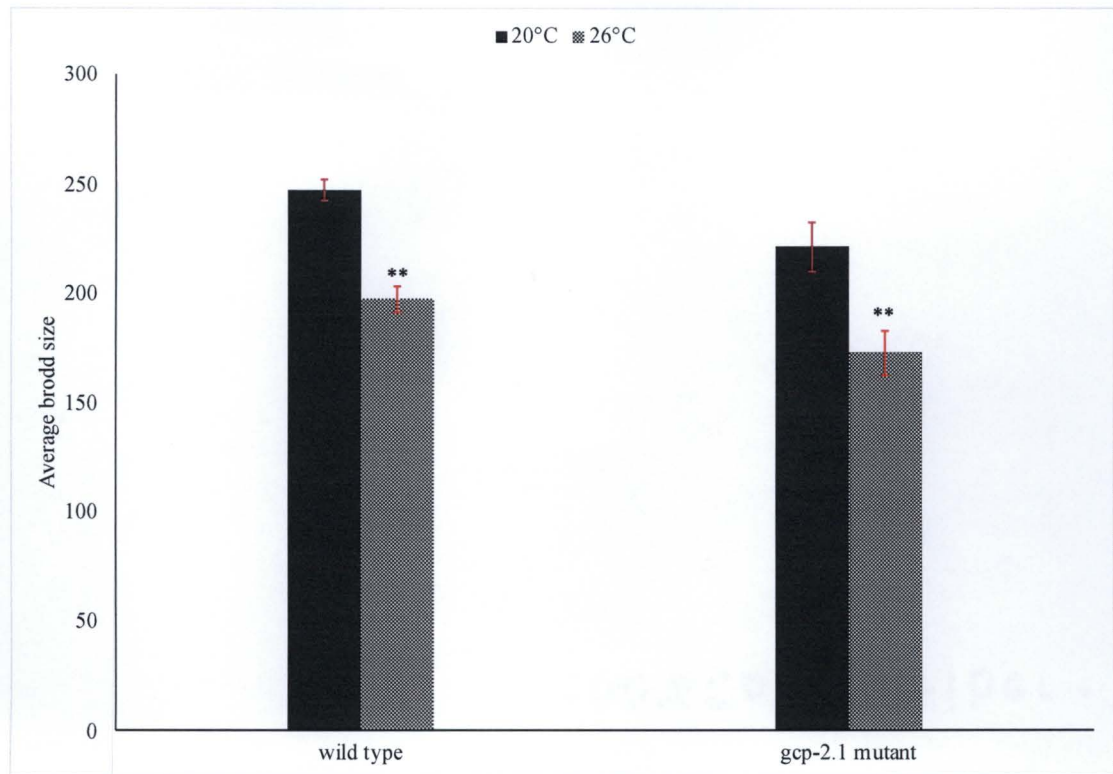


Figure 22. The effect of temperature on brood size of the wild-type and *gcp-2.1* mutant *C. elegans*.

The brood size of wild-type and *gcp-2.1* mutant worms at 20 °C and 26 °C (RT). Statistical significance was determined using two sample T-test (*p > 0.005, **p < 0.005). **p < 0.005 considered significant. The error bars represent \pm SEM. The mean brood size of wild-type at 20 °C, 247.5; at 26 °C, 197.5 (p= 9.91E-06). The mean brood size of *gcp-2.1* mutant at 20 °C, 221.6; at 26 °C, 172.7 (p= 0.00357). Data shown are representative of two biological replicates of five animals each.

2.4.5 Investigation of the Effect of RNAi

Verification of RNAi Feeding Strains

This is a quality control test conducted to verify RNAi feeding strains. First, the transformation of the feeding vector to into the *E. coli* HT115 feeding bacteria was confirmed by gel electrophoresis by detecting the presence of plasmids as shown in the Figure 23. The proper insertion of the *gcp-2.1*, *gcp-2.2* and *gcp-2.3* sequences into the L4440 vector was determined by RNAi plasmids sequencing.

Gel Electrophoresis

Gel electrophoresis was used to detect the presence of plasmids in feeding bacteria.

RNAi Sequence Alignment

The proper insertion of the *gcp-2.1*, *gcp-2.2* and *gcp-2.3* sequences into the L4440 vector was detected by RNAi sequencing and alignment. RNAi plasmid sequencing results obtained from the Core Sequencing Facility at the University of Illinois at Urbana-Champaign was compared to the known reference sequences if each *gcp-2* paralog. *gcp-2.1* showed 95% (971/1027) sequence identity whereas *gcp-2.2* and *gcp-2.3* showed 99% (858/867) and 98% (824/837) sequence identity respectively. The alignment results obtained from the NCBI sequence nucleotide alignment tool “BLAST engine” is shown in the appendix 3. This indicates that accurate *gcp-2.1*, *gcp-2.2* and *gcp-2.3* sequences are inserted into the L4440 vector.

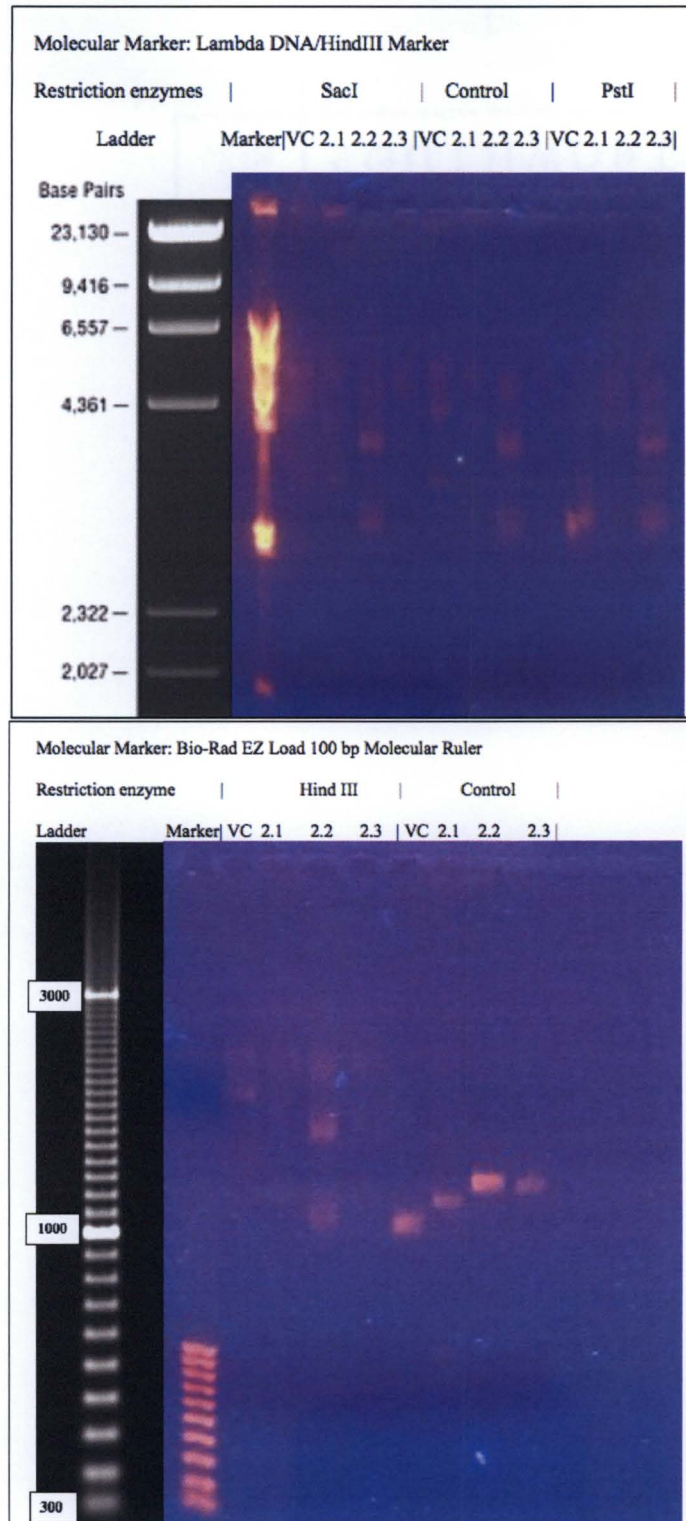


Figure 23. The gel electrophoresis images of RNAi plasmids.

The Effect of RNAi Induced GCP-2 Inhibition on Reproduction

In order to determine the effect of GCPII in *C. elegans* reproduction using RNAi mediated GCP-2 knock down technique, the brood size assay was conducted in wild-type worms shown in Figure 24. Quantification of the reproduction was measured by the brood size. Wild-type *C. elegans* were fed with RNAi feeding strains for GCP-2.1, GCP-2.2, GCP-2.1 and vector control. Additionally, worms were fed with a mixture of feeding strains (GCP-2.1, GCP-2.2, GCP-2.1 and vector control) to induce complete knock down of *gcp-2*. The data of this experiment was representative of one biological replicate with 5 worms.

The average brood size of wild-type worms fed with vector control was 130.2 whereas GCP-2.1, 117.8 ($p= 0.01932146$); GCP-2.2, 129.6 ($p= 0.465578589$); GCP-2.3, 118.2 ($p= 0.029034692$) and mixture of all plasmids, 116 ($p= 0.073427447$). Therefore, data did not show a significant ($p < 0.001$) difference between wild-type worms fed with vector control and GCP-2 plasmids.

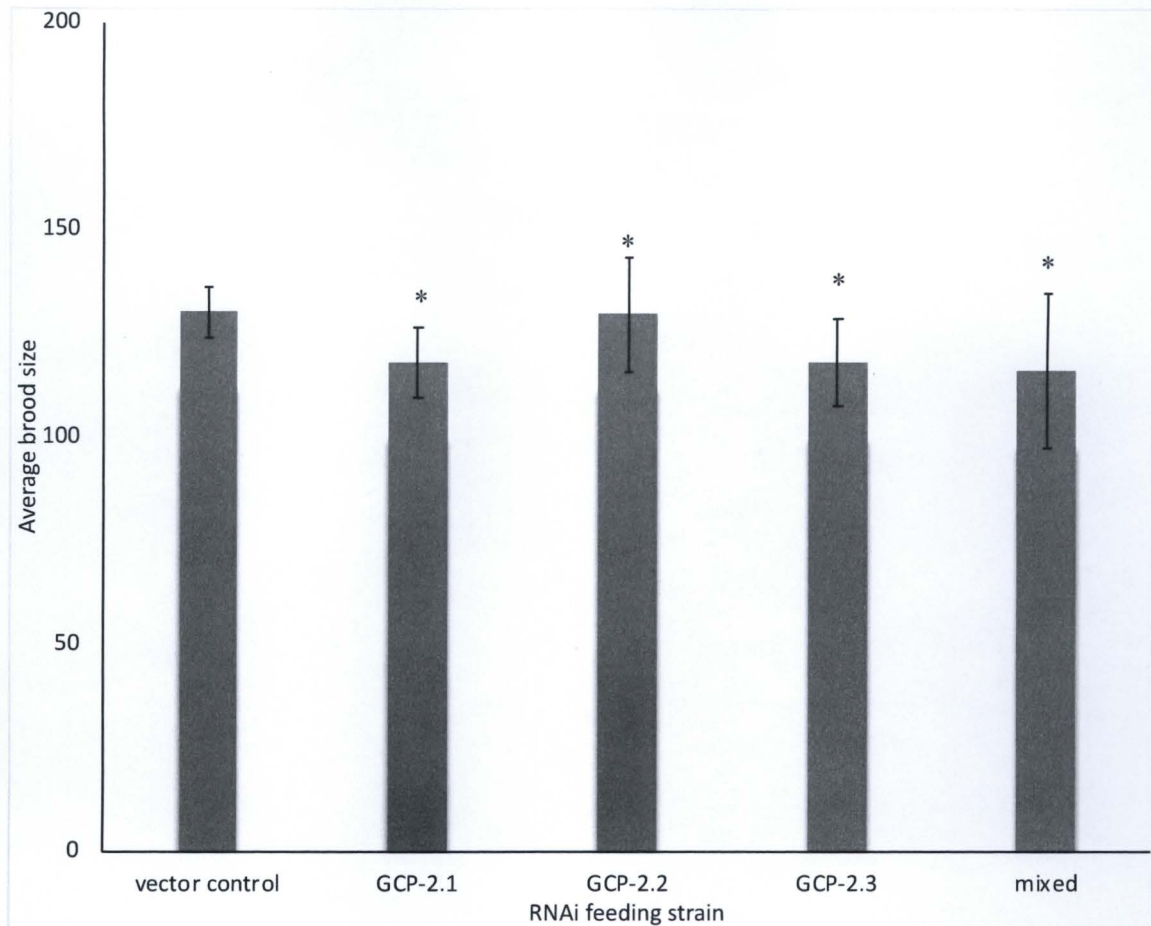


Figure 24. The effect of RNAi induced GCP-2 inhibition on brood size of wild-type *C. elegans*.

Mean brood size of wild-type worms fed with vector control, 130.2; GCP-2.1, 117.8 ($p=0.01932146$); GCP-2.2, 129.6 ($p=0.465578589$); GCP-2.3, 118.2 ($p=0.029034692$) and mixture of all strains, 116 ($p=0.073427447$). Statistical significance was determined using two sample T-test (* $p > 0.001$, ** $p < 0.001$). ** $p < 0.001$ considered significant.

The error bars represent \pm standard deviation. Data shown are representative of 1 biological replicate with 5 worms.

2.5 Discussion

In this study I describe the role of cGCPII and its paralogs in reproduction, aging and development of *C. elegans*. I have shown that *gcp-2* paralogs affect these physiological parameters at different levels. Paralogs as discussed in the Section 1.3.4, is a product of gene duplication followed by mutations. This is a mechanism of neofunctionalization in which genes acquire functional divergence. In other words, paralogs can take on a different function after a gene duplication event (44). Furthermore, sometimes, over a long evolutionary period, the function and the expression patterns of a paralogous gene pair may diverge significantly. This will give rise to totally new functions and specializations in the organism (107). Therefore, it is possible that the *gcp-2* paralogs may or may not have the same role in reproduction, aging, development and other physiological functions in any organism. The reproduction and growth are affected by cGCPII. The absence of *gcp-2* paralogs reduce reproduction and growth at different levels in *C. elegans*. This indicates that cGCPII play a role in *C. elegans* reproduction and growth. However, the effect of cGCPII in longevity does not appear statistically significant.

As discussed in the Chapter 1, hGCPII plays a role in neuronal signaling and folate absorption. Therefore, the observed deterioration in *C. elegans* reproduction and growth can be due to disruptions to cGCPII dependent neuronal signaling or folate metabolism caused by mutations in *gcp-2* paralogs. hGCPII contributes to neural signaling by hydrolyzing NAAG and producing free glutamates to induce fast excitatory neurotransmission through the free glutamate acting on mGlu receptors (Chapter 1). *C. elegans* also expresses glutamatergic signaling and 10 genes encoding putative ionotropic glutamate receptor subunits have been identified (108–110). Previous studies using mice

models had shown that dyshomeostasis of glutamatergic signaling can disrupt insulin signaling in the brain (111). In *C. elegans*, mutation in *daf-2*, a gene encoding an insulin receptor-like protein, was shown to reduce the progeny size by 20% at 20 °C (112). This suggests a relationship between glutamate and reproduction through the insulin signaling pathway. Therefore, the observed reduction in *C. elegans* reproduction and growth can be caused by mutated *gcp-2* reducing the overall glutamate levels which leads to reduced/altered insulin signaling. However, it should be noted that NAAG has been reported as a mammalian neuropeptide and yet there are no reports of NAAG in *C. elegans*. Therefore, if indeed there is link between glutamate-mediated signaling and progeny production, then the source of glutamate must be established. Additionally, the observed effect cGCPII in reproduction and growth can also be related to GCPII function in folate metabolism. This is further discussed in the Chapter 3.

The reduced but statistically significant effect of all three *gcp-2* paralogs on the reproduction and physiological functions may be due to functional complementation by one *gcp-2* paralog for the loss of another *gcp-2* paralog in *C. elegans* as reported (113, 114). When the brood size data is taken into account both *gcp-2.1* and *gcp-2.2* paralogs showed similar but lower brood size than the wild-type and *gcp-2.3* paralog. This may indicate that *gcp-2.1* and *gcp-2.2* are important paralogs than *gcp-2.3* and compensating each other's role on progeny production. This functional compensation hypothesis is further strengthened by the fact that none of the paralog shows a striking reduction or complete abolition of progeny production. Availability of a double mutant of *gcp-2.1* and *gcp-2.2* will be an ideal model to test this hypothesis but such double mutants are not currently available from the worm sources.

The RNAi experiment did not show a significant difference in reproduction between the wild-type and *gcp-2* mutants. However, when *gcp-2* paralogs were genetically mutated, then there was a significant reduction in brood size of *gcp-2* mutants compared to wild-type. These disparities in results shows that the RNAi experiment was not successful. Although, the quality control experiments showed that proper *gcp-2.1*, *gcp-2.2* and *gcp-2.3* sequences are inserted into the L4440 vector and this vector is transformed into the *E. coli* HT115 feeding bacteria, it is still possible that the dsRNA production was induced. This can be confirmed by following methods in a future study (115, 116),

- Real-time quantitative PCR (RT-qPCR) to quantify the knockdown of the mRNA
- SDS-PAGE and western blotting to visualize the knockdown of the protein

Suggestions for future successful RNAi experiments,

- Microinject worms with dsRNA (Protocol: (71, 116))
- Soak worms in dsRNA (Protocol: (71, 116))

Longevity assays were initially conducted in liquid media using 96 well microtiter plates as described before (97). However, this experiment was not successful. Bacteria settled to the bottom of the well, which resulted scattering of light (from the microscope light source to the objective lens) in the turbid medium making it hard to count the number of worms in each well. My suggestion for this experiment is to shake the microtiter plate on a microtiter plate shaker for at least 2-3 minutes before counting as mentioned in the protocol (97). However, our lab did not have a microtiter plate shaker. Therefore, I conducted the longevity assay in solid media as previously described (117). Measuring longevity in liquid media is an easy and efficient method to count a large number of worms compared to solid media. As in solid media worms need to be transferred to new plates

frequently whereas in this method, worms stay in the same 96 well plate throughout the experiment.

The observed similar longevity in wild-type and *gcp-2* mutants may be due to either cGCPII not playing a role in ageing or functional complementation by one *gcp-2* paralog for the loss of another *gcp-2* paralog in *C. elegans* as reported (113, 114).

2.7 Conclusions

Taken together, this chapter shows that *gcp-2* paralogs play a role in the reproductive and physiological biology at different levels in *C. elegans*. However, the underpinning mechanism is still unclear. The next chapter will focus on understanding underlying mechanism of cGCPII in the physiological parameter of *C. elegans*.

Chapter 3: Investigation of the Role of GCPII in Folate Metabolism

3.1 Introduction

The terminology “*folate*” is a generic name for a group of chemically associated compounds based on its structure. Folate or vitamin B₉ is a water-soluble B vitamin whose canonical role is in one-carbon transfer for the *de novo* synthesis of thymidine, purines, methionine, and the methyl donor S-adenosylmethionine (118, 119). Animals cannot synthesize folates and must be assimilated either through diet or food supplementation, whereas bacteria, fungi, algae and plants synthesize folates *de novo* (120). Dietary folates are naturally present in foods such as leafy green vegetables, legumes, egg yolk, liver, citrus fruit, meat, poultry and fish (118, 121). Folic acid (pteroylmonoglutamic acid) is the synthetic form which is found in dietary supplements and fortified foods (122). Dietary folates and folic acid are not metabolically active until they are reduced to various forms of dihydro (DHF)- or tetrahydrofolates (THF) (118). These reduced forms of folates are an essential cofactor for one carbon metabolic pathways and thereby, required for the biosynthesis of a range of cellular components in all prokaryotic and eukaryotic cells (123).

3.2 Chemistry and Stability

Folate is composed of three moieties: a pterine ring (pte), a para-aminobenzoate (*p*ABA) and one or more glutamates. These terminal glutamate residues are in γ -linkages (Figure 25A). Folates forms vary from each other by: (1) the oxidation states of the pteridine ring, *i.e.*, dihydrofolate or tetrahydrofolate; (2) modification of the N⁵ and/or N¹⁰ positions of the pteridine ring by substitution with formate (5-formyl-THF (*aka* as folinic acid), 10-formyl-THF, and 5,10-methenyl-THF), formaldehyde (5,10-methylene-THF), or

methanol (5-methyl-THF) (Table 5); and (3) the number of terminal glutamate residues. The three forms of formylated-THFs are interconvertible at different conditions. For example, 5,10-methenyl-THF is stable at pH 1.5–2.6, and at pH 4.0–5.5 it is converted to 5-formyl-THF. In neutral and higher pH, it is converted to 10-formyl-THF and *vice versa* (119).

Folates are soluble in alkaline solutions due to the polar hydrophilic character of the α -carboxyl group. The presence of additional ionizable α -carboxyl groups in polyglutamated folates makes it more anionic than monoglutamated folic acid. Therefore, folates with long polyglutamated tail are more hydrophobic compared to shorter tail as the α -carboxyl groups are highly protonated at lower pH. In neutral pH 5-Formyl-THF is stable. In acidic pH with heating, it is converted to 5,10-methenyl-THF. The synthetic folic acid is more stable than dietary folates at different temperatures. For example, folic acid is stable in 100 °C at pH 5.0–12.0 (121).

The number of terminal glutamate residues does not affect the folate stability. Oxidative cleavage of the C9 and N10 bonds results in loss of biological activity. Reducing agents such as ascorbic acid, 2-mercaptoethanol and dithiothreitol can be used to stabilize folates. The quantity of oxygen and exposure to light have an inverse relationship with folate stability *i.e.* higher levels of oxygen reduces the stability. Therefore, the optimal condition folates are where there is a minimal amount of oxygen and light in higher pH (121).

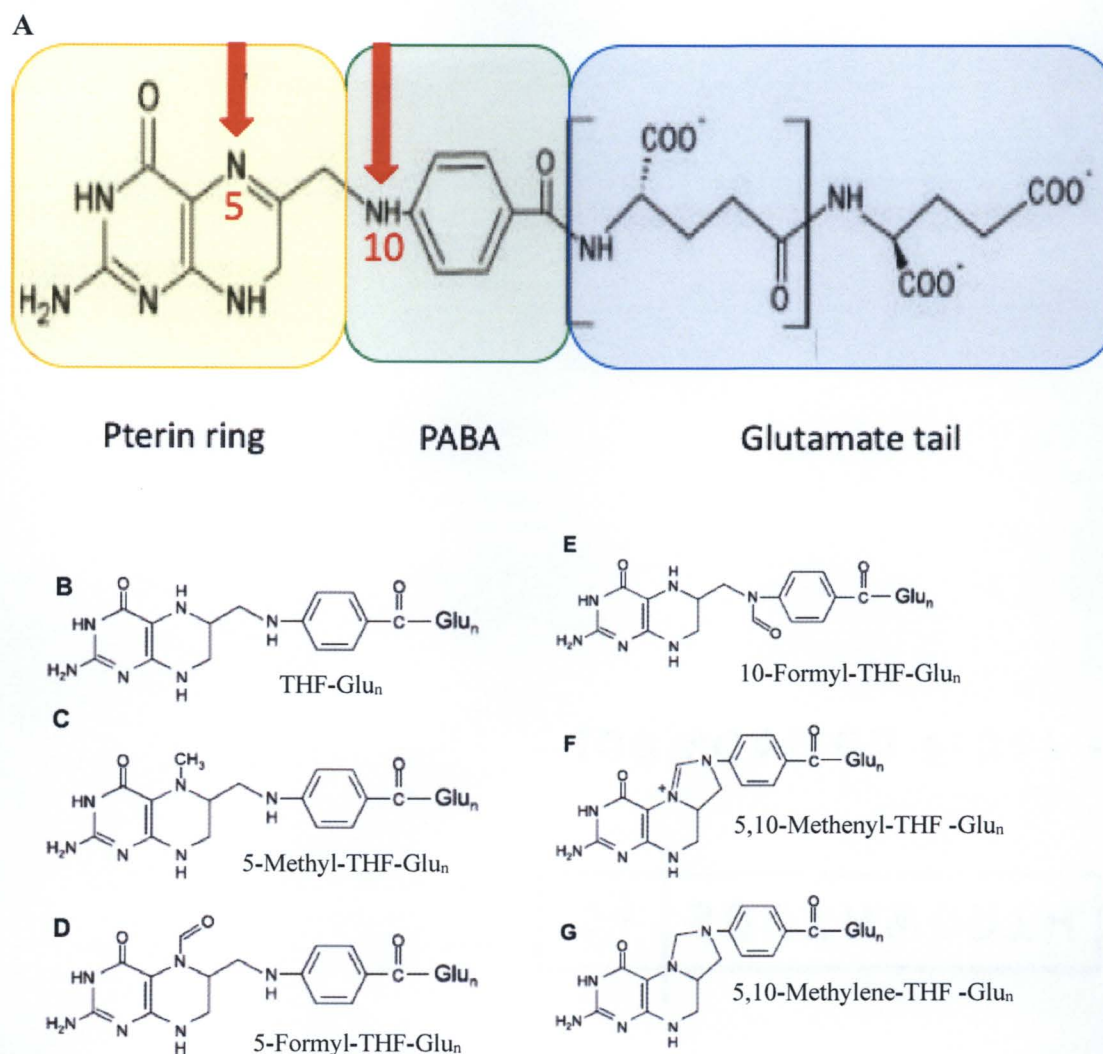


Figure 25. Chemical structure of Folates.

(A) Structure of polyglutamated THF. Red arrows indicate positions of one-carbon groups. N5 and N10 represent various one-carbon substituents. (B-G) Chemical structure of different forms of folates. Glu_n indicates one or more glutamate residues (119).

Table 5. Substituents carried by a THF molecule.			
Folate form	N ⁵ ^a	N ¹⁰ ^a	Figure ^b
Tetrahydrofolate	-H	-H	B
5-Methyltetrahydrofolate	-CH ₃	-H	C
5-Formyletetrahydrofolate	-CHO	-H	D
10-Formyletetrahydrofolate	-H	-CHO	E
5,10-Methenyltetrahydrofolate	-CH=N ⁺	-CH=N ⁺	F
5,10-Methylenetetrahydrofolate	-CH ₂ -	-CH ₂	G
^a Refer to Figure 25 A			
^b Refer to Figure 25B-G			

3.3 Biosynthesis in Bacteria

Folates are synthesized *de novo* in plants, fungi, certain protozoa, and several archaea and bacteria (124). As mentioned in the Section 3.1, folate is composed of three moieties: a pterine ring, *p*ABA and one or more glutamates. Therefore, *de novo* synthesis requires 6-hydroxymethyl-7,8-dihydropterin pyrophosphate (DHPPP) and *p*ABA as precursors.

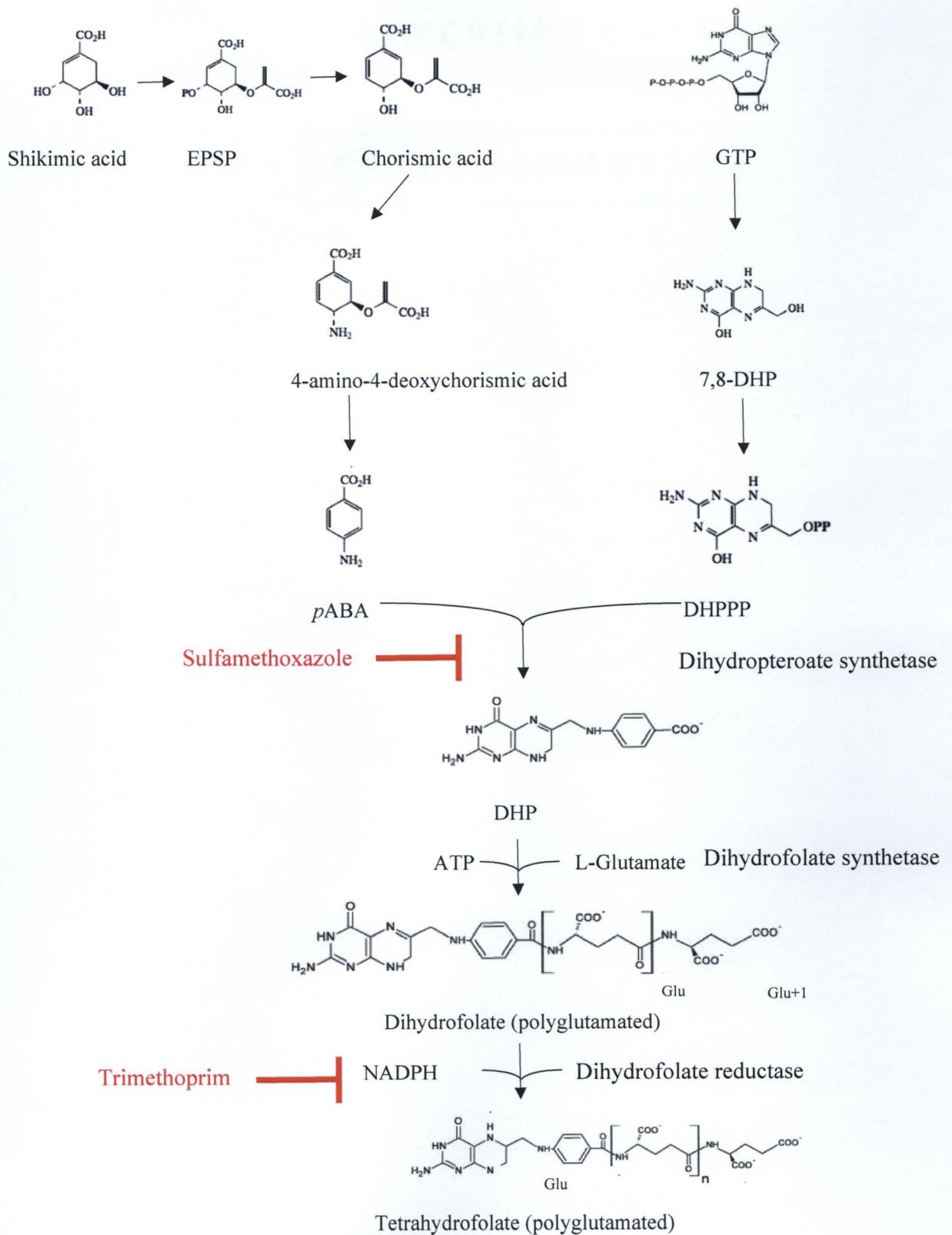


Figure 26. Pathway of *de novo* bacterial biosynthesis of folate.

Sulfamethoxazole and Trimethoprim inhibits folate synthesis. Abbreviations: EPSP, 3-enolpyruvylshikimic acid 3-phosphate; GTP, guanosine triphosphate; DHP, 7,8-dihydropteroate; DHPPP, 6-hydroxymethyl-7,8-dihydropterin pyrophosphate; *p*ABA, para-aminobenzoic acid; ATP, Adenosine triphosphate; NADPH, Nicotinamide Adenine Dinucleotide Phosphate.

*P*ABA (vitamin B₁₀) and aromatic amino acids are produced from the shikimate pathway (Figure 26) which is employed by microorganisms and plants only and not by animals (125). Thus, animals need to acquire folates through their diet or gut microbes. The shikimate pathway initiates by pairing phosphoenolpyruvate (from glycolysis) and D-erythrose-4-phosphate (from pentose phosphate pathway). Phosphoenolpyruvate combines with Shikimic acid through an addition–elimination reaction giving 3-enolpyruvylshikimic acid 3-phosphate (EPSP). EPSP is transformed to chorismic acid by eliminating 1,4-phosphoric acid. Chorismic acid is aminated at C-4 to give 4-amino-4-deoxychorismic acid by aminodeoxychorismate synthase. Subsequently, pyruvate is cleaved by 4-amino-4-deoxychorismate lyase to give *p*ABA (124, 125).

DHPPP is produced by guanosine triphosphate (GTP) in four consecutive steps (Figure 26). First, GTP is transformed to form a pterin ring structure via Amadori rearrangement followed by dephosphorylation, aldolase and pyrophosphokinase reactions ultimately leading to active pyrophosphorylated DHPPP (124). DHPPP and *p*ABA is coupled by dihydropteroate synthase forming a C–N bond. This condensation reaction produces 7,8-dihydropteroate (DHP). Dihydrofolate (DHF) is produced from DHP by incorporating L-glutamate and reduction by DHF reductase yields tetrahydrofolate (THF).

Addition of multiple glutamate moieties by polyglutamate synthase leads to polyglutamated THF. Polyglutamylation can occur before the reduction step by DHF synthase (124, 125). Plants and other microorganisms has the same general biosynthetic pathway with slight modifications (126).

3.4 Intestinal Absorption

Firstly, dietary polyglutamated-folates are hydrolyzed to monoglutamated folates by GCPII as folate carriers (discussed later) that transport folates across the mucosal membrane are highly specific to monoglutamated folates. GCPII mediated folate hydrolysis occur at surface of the jejunal brush border membrane. The optimal pH for this reaction is 6.5. As discussed in the chapter 1.2, like in NAAG, GCPII cleaves terminal γ -linked glutamate residues of folate molecule yielding monoglutamated folates and free glutamates (Figure 27) (127).

Secondly, the monoglutamated folates are absorbed into enterocytes (intestinal epithelial cells) via three major genetically distinct and functionally diverse folate transport systems: reduced folate carriers (RFC), proton-coupled folate transporters (PCFT) and folate receptors (FR) (128). These carriers absorb monoglutamated-folates within the low pH (acidic) microenvironment in the duodenum and jejunum, thus, absorption negatively correlate with pH *i.e.* lower the pH, higher the affinity of receptors for folates (127).

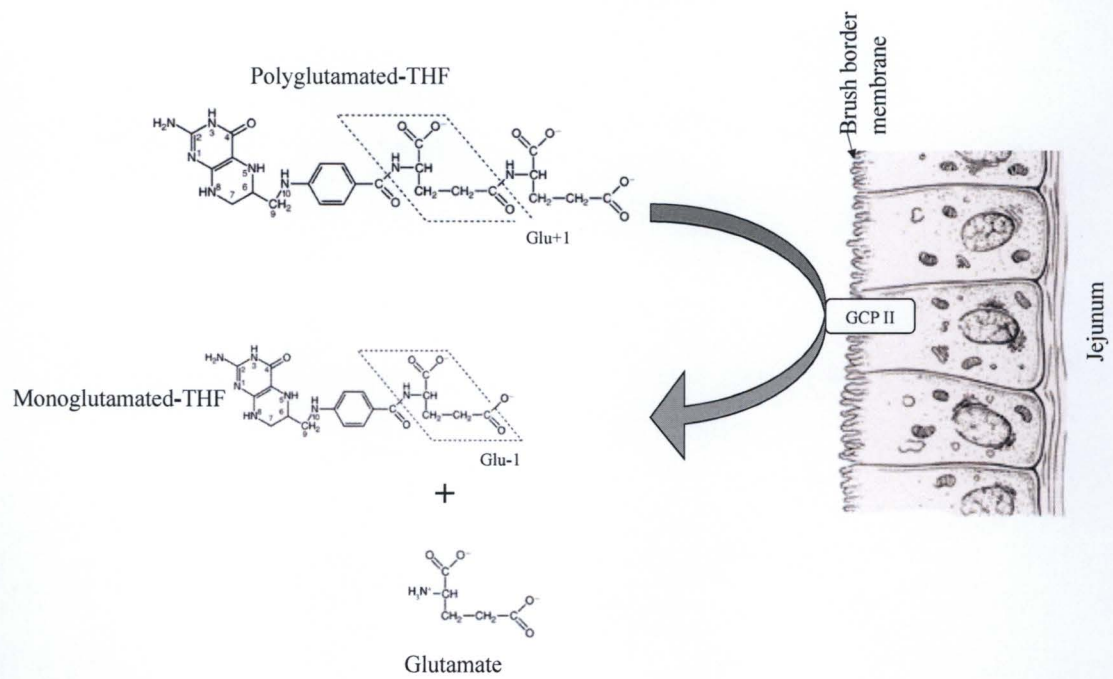


Figure 27. Hydrolysis of dietary folates by GCPII in the jejunal brush border membrane.

GCPII cleaves off γ -linked glutamates from folylpoly- γ -glutamates.

RFC has high affinity for reduced folate forms: 5-methyl-THF and 5-formyl-THF. It has approximately ~100-fold lower affinity for synthetic folic acid. RFC is an active anionic exchanger that counter-transport folates with organic anions. This is the main transport system for reduced folates in mammalian cells. Human RFC are expressed in small intestine, colon, placenta, liver, kidney, lung, bone marrow, brain, hepatocyte membranes, choroid plexus (a branching network of cells that produce cerebrospinal fluid), renal tubular epithelium, and cells lining the spinal canal. Thus, RFC transport folates from the intestinal lumen to enterocytes, which is then transported through blood to peripheral tissues as shown in Figure 28 (128).

PCFT is expressed in the duodenum and proximal jejunum, and primarily involved in folate absorption in the intestine. It is a proton-folate symporter, which couple protons down an electrochemical gradient to the uptake of different forms of folates into enterocytes (128).

FR has high affinity for folic acid, reduced folates, and folate conjugates. FR transports folate across the cell membrane by endocytosis. When folates bind to FR at the cell surface, cytoplasmic vesicles form which releases bound folates to the cytoplasm upon endosomal acidification. It is present in choroid plexus, retina, kidney, uterus, placenta, bone marrow, blood cells and adenocarcinomas. Therefore, FR are involved in folate transport from blood to peripheral tissues (128).

Upon absorption, enterocytes metabolize all different folates to 5-Methyl-THF as shown in Figure 28. However, this metabolization is limited in folic acid. Metabolized 5-Methyl-THF and folic acid are transported out into the hepatic portal vein to hepatocytes (liver cells) (129–131). The mechanism by which folates are transported into the hepatic

portal vein is still not clear. But there are evidences that multidrug resistance proteins-3 (MRP3) expressed at the basolateral membrane of enterocytes is involved this transport process (130).

Monoglutamated folates, primarily monoglutamated methyl-THF from hepatic portal vein are actively transported via PCFT expressed on across the cell membrane of hepatocytes (129). In order to retain folates within the hepatocytes monoglutamated folates are converted to polyglutamated folates by folate polyglutamate synthetase (FPGS). This weakens their affinity for folate transporters, thus, can be stored (132).

γ -Glutamyl hydrolase (GGH) possesses similar enzymatic activity as GCPII. It is expressed in the tissues that store high levels of polyglutamated folates like liver and kidney. GGH is essential to ensure that stored polyglutamated folates are converted to folate monoglutamates when needed. This strengthens their affinity for folate transporters, thus, can be transported out of the stored sites to meet systemic folate needs. This enzyme is localized within lysosome and the optimal pH for this reaction is acidic at 4.5-6.0 (127).

In addition to dietary folates, gut microbes in the colon also produces folates. This is absorbed by PCFT in the colon. However, the colon pH (6-7) is not favorable for this process. Therefore, the rate of absorption is less compared to the duodenum and jejunum. Folates produced by the gut microbes are polyglutamated and terminal glutamate residues are cleaved by GCPII (Figure 27). Monoglutamated folates are then absorbed by a similar pathway as dietary folates as shown in Figure 28 (127).

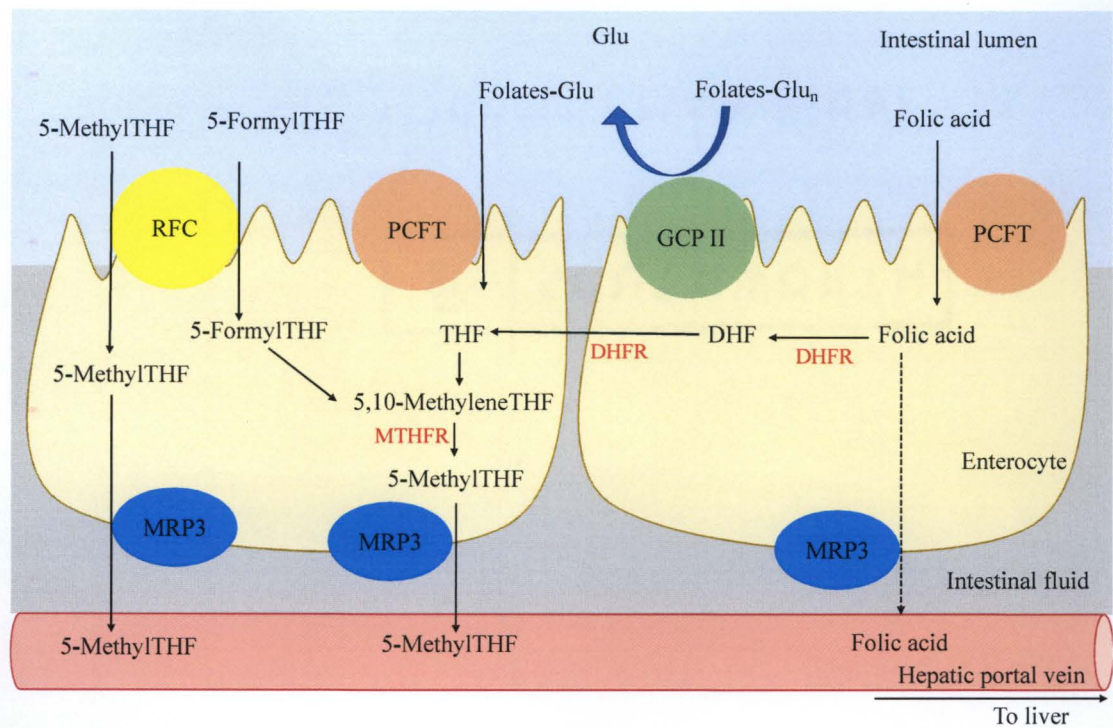


Figure 28. Folate absorption from intestinal lumen, metabolism in enterocytes, and transportation out into the hepatic portal vein as 5-Methyl-THF.

PCTF, proton-coupled folate transporter; GCP II, glutamate carboxypeptidase II; RFC, reduced folate carriers; Folate-Glu_n, polyglutamated folates; Folate-Glu₁, monoglutamated folates; THF, tetrahydrofolate; DHF, dihydrofolate; DHFR, dihydrofolate reductase; MTHFR, methylenetetrahydrofolate reductase; 5-Methyl-THF, monoglutamated methyl-THF; 5-Formyl-THF, monoglutamated formyl-THF; MRP3, multidrug resistance protein-3.

3.5 Metabolism

Monoglutamated folates (primarily 5-methyl-THF and folic acids) are released into the circulatory system from store sites such as liver. This is then taken up by cells via folate transporters (RFC and FR) and converted to folate polyglutamates by folate polyglutamate synthetase (FPGS) to retain within the cell (131–133). These folate molecules act as one carbon (1C/methyl groups) units for several biosynthetic processes including pyrimidine, purine and thymidine synthesis and homocysteine remethylation. This pathway is known as “1C metabolism” and shown in Figure 29.

One-carbon units are covalently attached to N⁵ position and N¹⁰ position of the pteridine ring and *p*ABA respectively (Figure 25A) and can be held in three different carbon oxidation states. Firstly, a carbon unit from amino acid serine or glycine is transferred to THF to form 5,10-methylene-THF. Afterward, this 1C unit can be interconverted between different carbon oxidation states: 5,10-methylene--THF, 5-methyl-THF, and 10-formyl-THF. Each of this oxidation state supports distinct biosynthetic functions. Folates loaded with 1C units does not cross membranes, thus, produced in both the mitochondria and cytosol (Figure 29) (132).

As shown in Figure 29, 5,10-methylene-THF can be used in four ways. First it is used to synthesize thymidine. Secondly, when 5,10-methylene-THF is oxidized to 10-formyl-THF, it is used to synthesize purines. Thirdly, 5,10-methylene-THF can provide a carbon group for the pyrimidine biosynthesis when oxidized to DHF (134, 135). These are building blocks of RNA and DNA. Finally, when it is reduced to 5-methyl-THF, can be utilized to methylate homocysteine to form methionine. Methionine is then converted to S-

adenosylmethionine (SAM) which is a methyl group donor. This process methylate DNA, RNA, hormones, neurotransmitters, membrane lipids, proteins and others (135).

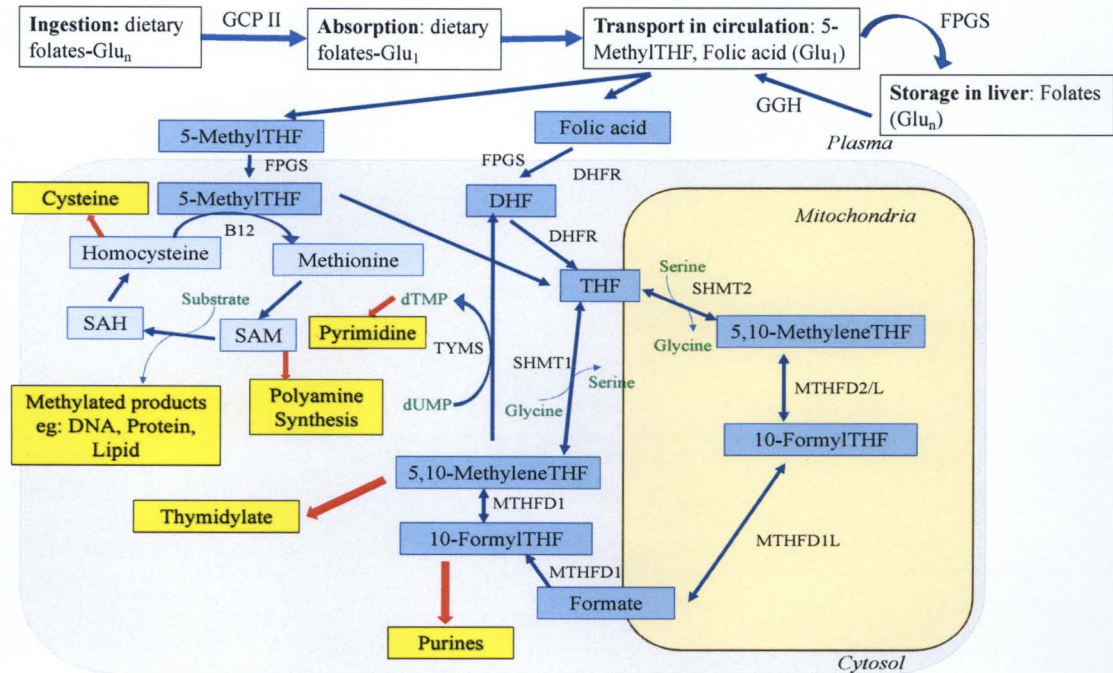


Figure 29. Folate-mediated one-carbon metabolism.

FPGS, Folate polyglutamate synthetase; THF, tetrahydrofolate; DHF, dihydrofolate; DHFR, dihydrofolate reductase; SHMT1/2, serine hydroxymethyl transferase, cytosolic (1)/ mitochondrial (2); MTHFD2/L, methylenetetrahydrofolate dehydrogenase 2/ 2-like; MTHFD1L, monofunctional tetrahydrofolate synthase, MTHFD1, methylenetetrahydrofolate dehydrogenase; B12, vitamin B12; SAM, S-adenosylmethionine; SAH, S-adenosyl homocysteine; TYMS, thymidylate synthetase; dUMP, deoxyuridine monophosphate; dTMP, deoxythymidine monophosphate; Glu_n, polyglutamated folates; Glu₁, monoglutamated folates; GCP II, glutamate carboxypeptidase II; GGH, γ -Glutamyl hydrolase.

3.6 Deficiencies

Folate deficiencies can occur due to multiple reasons such as inadequate dietary consumption, malabsorption in the gut and consumption of certain drugs: sulfonamides, aminopterin, methotrexate, pyrimethamine, trimethoprim and triamterene, which act as folate antagonists (136, 137). Folate deficiencies have long been known to have adverse effects on health, such as megaloblastic anemia, neuropathy (138), metabolic dysfunction (139), abnormal red cell precursors in bone marrow (140), neuropsychiatric disorders (141) heart diseases and cancer (142). Folate deficiency during pregnancy can lead to severe defects in brain and spine, termed Neural Tube Defects (NTD) and developmental delay in neonates (142). Low levels of 5-MTHF in the cerebrospinal fluid can lead to cerebral folate deficiency. This can cause delayed development, with deceleration of head growth, hypotonia, and ataxia, dyskinesias (choreo-athetosis, hemiballismus), spasticity, speech difficulties, and epilepsy (143).

In 1992, the U.S. Public Health Service recommended women capable of becoming pregnant to consume 400 μg of folic acid per day to decrease NTD. In 1998, the U.S. mandated fortification of enriched cereal grain products with 140 μg of folic acid per 100 g. These interventions reduced the prevalence of NTD cases (144).

3.7 The Mechanism of Sulfamethoxazole Action

Sulfa drugs are widely used to treat a broad range of bacterial and protozoal infections. Most sulfa drugs, including Sulfamethoxazole (SMX) and Sulfasalazine (SSZ) are close structural analogs of pABA, which exhibit the antimicrobial activity by

competing with pABA. This forms sulfa drug-pterin adducts instead of pABA-pterin adducts of dihydrofolate and thereby depletes bacterial cellular folate levels as shown in Figure 30 (137).

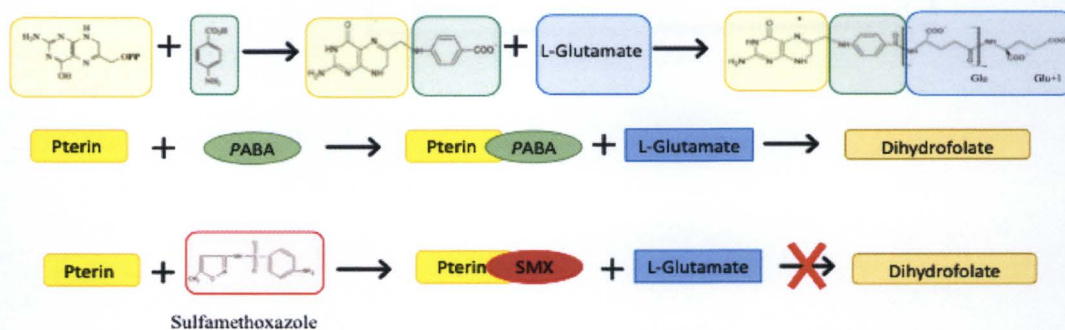


Figure 30. Sulfamethoxazole (SMX) is a structural analogue for PABA and inhibits bacterial folate biosynthesis.

3.8 Hypothesis and Objectives

The hypothesis that governs this study is that cGCPII plays an essential role in folate metabolism of *C. elegans*. The Chapter 2 focused on understanding the role of cGCPII and its paralogs in reproduction, aging and development of *C. elegans*. The two objectives of this study are (i) to illustrate the function of cGCPII in folate metabolism and (ii) to understand how altered folate levels affect the reproduction and development of wild-type and cGCPII mutants. Thirdly, the efficiency of folate supplementation in reproduction and development in wild-type and cGCPII mutants will be determined. In order to provide further information into the different forms of folates present in *E. coli* OP50 and consumed by *C. elegans*, NMR and HPLC based method development are attempted.

3.9 Materials and Methods

3.9.1 Preparation of NGM Assay Plates

Bacterial Food Source: SMX treated *E. coli* OP50

50 μ L of bacteria from the frozen stock at -80 °C was inoculated into 100 mL LB broth containing varied SMX concentrations: 1 μ g/mL, 100 μ g/mL, 1000 μ g/mL and 2000 μ g/mL. Then bacteria were incubated overnight at 35 °C and 250 rpm using an incubating orbital shaker. Obtained bacterial pellet by centrifuging at 3500 rpm for 5 minutes. Afterwards, removed the supernatant, resuspend bacteria in sterile water. Again, centrifuged at 3500 rpm for 5 minutes and removed the supernatant to get rid of SMX. Measured the pellet weight and added sterile water to normalize bacterial concentration to 200 mg/mL. Growth curve for *E. coli* OP50 is shown in the Appendix 6.

Preparation of NGM Plates

NGM petri dishes were prepared as mentioned in the Section 2.3.2. Plates were seeded with 100 μ L of SMX treated *E. coli* OP50. For the Folinic acid (5-formyl-THF) supplementation experiments, prior seeding 10 μ L Folinic acid was added to SMX treated 200 mg/ml *E. coli* OP50.

3.9.2 Brood Size Assay

Brood size assay was conducted as mentioned in the Section 2.3.6. Prior to the experiments, worms were maintained in the same experimental conditions for at least three generations. *i.e.* worms were maintained on SMX-treated bacteria for three generations before the brood size assay. Two replicates were performed for each experiment. Statistical

Analysis was conducted using two-sample t-test assuming equal variances. p value < 0.001 considered significant. Error bars represent \pm SEM.

3.9.3 Body Length Assay

Body length assay was conducted as mentioned in the Section 2.3.9. Prior to the experiments, worms were maintained in the same experimental conditions for at least three generations. *i.e.* worms were maintained on SMX-treated bacteria for three generations before the body length assay. Three replicates were performed for each experiment. Statistical Analysis was conducted using two-sample t-test assuming equal variances. p value < 0.001 considered significant. Error bars represent \pm SEM.

3.9.4 Bacterial Folate Extraction

100 mL of *E. coli* OP50 was grown for 14 hours at 37 °C at 220 rpm. Bacterial culture was centrifuge at 5000 rpm for 5 mins and supernatant was discarded. Bacterial pellet was resuspended in 10 mL extraction buffer, capped, vortexed and flushed with Nitrogen for 30 s. Samples were sonicated in ice for 20 seconds, cooled tubes on ice 30 s and repeated for 9 times. Then, flushed with nitrogen for 1 min, boiled in water for 12 min. Allowed samples cool on ice for 5 min, centrifuged at 9500 rpm for 15 min at 4 °C and transferred supernatant to a clean tube (Folate Extract 1). Bacterial pellet resuspended in 5 mL extraction buffer, vortexed, flushed with Nitrogen for 30 and rotated for 10 mins. Sonicated as before for 9 times. Then, flushed with nitrogen for 1 min, boiled in water for 10 min. Allowed samples cool on ice for 5 min, centrifuged at 9500 rpm for 15 min at 4 °C and pooled supernatant with Folate Extract 1. All extracts (supernatant) were filtered

through Whatman filter Grade No. 4 (20-25 μM). All the samples, extraction buffer, standard solutions and folate extract were prepared on the day of analysis. All composition and preparation details of buffers and solutions are given in the Appendix 4.

3.9.5 Bacterial Folate Extract Purification

Bacterial folate extracts were purified using Q Sepharose XL strong anion exchanger (GE Healthcare) and 0.1 M, 0.5 M and 1 M phosphate buffers. The purification steps are elaborated in the Figure 31.

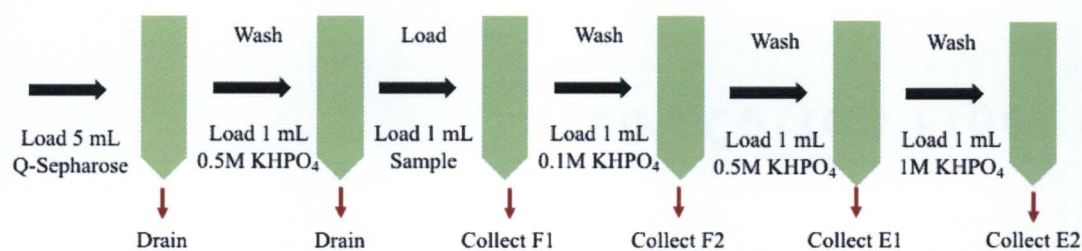


Figure 31. Bacterial Folate Purification Steps.

KHPO_4 , potassium phosphate buffer; Sample, bacterial folate extract; F1, flow 1; F2, flow 2; E1, elution 1; E2, elution 2.

3.9.6 Folate Standard Preparation

Standards Used: Folinic acid calcium salt hydrate 98% (Alfa Aesar™), Dihydrofolic acid $\geq 90\%$ (Sigma-Aldrich), 5-Methyltetrahydrofolic acid disodium salt $\geq 88\%$ (Sigma-Aldrich) and Tetrahydrofolic acid $\geq 65\%$ (Sigma-Aldrich).

Standard Preparation: The standards were dissolved under subdued light (in a room with lights tuned off) immediately before analysis in the extraction buffer containing: 0.1M phosphate buffer (pH 6.1), with 2% sodium ascorbate (w/v) and 0.1% 2-mercaptoethanol (v/v). All samples and buffers were prepared using HPLC grade water (Fisher Chemical) and filtered through non-sterile 0.2 μm Whatman filter.

3.9.7 NMR Based Folate Analysis

1 mL of bacterial folate extract without SMX and 100 mg/mL folic acid dissolved in extraction buffer were added to petri dishes and stored in an oven set to 37 °C for ~5 hours to get rid of extraction buffer. Once samples are completely dried 1 mL of DMSO was added and swirled until dissolved. Samples were analyzed using ^1H NMR. The NMR experimental conditions are given in the Appendix 5.

3.9.8 HPLC Based Folate Analysis

Analyses of bacterial folate extracts, and folate standards were performed using an HPLC system (Hitachi Chromaster) consisting of a gradient quaternary pump (5110), an autosampler (5210), a thermostated column compartment (5310), a diode array detector (DAD-5430), and a fluorescence detector (5440). The HPLC system was controlled by a personal computer running software (Chromaster System Manager). The separation of

folates was performed on a Thermo Scientific™ Hypersil™ ODS C18 analytical column, 5 µm x 4.6 mm x 200 mm, with a guard column (Thermo Scientific™).

The flow rate was 0.8 mL/min and the temperature of thermostated column compartment was set to 4 °C. Injection volume was 10 µL. Two Buffers were used for analysis: Buffer A (1L), 28 mmol dibasic potassium phosphate and 60 mmol phosphoric acid in water; Buffer B (1L), 28 mmol dibasic potassium phosphate and 60 mmol phosphoric acid in 200 mL acetonitrile and 800 mL water. The mobile phase program consisted of 3 min with 100% A, 10 min with 70% A:30% B, 17 min with 45% A:55% B, 15 min with 43% A:57% B followed by 10 min with 100% A and another sample analysis began immediately. The fluorescence intensity of standards and folate extracts monitored with a fluorescence detector (excitation at 295 nm and emission at 360 nm). Peaks were identified on the basis of the retention time folate standards.

HPLC program was stored at Protocatechuic Acid Folder >
Folate_DAD_Hypersil_ODS_Gra.

3.10 Results

3.10.1 The Effect of Reduced Dietary Folates on Reproduction

In order to determine the effect of GCPII dependent folate metabolism on reproduction and brood size assays were conducted in wild-type and *gcp-2* mutant worm strains that were maintained on *E. coli* OP50 with various concentrations of SMX for at least three generations. As mentioned in the Section 3.7, SMX inhibits folate biosynthesis and the level of inhibition increases with increasing concentration of SMX (105, 106). Thus, the available amount of folate and its derivatives reduces with increasing SMX used in treating the bacterial food. This allows to investigate the effect of reduced dietary folate levels on *C. elegans*. Reproduction was quantified as brood size and the data shown are representative of 2 biological replicates with 5 worms each.

As shown in the Figure 32, wild-type worms showed a concentration dependent decline in brood size. The average brood size without SMX was 283.11 (± 3.8) whereas when the worms consumed bacteria treated various concentrations of SMA were as follows: 1 $\mu\text{g/mL}$ SMX - 272.5 (± 6.5); 100 $\mu\text{g/mL}$, 178.7 (± 6.7); 1000 $\mu\text{g/mL}$, 81.2 (± 8.1) and 2000 $\mu\text{g/mL}$, 1.33 (± 2.5). There was not a significant difference at 1 $\mu\text{g/mL}$ ($p > 0.001$) compared to untreated control. However, there was a significant ($p < 0.001$) decline in brood size at 100 $\mu\text{g/mL}$, 1000 $\mu\text{g/mL}$ and 2000 $\mu\text{g/mL}$ SMX. Therefore, SMX resulted 3.7%, and 36.8% decline in progeny production at 1 $\mu\text{g/mL}$ and 100 $\mu\text{g/mL}$, respectively. At the half maximal inhibitory concentration ($\text{IC}_{50} = 1025 \mu\text{g/ml}$) of SMX, 71.3% drop in progeny production was shown and at twice the IC_{50} of SMX, 99.9% decline in progeny production was observed. Hence, data indicates that the reproduction of wild-type worms were affected by SMX induced folate synthesis inhibition in a concentration dependent manner.

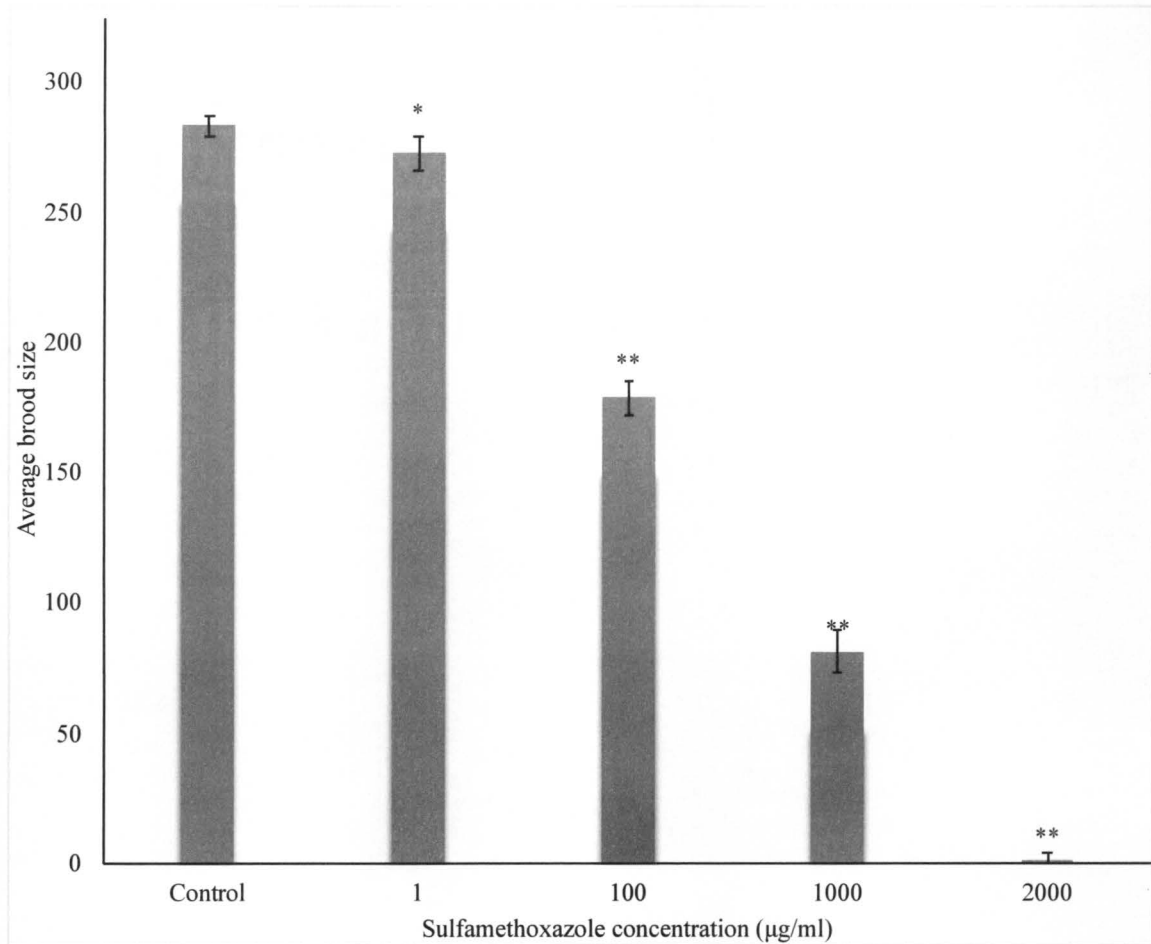


Figure 32. The effect of SMX dependent folate inhibition on brood size of wild-type *C. elegans*.

The mean brood size of control (no SMX), 283.1. The mean brood size of worms maintained on *E. coli* treated with 1 µg/mL, 272.5 ($p=0.09$); 100 µg/mL, 178.7 ($p=3.87094E-11$); 1000 µg/mL, 81.2 ($p=4.47966E-20$) and 2000 µg/mL, 1.33 ($p=1.28891E-22$). Statistical significance was determined using two sample T-test (* $p > 0.001$, ** $p < 0.001$). ** $p < 0.001$ considered significant. The error bars represent \pm SEM. Data shown are representative of two biological replicates of five worms each.

Similarly, *gcp-2.1* mutant worms showed a concentration dependent decline in brood size (Figure 33). The average brood size without SMX was 242.5 (± 4.3) and when the worms consumed bacteria treated various concentrations of SMA the brood size measurements were as follows: 1 $\mu\text{g}/\text{mL}$ SMX, 247.4 (± 9); 100 $\mu\text{g}/\text{mL}$, 13.1 (± 1.3); 1000 $\mu\text{g}/\text{mL}$, 2.9 (± 0.4) and 2000 $\mu\text{g}/\text{mL}$, 0.8 (± 0.4). There was not a significant difference at 1 $\mu\text{g}/\text{mL}$ ($p > 0.001$) compared to non-treated control. However, there was a significant ($p < 0.001$) decline in brood size at 100 $\mu\text{g}/\text{mL}$, 1000 $\mu\text{g}/\text{mL}$ and 2000 $\mu\text{g}/\text{mL}$ SMX. Therefore, SMX resulted 94.5% decline in progeny production at 100 $\mu\text{g}/\text{mL}$. At IC_{50} and twice the IC_{50} concentrations of SMX, there was a 99.9% drop in progeny production. Hence, data indicate that the reproduction of *gcp-2.1* mutants were affected by SMX induced folate inhibition in a concentration dependent pattern. Furthermore, the data indicate that the reduction in brood size severe in *gcp-2.1* mutant compared to the wild type at same concentrations of SMX.

As shown in Figure 34, *gcp-2.2* mutant worms also showed a similar concentration dependent decline in brood size as seen in *gcp-2.1* mutant. The average brood size without SMX was 238.6 (± 5.5) and when the worms consumed bacteria treated various concentrations of SMA the brood size measurements were as follows: 1 $\mu\text{g}/\text{mL}$ SMX, 235.3 (± 3.5). There was not a significant difference at 1 $\mu\text{g}/\text{mL}$ ($p > 0.001$) compared to non-treated control. Interestingly, in contrast to *gcp-2.1*, *gcp-2.2* mutants were sterile at 100, 1000 and 2000 $\mu\text{g}/\text{mL}$ SMX. In the 2nd and 3rd generations at 100 and 1000 $\mu\text{g}/\text{mL}$ SMX, worms laid eggs as shown in Figure 36, however, only few eggs hatched. An attempt to obtain an age synchronized population using these eggs to conduct the brood size assay failed as eggs did not survive after treating with bleach. In addition, at twice the IC_{50} (2000

$\mu\text{g/mL}$) of SMX was lethal to the test worms (all the worms were dead after few days). Hence, data indicates that the reproduction of *gcp-2.2* mutants were intensely affected by SMX induced folate inhibition in a concentration dependent pattern. It is important to note that at 2000 $\mu\text{g/mL}$ of SMX both wild type and *gcp-2.1* mutant survived and laid eggs.

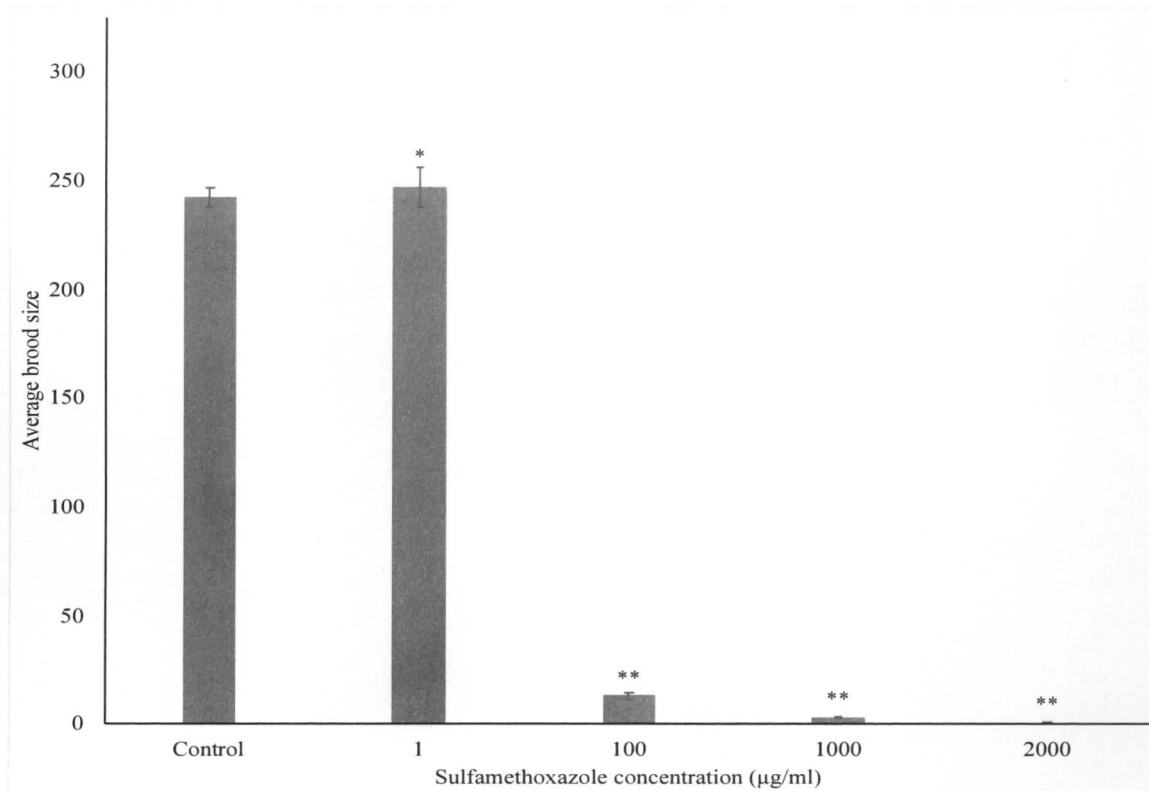


Figure 33. The effect of SMX dependent folate inhibition on brood size of *gcp-2.1* mutant *C. elegans*.

The mean brood size of control (no SMX), 242.5. The mean brood size of worms maintained on *E. coli* treated with 1 $\mu\text{g/mL}$, 247.4 ($p= 0.316$); 100 $\mu\text{g/mL}$, 13.1 ($p= 3.380069\text{E-}21$); 1000 $\mu\text{g/mL}$, 2.9 ($p= 8.93304\text{E-}22$) and 2000 $\mu\text{g/mL}$, 0.8 ($p= 7.43351\text{E-}22$). Statistical significance was determined using two sample T-test (* $p > 0.001$, ** $p < 0.001$). ** $p < 0.001$ considered significant. The error bars represent \pm SEM. Data shown are representative of two biological replicates of five worms each.

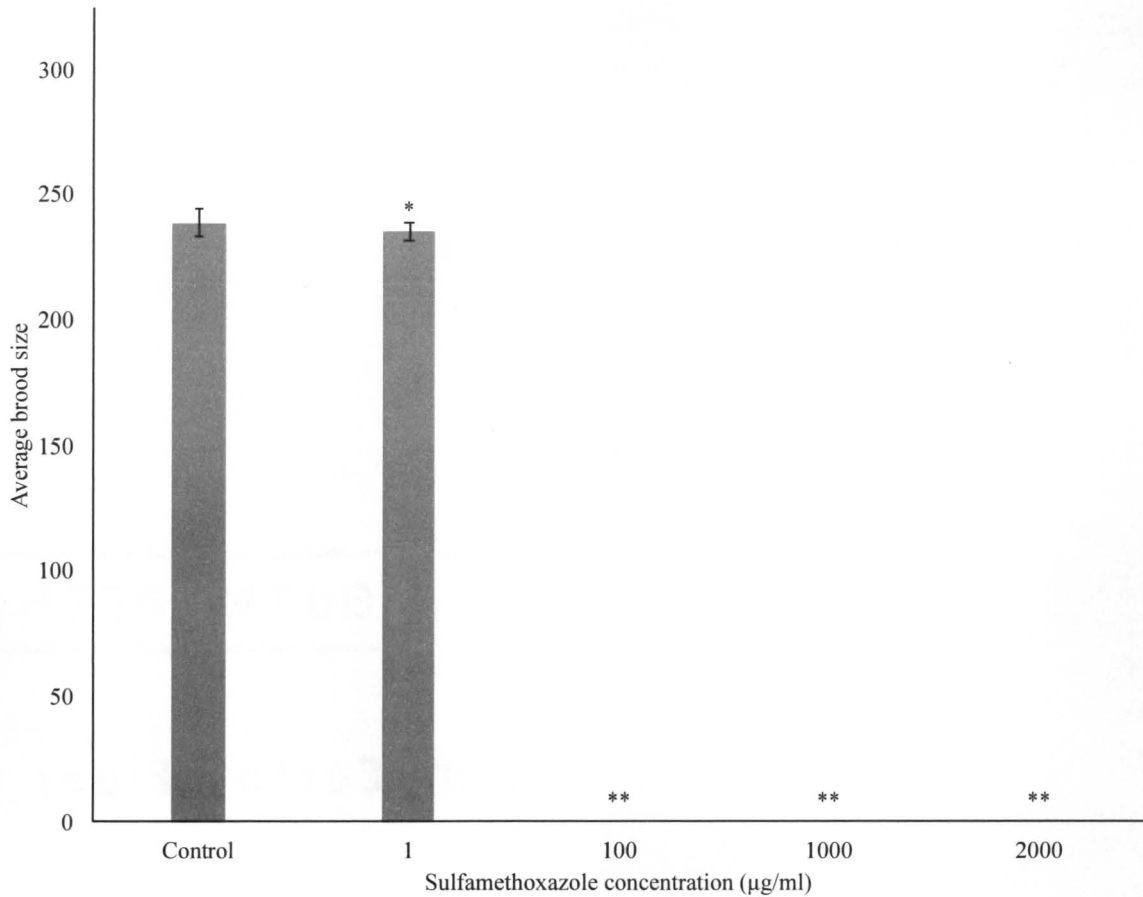


Figure 34. The effect of SMX dependent folate inhibition on brood size of *gcp-2.2* mutant *C. elegans*.

The mean brood size of control (no SMX), 238.6. The mean brood size of worms maintained on *E. coli* treated with 1 µg/mL, 235.3 ($p = 0.31196332$). Worms did not reproduce at 100, 1000 and 2000 µg/mL ($p = 7.60113E-20$). Statistical significance was determined using two sample T-test (* $p > 0.001$, ** $p < 0.001$). ** $p < 0.001$ considered significant. The error bars represent \pm SEM. Data shown are representative of two biological replicates of five worms each.

As shown in the Figure 35, *gcp-2.3* mutants showed a concentration dependent decline in brood size in. The average brood size without SMX was 249.8 (± 5.8) and when the worms consumed bacteria treated various concentrations of SMA the brood size measurements were as follows: 1 $\mu\text{g}/\text{mL}$ SMX, 252.89 (± 4.4); 100 $\mu\text{g}/\text{mL}$, 188.1 (± 7.6); 1000 $\mu\text{g}/\text{mL}$, 43.7 (± 5.5) and 2000 $\mu\text{g}/\text{mL}$, 3 (± 0.6). There was not a significant difference at 1 $\mu\text{g}/\text{mL}$ ($p > 0.001$) compared to non-treated controls. However, there was a significant ($p < 0.001$) decline in brood size at 100 $\mu\text{g}/\text{mL}$, 1000 $\mu\text{g}/\text{mL}$ and 2000 $\mu\text{g}/\text{mL}$ SMX. Therefore, SMX resulted 24.6% decline in progeny production at 100 $\mu\text{g}/\text{mL}$. At IC_{50} of SMX, 82.5% drop in progeny production was shown and at twice the IC_{50} of SMX, 98.8% decline in progeny production was observed. Hence, data indicates that the reproduction of *gcp-2.3* mutants were affected by SMX induced folate inhibition in a concentration dependent manner. However, the relative progeny production is higher than *gcp-2.1* and *gcp-2.2* as shown in Figure 36.

The Figure 36 shows the images of growth phenotype of the wild-type and *gcp-2* mutant *C. elegans* maintained on 1000 $\mu\text{g}/\text{mL}$ SMX treated *E. coli* OP50. These images displays how SMX induced folate inhibition affected the wild-type and *gcp-2* mutants differently. The NGM plates with *gcp-2.1* and *gcp-2.2* worms were drastically less crowded compared to wild-type and *gcp-2.3* mutants. The NGM plate with wild-type was the most crowded and contained a lot of gravid adults, eggs and L-L2 worms. The NGM plate with *gcp-2.2* mutants was the least crowded plate with few worms and eggs which did not develop into L1 larva. Taken together, wild-type and all *gcp-2* mutant strains were affected by SMX induced folate inhibition in a concentration dependent manner. *gcp-2.1* and *gcp-2.2* mutants were affected to higher extent compared to the wild-type and *gcp-2.1* mutants.

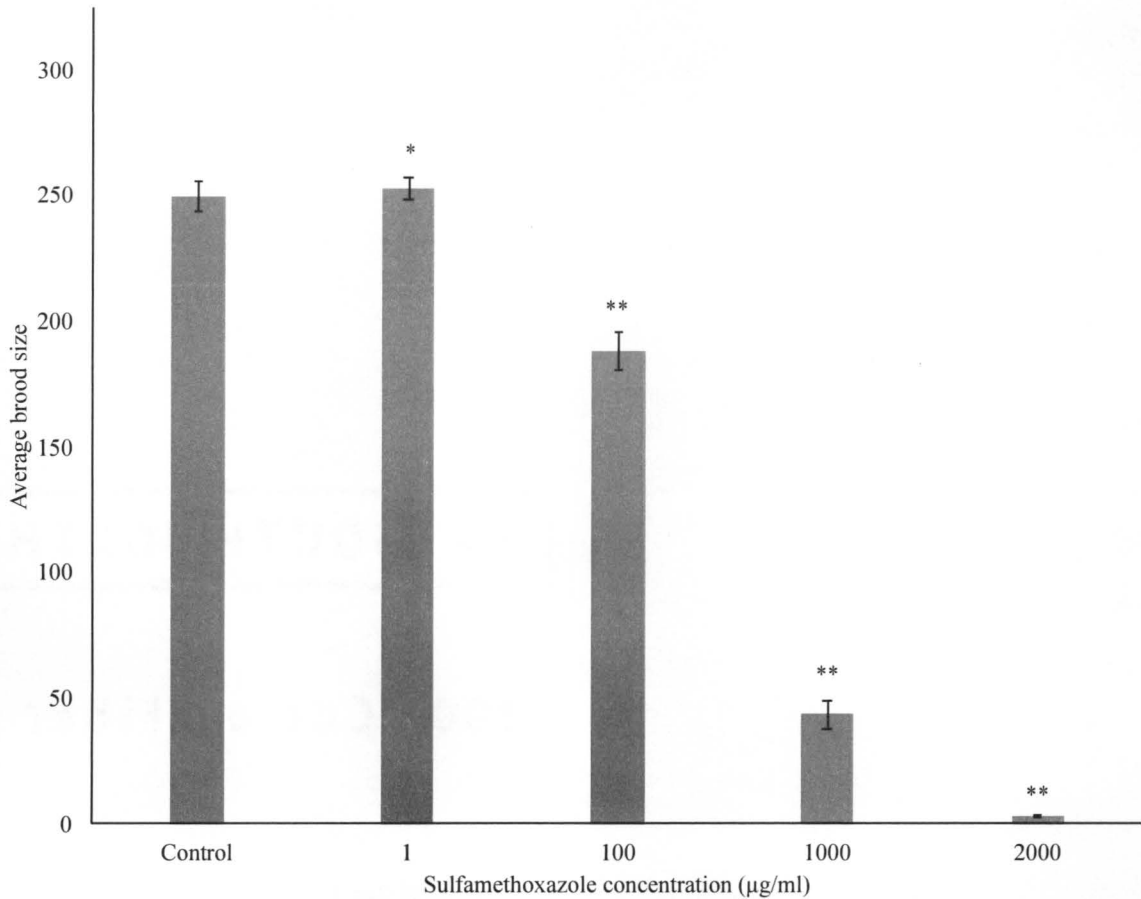


Figure 35. The effect of SMX dependent folate inhibition on brood size of *gcp-2.3* mutant *C. elegans*.

The mean brood size of control (no SMX), 249.8. The mean brood size of worms maintained on *E. coli* treated with 1 µg/mL, 252.89 (p= 0.34); 100 µg/mL, 188.1 (p= 2.54803E-06); 1000 µg/mL, 43.7 (p= 6.74562E-16) and 2000 µg/mL, 3 (p= 9.85037E-20). Statistical significance was determined using two sample T-test (*p > 0.001, **p < 0.001). **p < 0.001 considered significant. The error bars represent ± SEM. Data shown are representative of two biological replicates of five worms each.

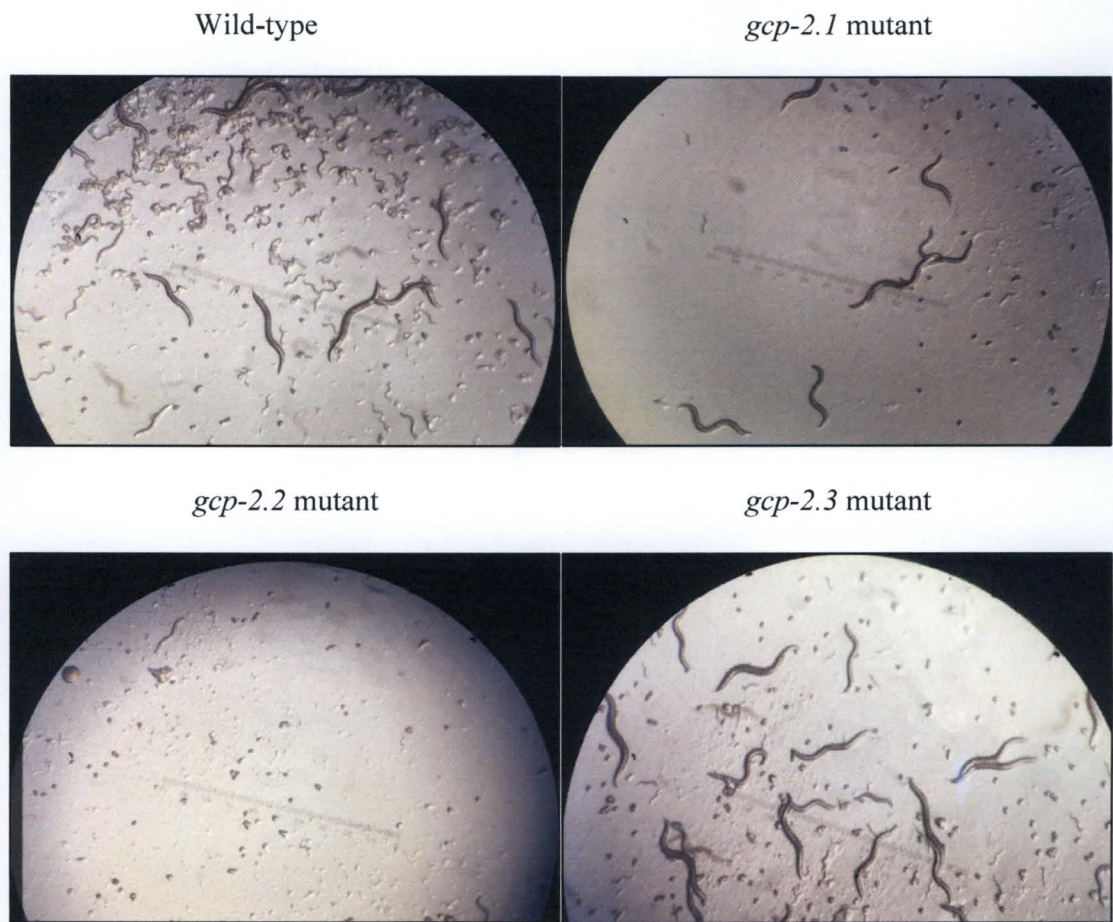


Figure 36. Growth assay showing growth phenotype of the wild-type and *gcp-2* mutants. *C. elegans* were maintained on 1000 $\mu\text{g}/\text{mL}$ SMX treated *E. coli* OP50.

3.10.2 The Effect of Reduced Dietary Folates on Development

In order to determine the effect of GCPII dependent folate metabolism on overall physiology and body development, body length assay was conducted in wild-type and *gcp-2* mutants maintained on *E. coli* OP50 grown with various concentrations of SMX. As mentioned in the Section 3.7, SMX inhibits folate biosynthesis and the synthesis of folates reduces with increasing SMX. This allows to investigate the effect of reduced dietary folate levels on *C. elegans*. Development was quantified as body length and the data shown are representative of three biological replicates of 3-5 worms each.

As shown in the Figure 37, the body length of wild-type worms was not affected by the varying concentrations of SMX. The average body length without SMX was 31.1 whereas when consumed on bacteria treated with 1 $\mu\text{g}/\text{mL}$ SMX, 31.9; 100 $\mu\text{g}/\text{mL}$, 27.7; and 1000 $\mu\text{g}/\text{mL}$, 30. Therefore, there was not a statistically significant ($p > 0.001$) body length change at the tested concentrations of 1 $\mu\text{g}/\text{mL}$, 100 $\mu\text{g}/\text{mL}$ and 1000 $\mu\text{g}/\text{mL}$ compared to that of the untreated control. The body length images of the wild-type worms at different SMX concentrations is shown in the Figure 38 which displays similar body length at various SMX concentrations.

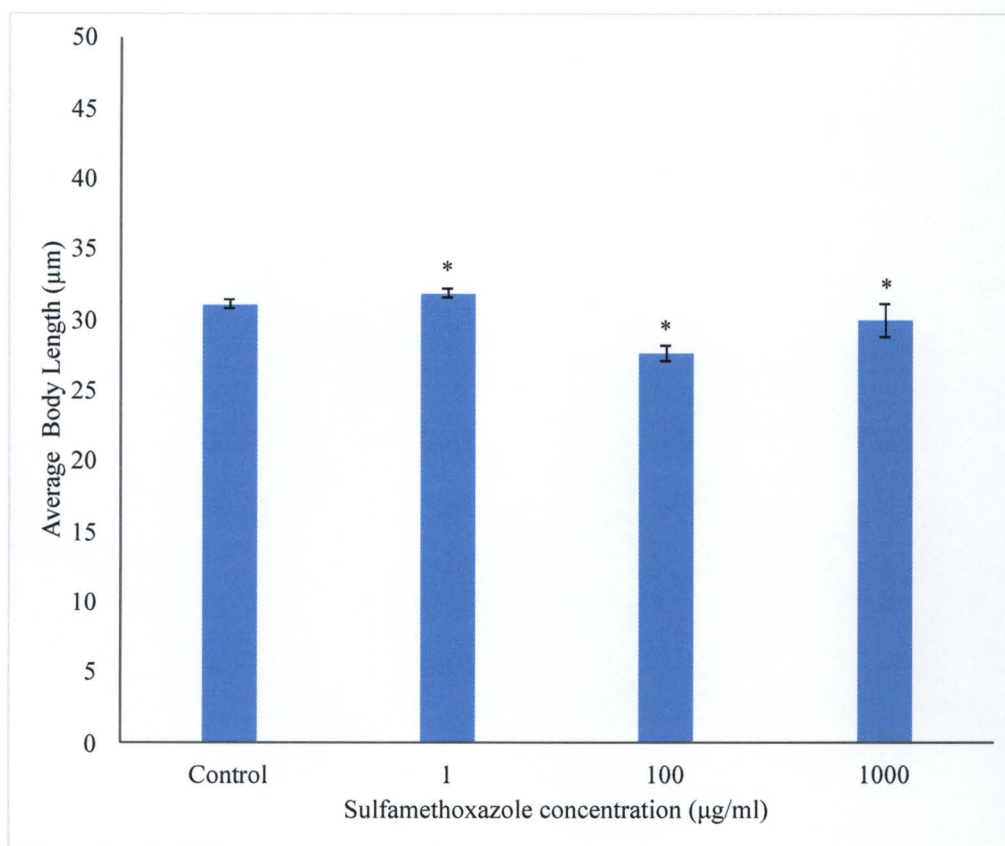


Figure 37. The effect of SMX dependent folate inhibition on body length of wild-type *C. elegans*.

The mean body length of control (no SMX), 31.1. The mean body length of worms maintained on *E. coli* treated with 1 µg/mL, 31.9 ($p = 0.04$); 100 µg/mL, 27.7 ($p = 0.0075$); and 1000 µg/mL, 30 ($p = 0.175616667$). Statistical significance was determined using two sample T-test ($*p > 0.001$, $**p < 0.001$). $**p < 0.001$ considered significant. The error bars represent \pm SEM. Data shown are representative of three biological replicates 3-5 worms each.

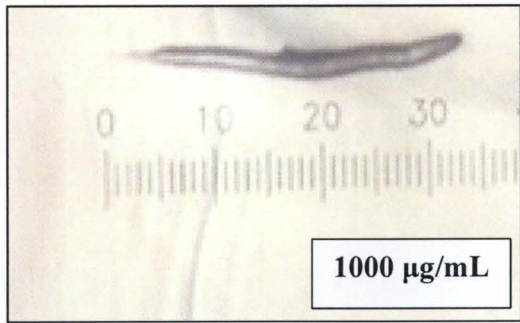
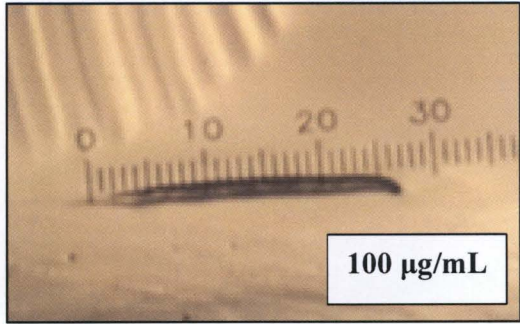
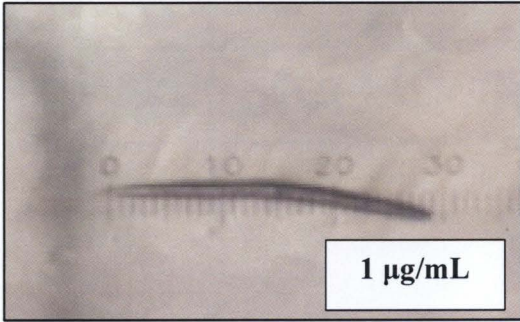
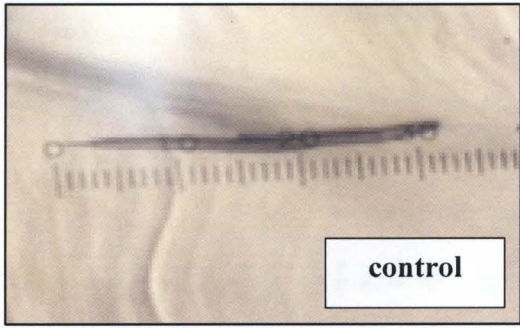


Figure 38. The images of wild-type worms at different concentrations of SMX.

As shown in the Figure 39, the body length of *gcp-2.1* worms were affected by the varying concentrations of SMX. The average body length without SMX was 37.4 (\pm) whereas when consumed on bacteria treated SMX showed the following body lengths: 1 $\mu\text{g}/\text{mL}$ SMX, 29.2 (\pm); 100 $\mu\text{g}/\text{mL}$, 27 (\pm); and 1000 $\mu\text{g}/\text{mL}$, 24.89 (\pm). There was a statistically significant ($p < 0.001$) decline in body length at 1 $\mu\text{g}/\text{mL}$, 100 $\mu\text{g}/\text{mL}$ and 1000 $\mu\text{g}/\text{mL}$ SMX compared to untreated worms. Therefore, SMX resulted 21.9% and 27% decline in body length at 1 $\mu\text{g}/\text{mL}$ and 100 $\mu\text{g}/\text{mL}$, respectively. At the IC_{50} concentration of SMX, 33.4% drop in body length was observed. The body length images of the *gcp-2.1* worms at different SMX concentrations is shown in the Figure 40. Furthermore, the worms that consumed SMX treated OP50 not only had shortened body length but also their body width was significantly reduced with increasing SMX concentrations, resulting in overall small sized worms compared to the control as visible from the Figure 40. Hence, data indicate that the development of *gcp-2.1* mutant worms were affected by SMX induced folate inhibition in a concentration dependent manner.

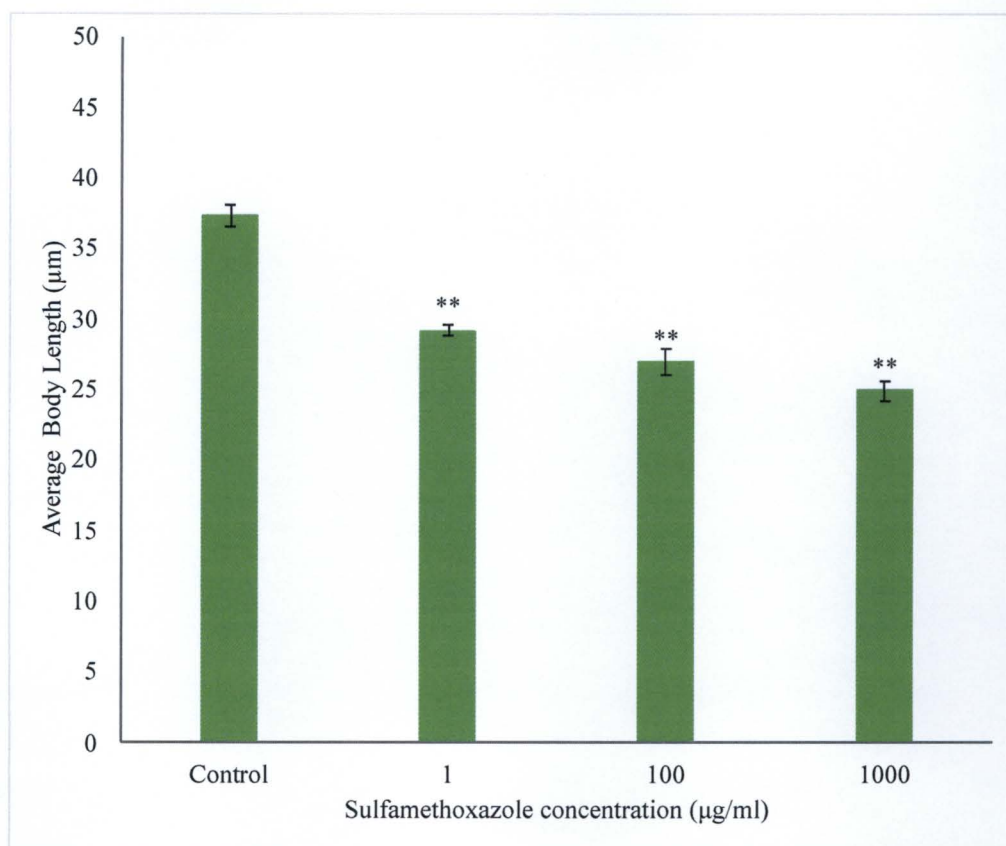


Figure 39. The effect of SMX dependent folate inhibition on body length of *gcp-2.1* mutant *C. elegans*.

The mean body length of control (no SMX), 37.4. The mean body length of worms maintained on *E. coli* treated with 1 µg/mL, 29.2 ($p= 1.35244E-08$); 100 µg/mL, 27 ($p= 8.8024E-08$); and 1000 µg/mL, 24.89 ($p= 9.6054E-10$). Statistical significance was determined using two sample T-test (* $p > 0.001$, ** $p < 0.001$). ** $p < 0.001$ considered significant. The error bars represent \pm SEM. Data shown are representative of three biological replicates 3-5 worms each.

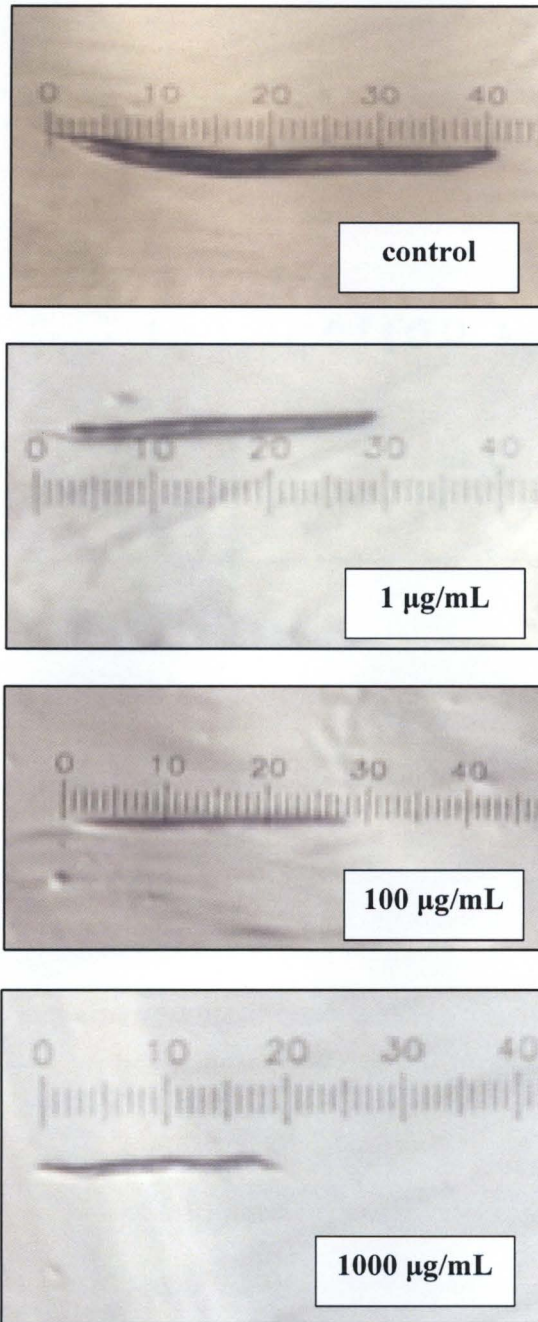


Figure 40. The images of *gcp-2.1* mutants at different concentrations of SMX.

As shown in the Figure 41, the body length of *gcp-2.2* worms were affected by the varying concentrations of SMX. The average body length without SMX was 43.1 (\pm) whereas when consumed on bacteria treated with SMX the body lengths were as follows: 1 $\mu\text{g}/\text{mL}$ SMX, 34.9 (\pm); 100 $\mu\text{g}/\text{mL}$, 32.6 (\pm); and 1000 $\mu\text{g}/\text{mL}$, 36.6 (\pm). There was a statistically significant ($p < 0.001$) decline in body length at 1 $\mu\text{g}/\text{mL}$, 100 $\mu\text{g}/\text{mL}$ and 1000 $\mu\text{g}/\text{mL}$ SMX. Therefore, SMX resulted 19% and 24.3% decline in body length at 1 $\mu\text{g}/\text{mL}$ and 100 $\mu\text{g}/\text{mL}$, respectively. At the IC_{50} concentration of SMX, 15% drop in body length was observed. The body length images of the *gcp-2.2* worms at different SMX concentrations is shown in the Figure 42. This displays the shortening of body length with SMX compared to the untreated control and body width was similar. Although, the development of worms was affected by SMX, there was not a significant variation among different concentrations. Hence, data indicates that the development of *gcp-2.2* mutant worms were affected by SMX induced folate inhibition in but not in a concentration dependent pattern.

As shown in the Figure 43, the body length of *gcp-2.3* worms were affected by SMX. The average body length without SMX was 28.2 (\pm) whereas when consumed on bacteria treated with SMX showed the following body lengths: 1 $\mu\text{g}/\text{mL}$ SMX, 30.8 (\pm); 100 $\mu\text{g}/\text{mL}$, 27.4 (\pm); and 1000 $\mu\text{g}/\text{mL}$, 20.7 (\pm). There was not a statistically significant ($p > 0.001$) decline in body length at 1 $\mu\text{g}/\text{mL}$, and 100 $\mu\text{g}/\text{mL}$. However, at the IC_{50} concentration of SMX (1000 $\mu\text{g}/\text{mL}$) SMX, 26.6% drop in body length was observed. Hence, data indicates that the development of *gcp-2.3* mutant worms were affected by SMX induced folate inhibition at higher concentrations of SMX.

Taken together, the development of wild-type and *gcp-2.3* mutant strains were not affected by SMX whereas the development of *gcp-2.1* and *gcp-2.2* mutants affected by SMX induced folate inhibition.

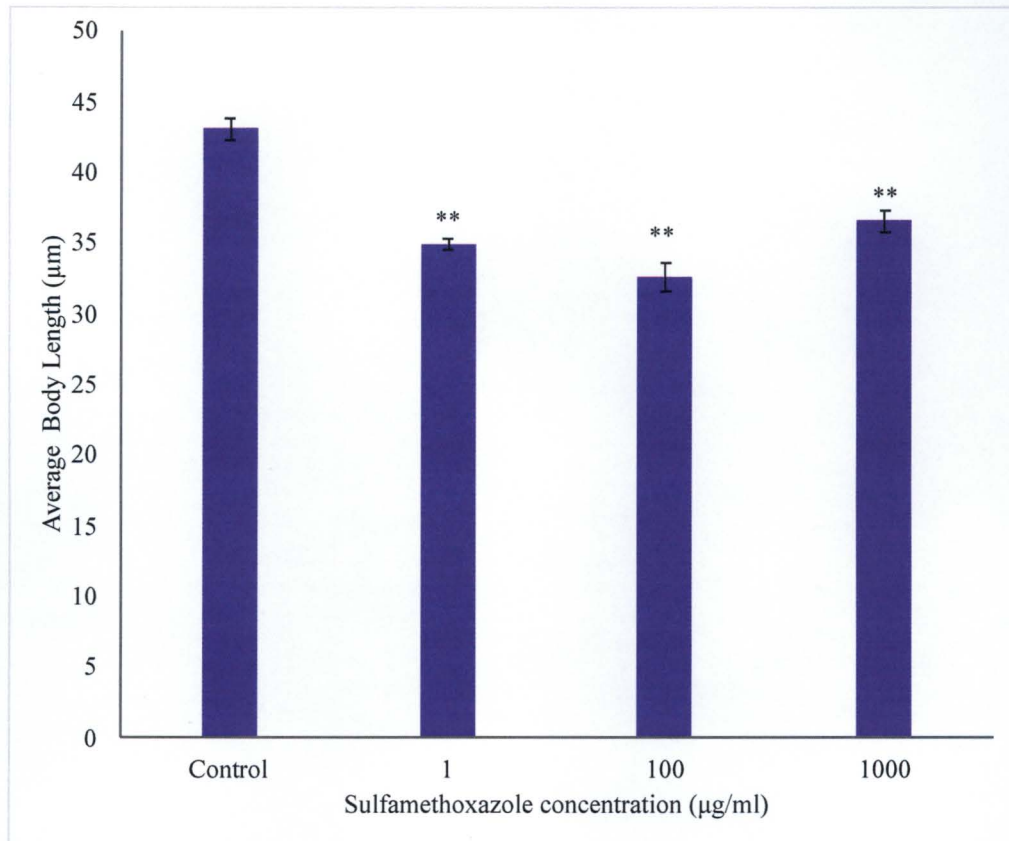


Figure 41. The effect of SMX dependent folate inhibition on body length of *gcp-2.2* mutant *C. elegans*.

The mean body length of control (no SMX), 43.1. The mean body length of worms maintained on *E. coli* treated with 1 µg/mL, 34.9. ($p=2.36531E-07$); 100 µg/mL, 32.6 ($p=2.58029E-06$); and 1000 µg/mL, 36.6 ($p=0.00036$). Statistical significance was determined using two sample T-test (* $p > 0.001$, ** $p < 0.001$). ** $p < 0.001$ considered significant. The error bars represent \pm SEM. Data shown are representative of three biological replicates 3-5 worms each.

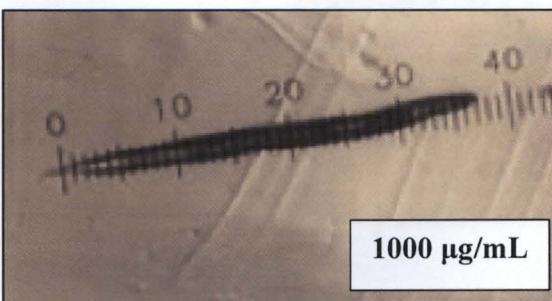
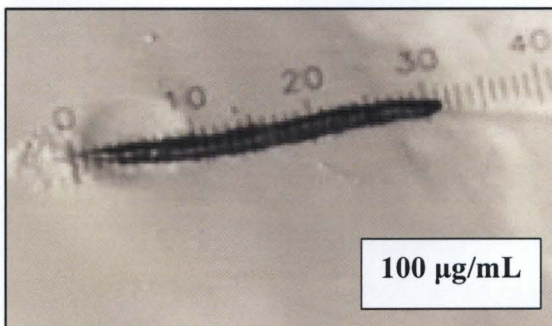
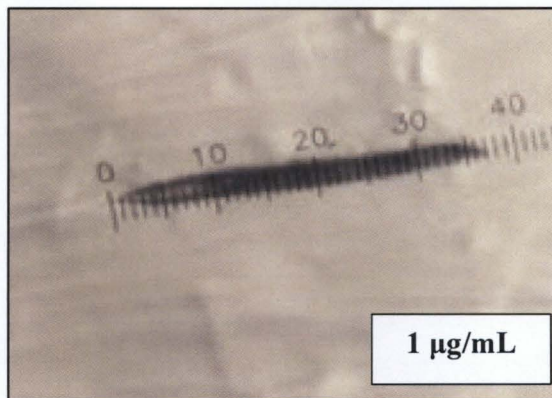
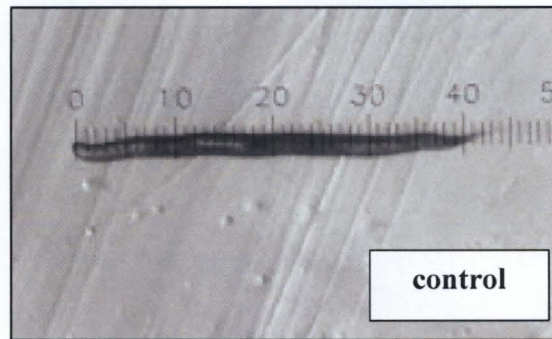


Figure 42. The images of *gcp-2.2* mutants at different concentrations of SMX

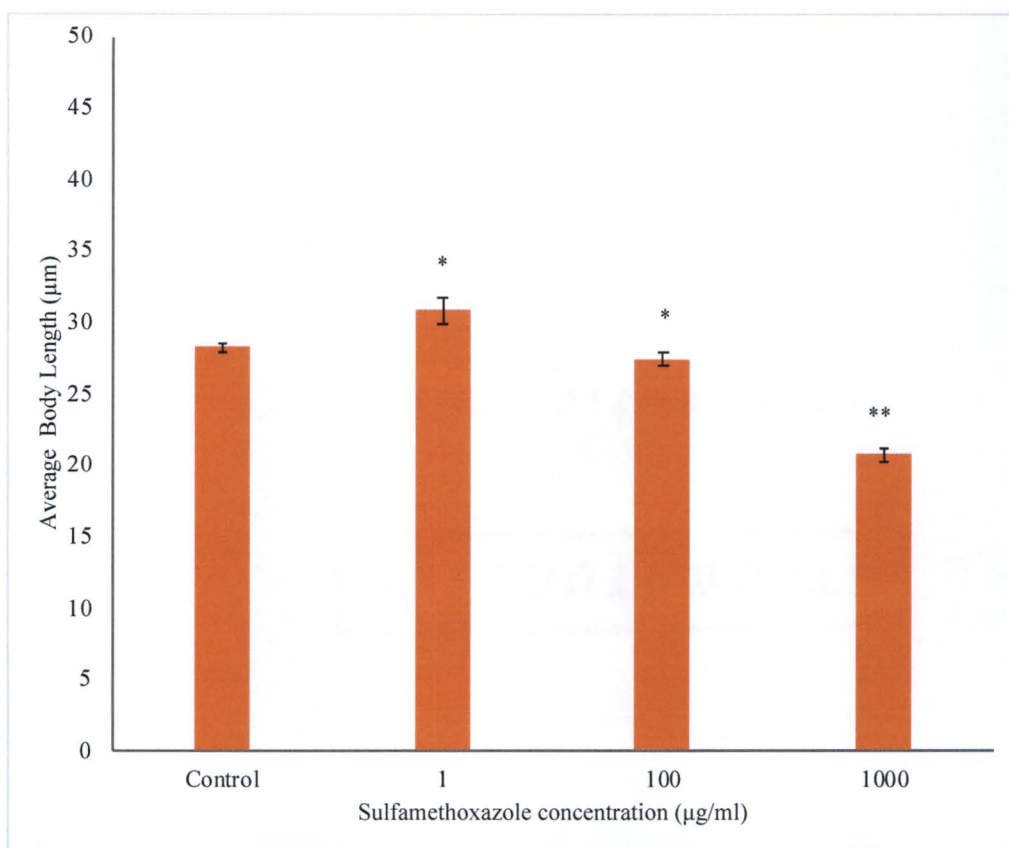


Figure 43. The effect of SMX dependent folate inhibition on body length of *gcp-2.3* mutant *C. elegans*.

The mean body length of control (no SMX), 28.2. The mean body length of worms maintained on *E. coli* treated with 1 µg/mL, 30.8 ($p = 0.01$); 100 µg/mL, 27.4 ($p = 0.091$); and 1000 µg/mL, 20.7 ($p = 1.9501E-11$). Statistical significance was determined using two sample T-test (* $p > 0.001$, ** $p < 0.001$). ** $p < 0.001$ considered significant. The error bars represent \pm SEM. Data shown are representative of three biological replicates 3-5 worms each.

3.10.3 The Effect of Folinic Acid (5-Formyl-THF) Supplementation

Folinic acid, 5-Formyl-THF, is an important folate derivative that can be transformed into other folate derivatives as shown in Figure 28. I hypothesize that supplementation of SMX treated OP50 food is expected to reverse the effects of SMX-mediated folate availability on brood size and body lengths. In order to determine the effect of folinic acid supplementation on GCPII dependent folate metabolism on reproduction, brood size assays were conducted in wild-type and *gcp-2* mutants maintained on *E. coli* OP50 grown with 1000 µg/mL of SMX and supplemented with 10 µM Folinic acid. This concentration of Folinic acid was used as it was previously reported to reverse the effects of folate inhibition in body length (106). This allows to investigate the efficacy of folate supplementation on folate deficient *C. elegans-E. coli* model. Reproduction was quantified as progeny size and the data shown are representative of one biological replicate with five worms.

The effect of folinic acid supplementation in reversing the effects of 1000 µg/mL SMX induced folate inhibition was shown in the Figure 44. The mean brood size of wild-type without supplementation, 81.2 (±3.9) and with supplementation, 105 (±2.5). This is a 29% increase in reproduction and statistically significant ($p < 0.001$). The mean brood size of *gcp-2.1* without supplementation, 2.9 (±0.4) and with supplementation, 2.7 (±0.4), showing no statistically significant ($p > 0.001$) effect in reproduction. The *gcp-2.2* were sterile without supplementation and with supplementation worms were slightly fertile with an average brood size of 2.2 (±0.5). This is a statistically significant ($p < 0.001$) increase in reproduction. The mean brood size of *gcp-2.3* without supplementation, 43.7 (±2.4) and with supplementation, 44.8 (±5.5). Therefore, there is no statistically significant ($p > 0.001$)

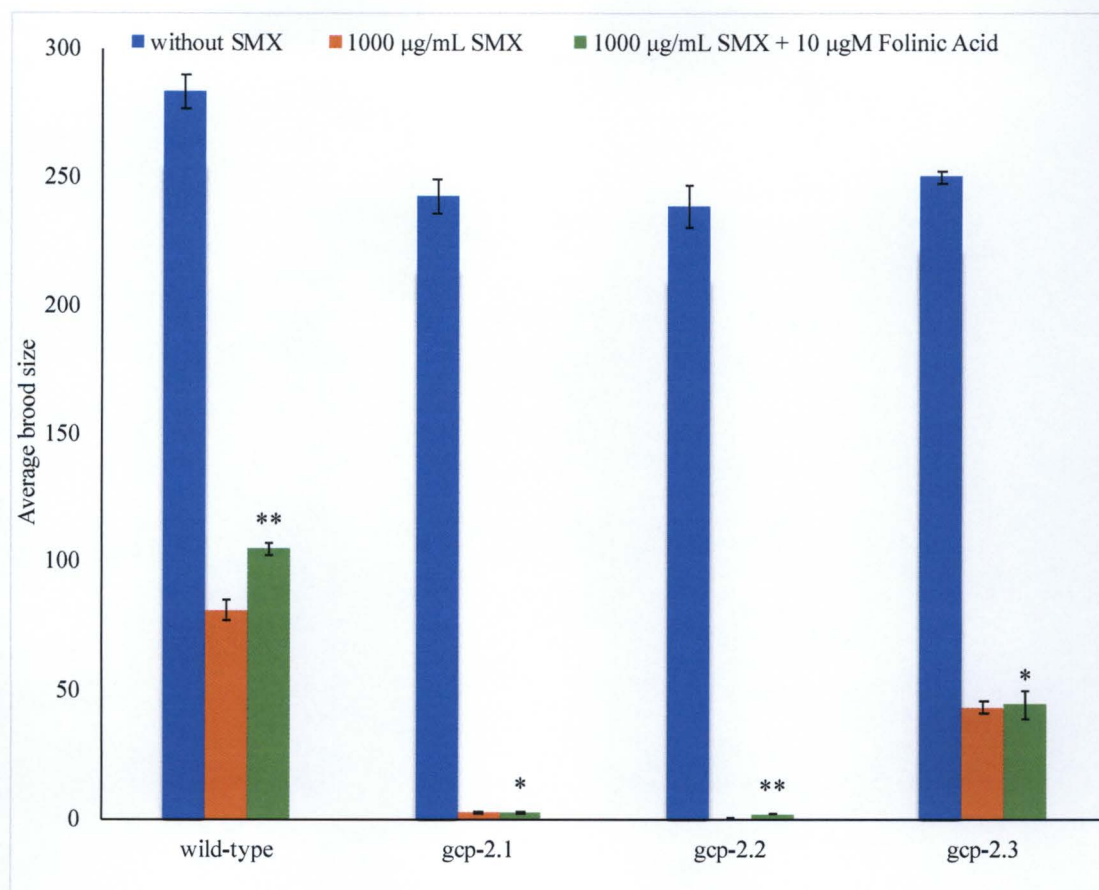


Figure 44. The effect of Folinic Acid supplementation on brood size of *C. elegans* that were supplied with 1000 µg/mL SMX treated OP50 as food.

The mean brood size of wild-type without supplementation, 81.2 and with supplementation, 105 ($p=3.7996E-05$). The mean brood size of *gcp-2.1* mutants without supplementation, 2.9 and with supplementation, 2.7 ($p=0.39$). The mean brood size of *gcp-2.2* mutants without supplementation, sterile and with supplementation, 2.2 ($p=0.0008$). The mean brood size of *gcp-2.3* without supplementation, 43.7 and with supplementation, 44.8 ($p=0.429$). Statistical significance was determined using two sample T-test (* $p > 0.001$, ** $p < 0.001$). ** $p < 0.001$ considered significant. The error bars represent \pm SEM. Data shown are representative of one biological replicate with 5 worms.

effect in reproduction. Hence, folic acid supplementation was effective in reversing the effect of SMX induced folate inhibition on reproduction of wild-type and to some extent in *gcp-2.2* worms but not *gcp-2.1* and *gcp-2.3* mutants.

In order to determine the effect of folic acid supplementation on GCPII dependent folate metabolism on development, body length assay was conducted in wild-type and *gcp-2* mutants maintained on *E. coli* OP50 grown with varying concentrations of SMX and supplemented with 10 μ M Folic acid. This allows to investigate the efficacy of folate supplementation on folate deficient *C. elegans-E. coli* model. Development was quantified as body length and the data shown are representative of two biological replicates with five worms each.

The effect of folic acid supplementation in reversing the developmental effects of SMX induced folate inhibition was shown in the Figures 47-49. When folic acid was supplemented to worms maintained on *E. coli* without SMX, only wild-type showed statistically significant ($p < 0.001$) increase in body length which was a 6.5% increase (Figure 45). When folic acid was supplemented to worms maintained on *E. coli* with 100 μ g/mL SMX, only *gcp-2.2* showed statistically significant ($p < 0.001$) increase in body length which was a 8.1% increase. When folic acid was supplemented to worms maintained on *E. coli* with 1000 μ g/mL SMX, only *gcp-2.2* showed statistically significant ($p < 0.001$) increase in body length which was a 22.4% increase. Therefore, folic acid supplementation induced development of wild-type and *gcp-2.2* mutants.

Taken together, folic acid supplementation was effective in reversing the effect of SMX induced folate inhibition on reproduction of wild-type worms not *gcp-2* mutants.

Additionally, folic acid supplementation was effective in reversing the effect of SMX induced folate inhibition on development of *gcp-2.2* mutants.

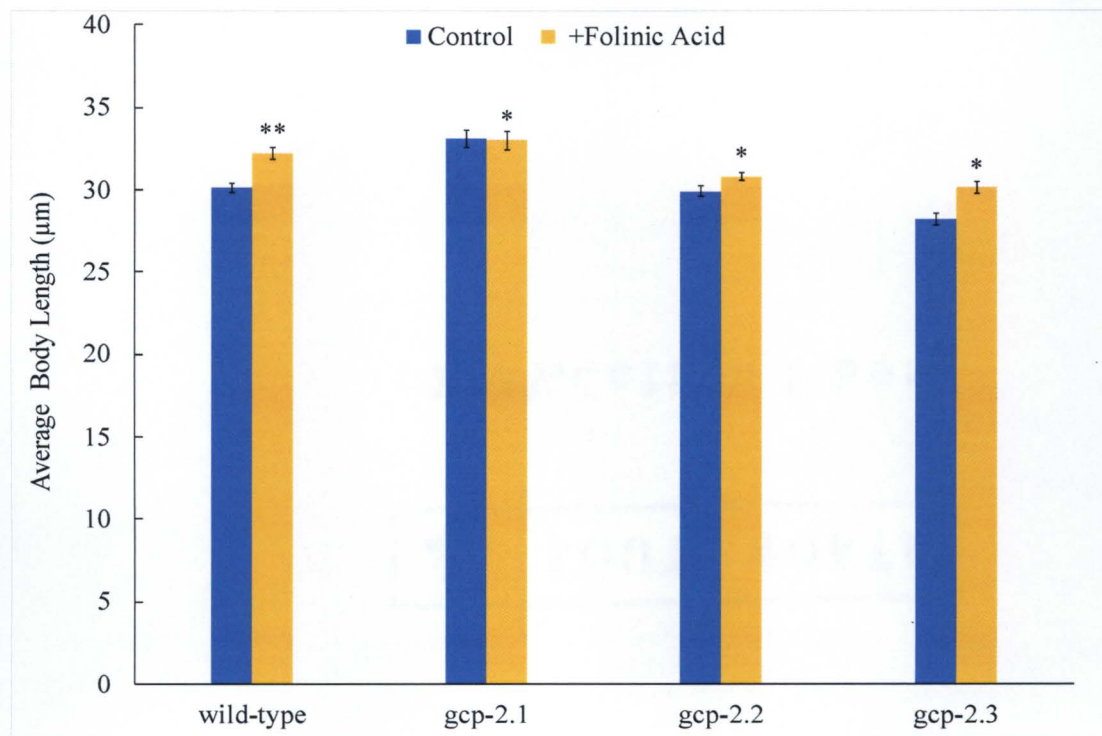


Figure 45. The effect of folic acid supplementation on the body length untreated controls.

The mean body length of wild-type without supplementation, 30.1 and with supplementation, 32.2 ($p=0.00066$). The mean body length of *gcp-2.1* mutants without supplementation, 33.1 and with supplementation, 33 ($p=0.43$). The mean body length of *gcp-2.2* mutants without supplementation, 29.9 and with supplementation, 30.8 ($p=0.033$). The mean body length of *gcp-2.3* without supplementation, 28.2 and with supplementation, 30.1 ($p=0.0059$). Statistical significance was determined using two sample T-test (* $p > 0.001$, ** $p < 0.001$). ** $p < 0.001$ considered significant. The error bars represent \pm SEM. Data shown are representative of two biological replicates with 5 worms each.

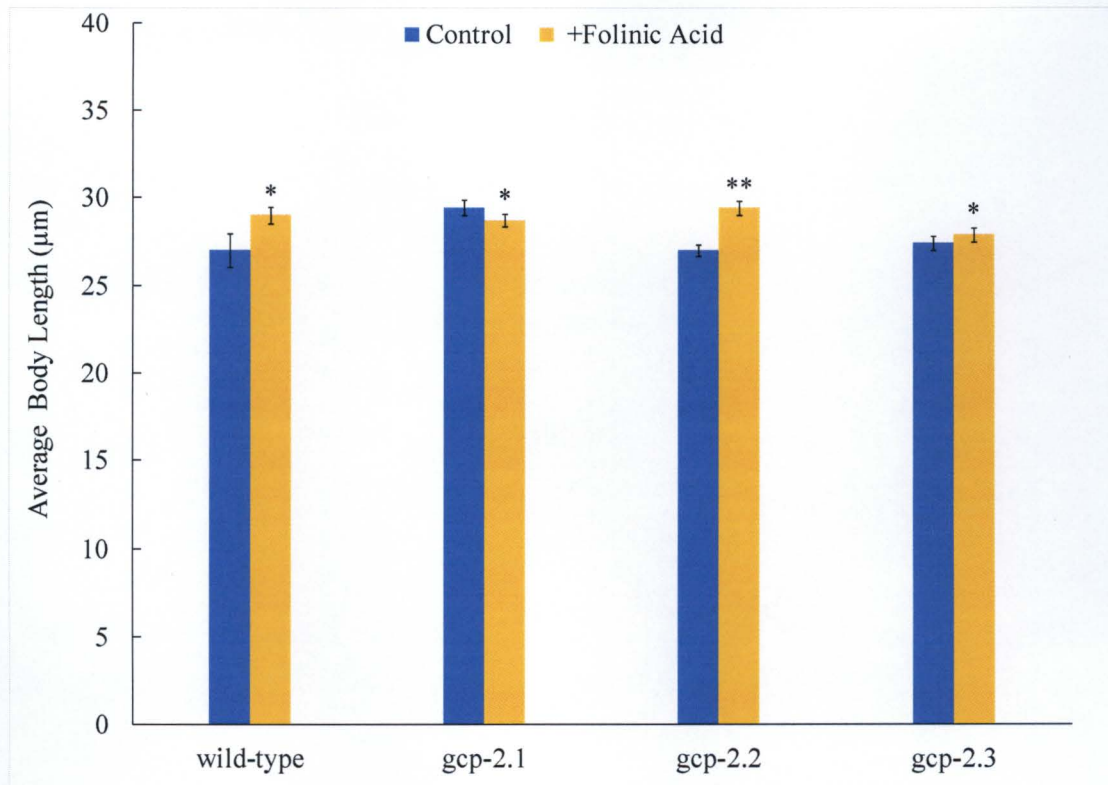


Figure 46. The effect of folinic acid supplementation on the body length of worms maintained on *E. coli* treated with 100 µg/mL SMX.

The mean body length of wild-type without supplementation, 27 and with supplementation, 29 ($p= 0.012$). The mean body length of *gcp-2.1* mutants without supplementation, 29.4 and with supplementation, 28.7 ($p= 0.149$). The mean body length of *gcp-2.2* mutants without supplementation, 27 and with supplementation, 29.4 ($p= 0.00035$). The mean body length of *gcp-2.3* without supplementation, 27.4 and with supplementation, 27.9 ($p= 0.1493$). Statistical significance was determined using two sample T-test (* $p > 0.001$, ** $p < 0.001$). ** $p < 0.001$ considered significant. The error bars represent \pm SEM. Data shown are representative of two biological replicates with 5 worms each.

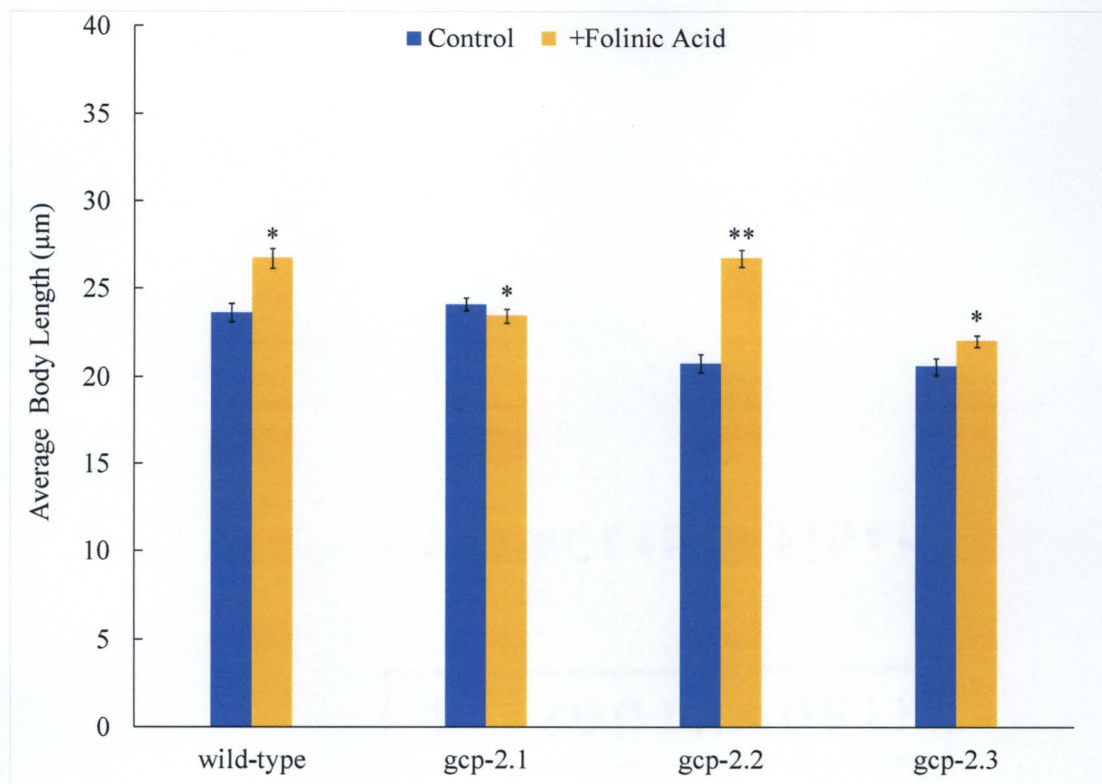


Figure 47. The effect of folic acid supplementation on the body length of worms maintained on *E. coli* treated with 1000 µg/mL SMX.

The mean body length of wild-type without supplementation, 23.6 and with supplementation, 26.7 (0.0016). The mean body length of *gcp-2.1* mutants without supplementation, 24 and with supplementation, 23.45 ($p=0.148$). The mean body length of *gcp-2.2* mutants without supplementation, 20.7 and with supplementation, 26.7 ($p=3.22583E-08$). The mean body length of *gcp-2.3* without supplementation, 20.54 and with supplementation, 22 (0.0073). Statistical significance was determined using two sample T-test (* $p > 0.001$, ** $p < 0.001$). ** $p < 0.001$ considered significant. The error bars represent \pm SEM. Data shown are representative of two biological replicates with 5 worms each.

3.10.4 Identification and Quantitation of Folate Derivative in *E. coli* OP50

In order to further understand the effect of folate derivatives mediated reproductive and physiological effects on wild type and GCPII mutant *C. elegans* we aimed to identify the folate derivatives present in the *E. coli* OP50 food source. In order to identify folate derivatives both ¹H-NMR and HPLC techniques were attempted. For the quantitation of folate derivatives HPLC methods were used.

NMR Based Folate Analysis

In order to detect different forms of folates present in bacterial folate extract folic acid standards were analyzed using ¹H-NMR. However, this experiment was not successful in identifying folates as I was not able to detect the distinct peaks that can be assigned to corresponding to folates unequivocally and therefore further analysis of folate were conducted using HPLC methods only. NMR spectra are shown the Appendix 4.

3.10.5 HPLC Based Folate Analysis

Analyses of Folate Derivative Standards

Analyses of folate standards were performed using HPLC to identify the peaks corresponding different forms of folates. All standards were dissolved in extraction buffer and monitored with a fluorescence detector set to excitation at 295 nm and emission at 360 nm. The peaks of each folate standard are shown in the Table 6.

Folate Extract

Analyses of folate extracts from *E. coli* OP50 were performed using HPLC to identify the different forms of folates present. The absorbance was monitored with a fluorescence

detector set to excitation at 295 nm and emission at 360 nm. The HPLC spectra for folate extracts is shown in figure 57. Spectra of bacterial folate extracts showed the peaks for Extraction Buffer

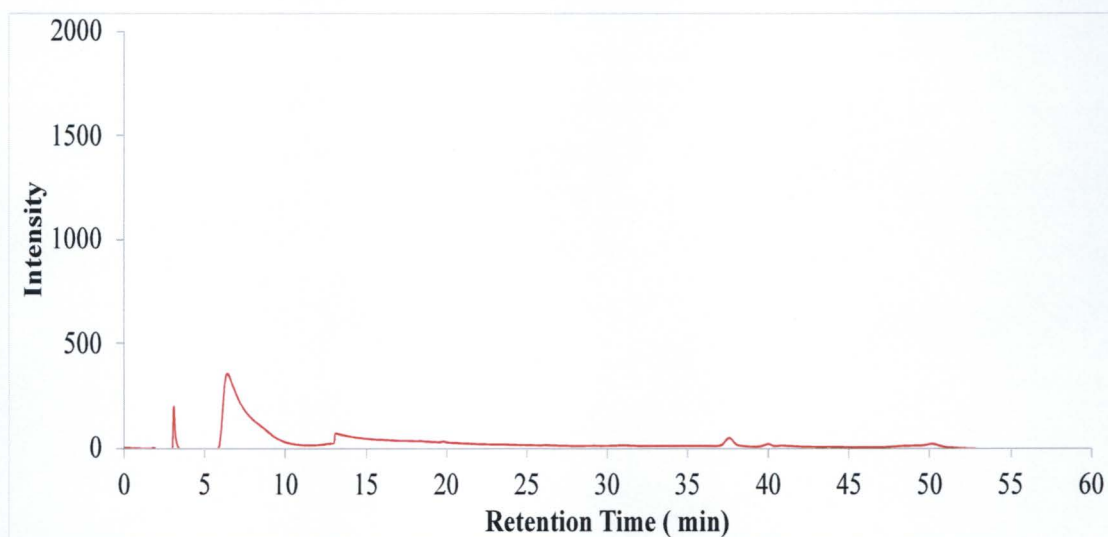


Figure 48. Chromatogram with florescence intensity of Extraction buffer without folates.

The separation of folates was performed using Hypersil ODS C18 analytical column with a flow rate of 0.8 mL/min at 4 °C. Intensity was monitored with a fluorescence detector set to excitation at 295 nm and emission at 360 nm.

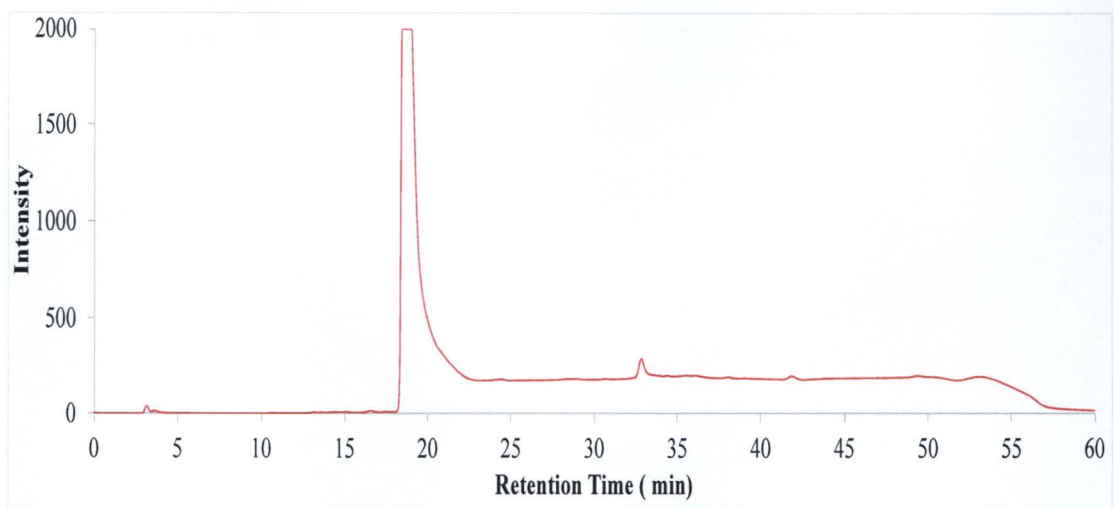


Figure 49. Chromatogram with fluorescence intensity of DHF standards.

DHF was dissolved in extraction buffer (5 mg/mL). Intensity was monitored with a fluorescence detector set to excitation at 295 nm and emission at 360 nm.

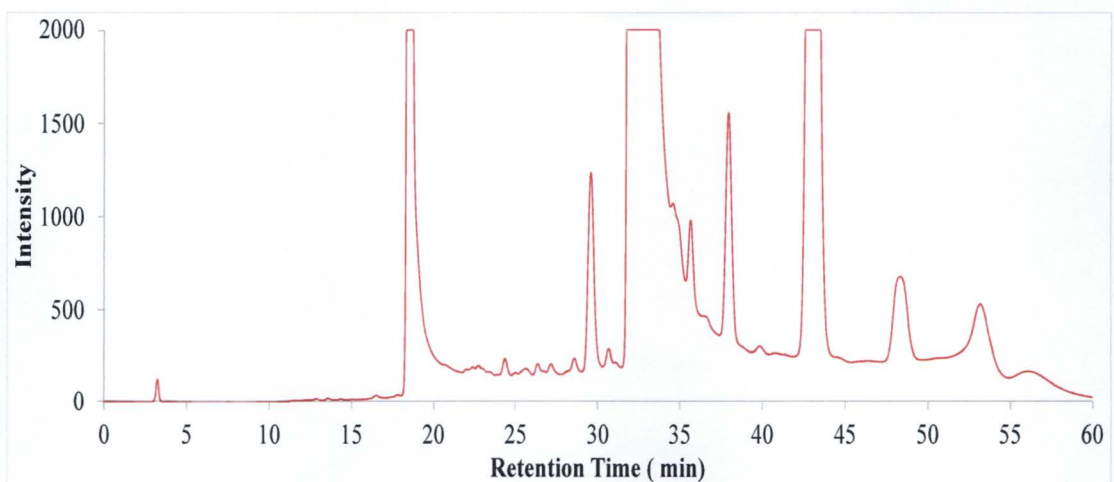


Figure 50. Chromatogram with fluorescence intensity of THF standard.

THF was dissolved in extraction buffer (5 mg/mL). Intensity was monitored with a fluorescence detector set to excitation at 295 nm and emission at 360 nm.

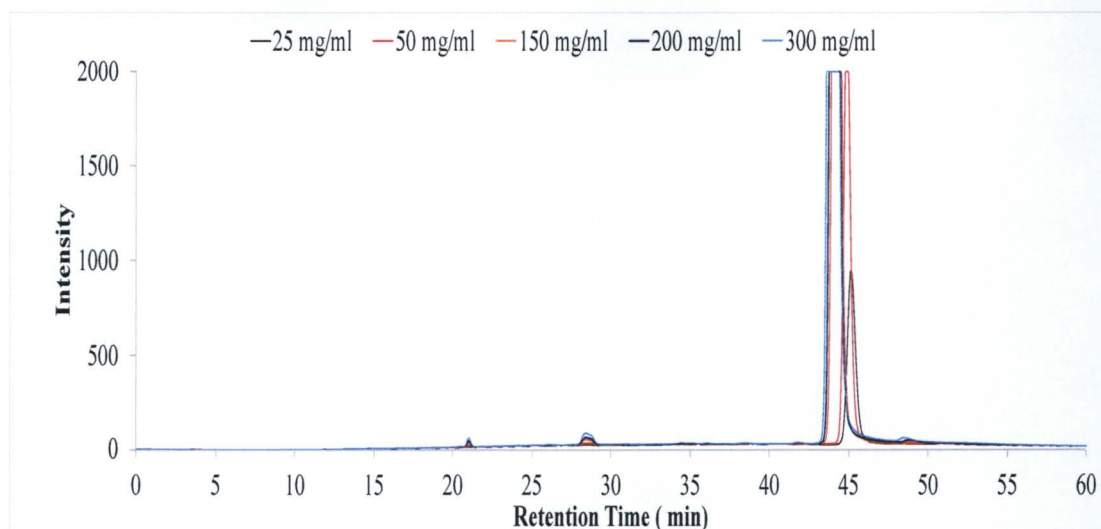


Figure 51. Chromatogram with fluorescence intensity of 5-Methyl-THF standard.

5-Methyl-THF was dissolved in extraction buffer (25-300 mg/mL). Intensity was monitored with a fluorescence detector set to excitation at 295 nm and emission at 360 nm.

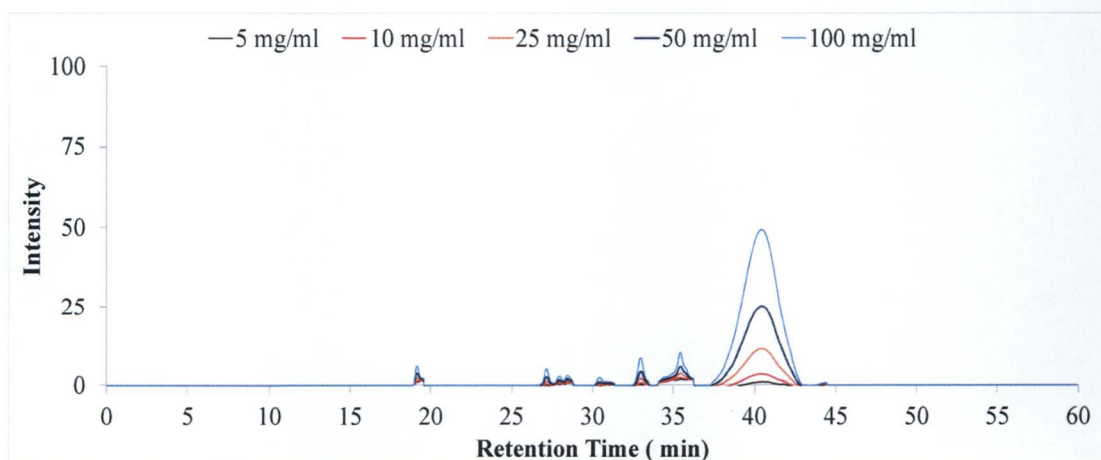


Figure 52. Chromatogram with fluorescence intensity of 5-Formyl-THF standard.

5-Formyl-THF was dissolved in extraction buffer (5-100 mg/mL). Intensity was monitored with a fluorescence detector set to excitation at 295 nm and emission at 360 nm.

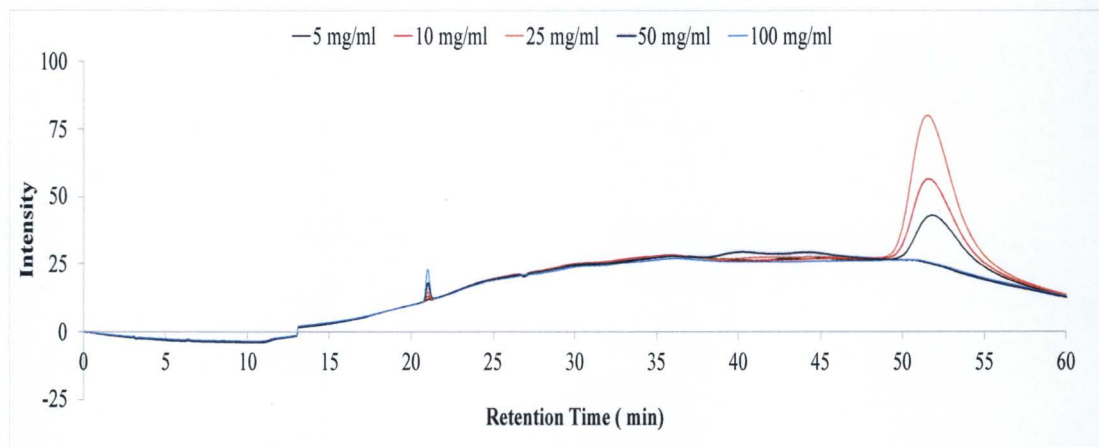


Figure 53. Chromatogram with fluorescence intensity of Folic Acid standard.

Folic Acid was dissolved in extraction buffer (5-100 mg/mL). Intensity was monitored with a fluorescence detector set to excitation at 295 nm and emission at 360 nm.

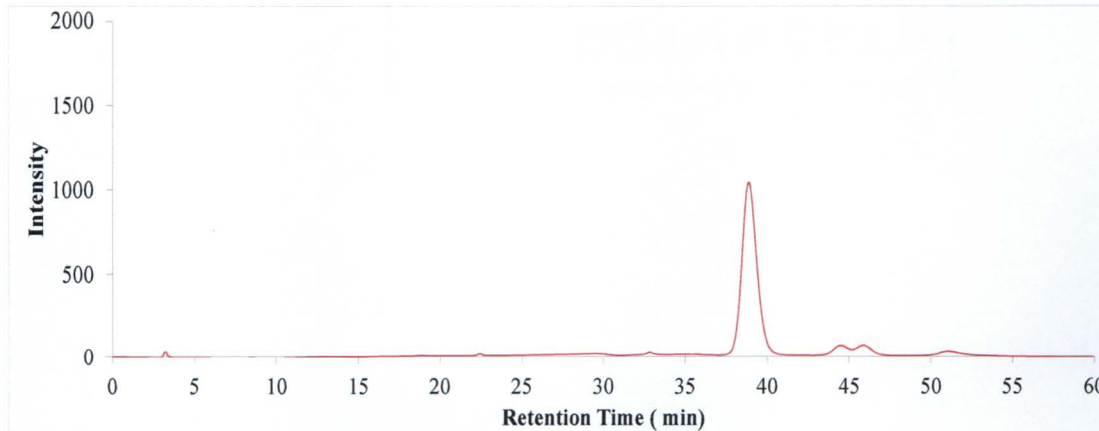


Figure 54. Chromatogram with fluorescence intensity of L-Glutamic Acid standard.

L-Glutamic acid was dissolved in extraction buffer (10 mg/mL). Intensity was monitored with a fluorescence detector set to excitation at 295 nm and emission at 360 nm.

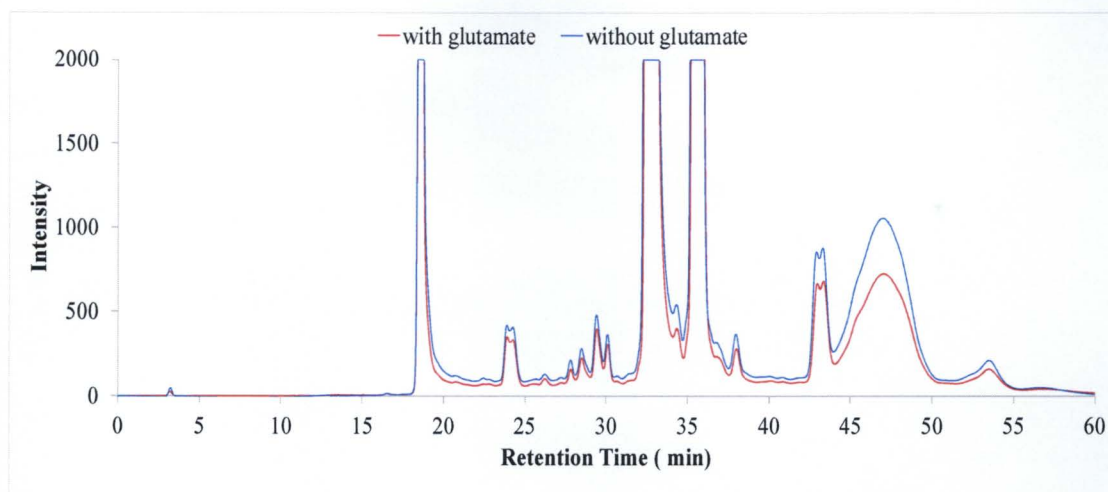


Figure 55. Chromatogram with fluorescence intensity of a mixture of different folate forms.

This sample contained 5 mg/mL DHF, THF, Folinic acid, Folic acid and 5-Methyl-THF. All folate derivatives were dissolved in extraction buffer. Intensity was monitored with a fluorescence detector set to excitation at 295 nm and emission at 360 nm.

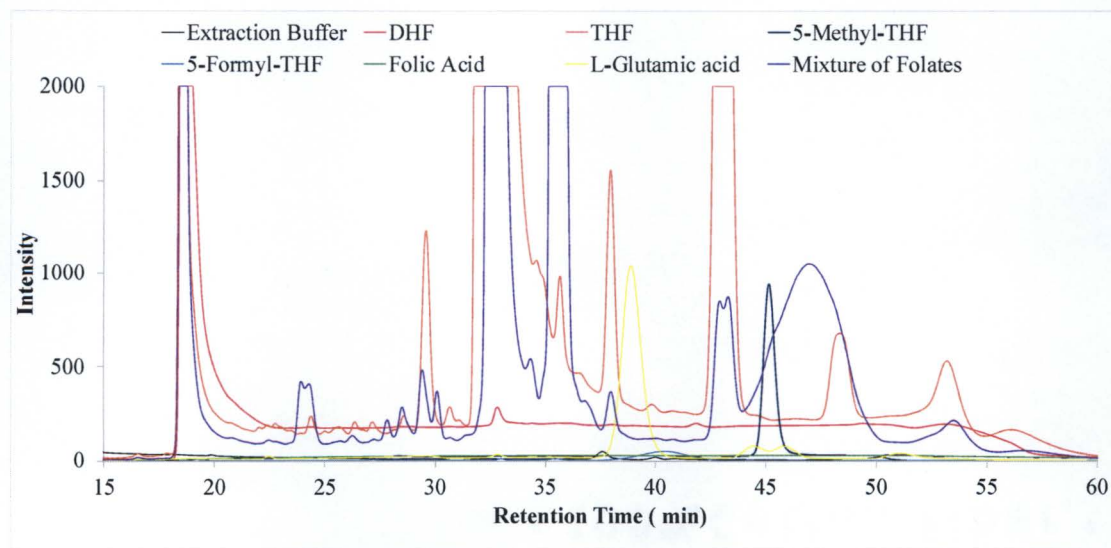


Figure 56. Comparative chromatogram of different folate forms.

This figure contains chromatograms from Figure 48-55

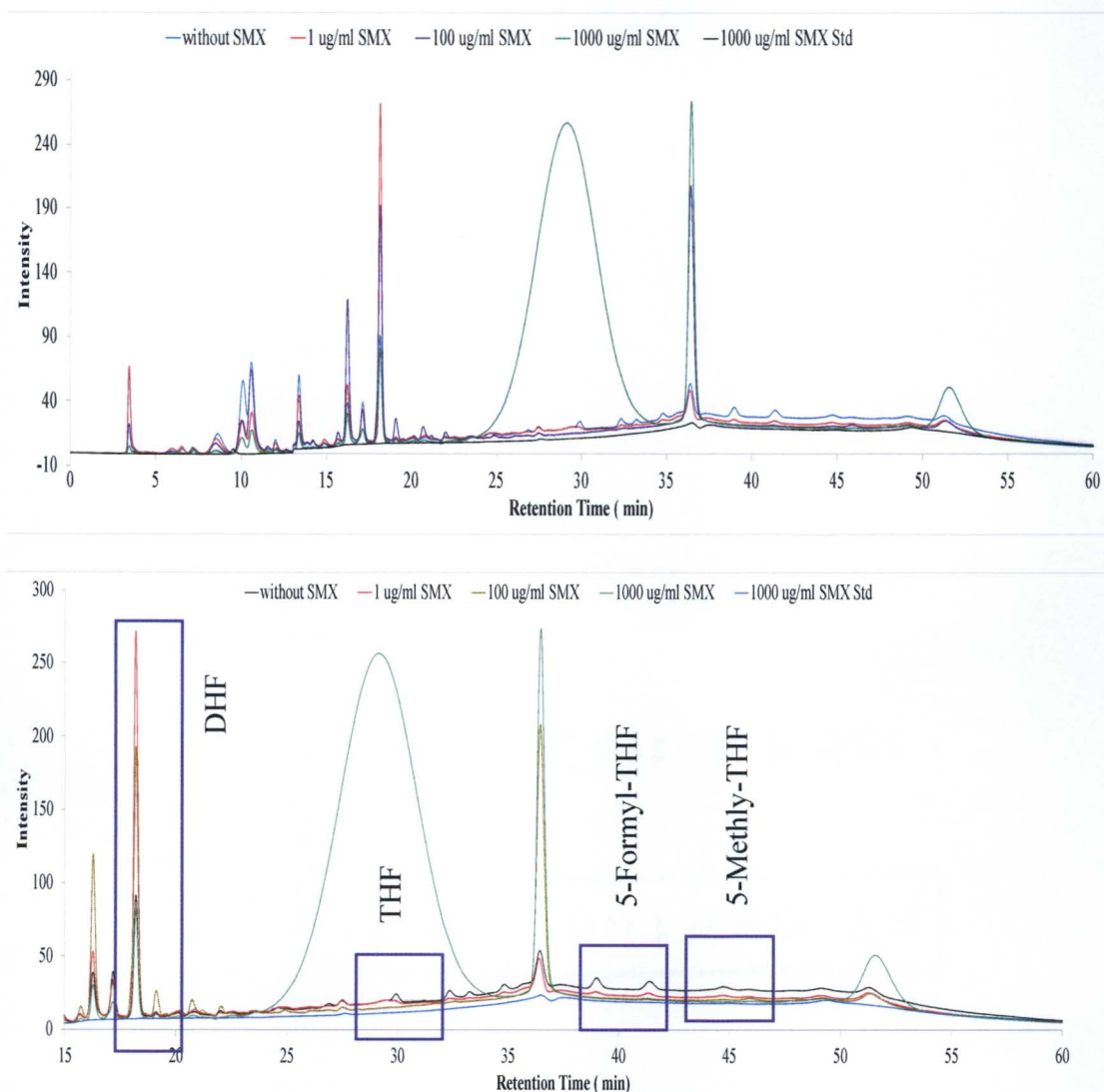


Figure 57. Overlaid Chromatograms with fluorescence intensity of *E. coli* OP50 folate extracts with varying concentrations of SMX.

Top – full chromatogram; bottom – zoomed in version (15-60 min). All folate extracts were prepared in extraction buffer. Intensity was monitored with a fluorescence detector set to excitation at 295 nm and emission at 360 nm. *E. coli* OP50 folate extracts exhibited peaks for DHF, THF, 5-Formyl-THF, and 5-Methyl-THF.

Table 6. Fluorescence Detection of Folate Standard. ^a

Compound ^b	Concentration (mg/mL)	Retention Time (min)	Peak Height (intensity)	<i>E. coli</i> OP50 Extract
DHF	5	18.1-22.7	2000	✓ ^c
		18.12-20.32	2000	✓
THF	5	29.1-30.29	1197	
		31.48-37.41	2000	
		37.51-38.94	1559	
		42.1-44.46	2000	
		47.52-49.2	658	
		52.25-54.9	504	
5-Methyl-THF	25	44.61-45.8	903	✓
	50	44.37-45.7	2000	
	150	43.6-44.95	2000	
	200	43.3-44.98	2000	
Folic acid	50	20.81-21.26	18.14	ND ^d
	200	20.80-21.29	23.24	
5-Formyl-THF	50	37.38-42.85	25	✓
(Folinic acid)	100	37.39-42.91	49	
L-Glutamic acid	10	37.1-40.57	1012	ND

^a All compounds were dissolved in extraction buffer and monitored with a fluorescence detector (excitation at 295 nm and emission at 360 nm)

^b Refer to Figure 50-56

^c ✓, detected in *E. coli* OP50 folate extract

^d ND, not detected in *E. coli* OP50 folate extract

3.11 Discussion

Chapter 2 concludes that mutations in cGCPII and *gcp-2* paralogs reduced progeny production and negatively impacted development of *C. elegans* to different extents. However, the underlying mechanism for these observations is unclear. Therefore, Chapter 3 aims to shed light on the predicted multiple biological functions, biochemical mechanisms and pathways by which cGCPII affects these physiological parameters. In particular, this chapter focuses on illustrating the function of cGCPII and *gcp-2* paralogs in folate metabolism in regulating reproduction, embryonic and post-embryonic development of *C. elegans*.

As shown in the comparative Figure 58, all the *gcp-2* mutants show slightly reduced progeny production compared to wild-type. Furthermore, more strikingly, all strains showed a concentration dependent decline in brood size *i.e.* as SMX induced folate biosynthesis inhibition increases, progeny size decreases. Therefore, the decrease of reproduction with increasing folate inhibition indicate that there is a link between folate metabolism and reproduction. Furthermore, the observed differences in progeny production between wild-type and strains with mutations in *gcp-2* paralogs indicate that cGCPII plays a role in reproduction through regulating folate metabolism.

C. elegans has two putative orthologs to the human reduced folate carrier (hRFC), referred as *folt-1* and *folt-2*. The expression of these genes is regulated during development and present in different tissues with highest expression levels in pharynx and intestine (145). FOLT-1 and FOLT-2 exhibits similar characteristics to hRFC such as similar affinity for oxidized, reduced, and substituted folate derivatives. Furthermore, the amino acid sequence of *folt-1* has high sequential similarity with the substrate binding domains of

hRFC (145). As mentioned in the Section 3.4, hRFC are highly selective towards monoglutamated folates. However, whether the folate carriers in *C. elegans* display similar selectivity for monoglutamated folates have not yet been reported. Nevertheless, if *folT-1* and *folT-2* shows similar functional characteristics and similar protein sequence in substrate binding domains with hRFC, therefore, it is possible that these transporters could be selective towards monoglutamated folates. Folate derivatives in *E. coli* OP50 is produced as polyglutamates with three to seven glutamate residues (119). In those instances, the hydrolytic enzyme function of GCPII can be vital in cleaving off γ -linked glutamates from polyglutamated folates (Figure 27) in *C. elegans*. Bases on this information, a hypothetical model elaborating the mechanism of GCPII in folate metabolism in *C. elegans* is shown in the Figure 59. In brief, (i) cGCPII hydrolyzes dietary polyglutamated-folates to monoglutamated folates in the intestinal lumen, (ii) monoglutamated folates are absorbed into enterocytes via folate transporters (FOLT-1/FOLT-2) present in the enterocyte membranes facing the intestinal lumen, (iii) enterocytes metabolize all different folates to 5-Methyl-THF and (iv) Folates are transported out into interstitial space and carried around the body by the interstitial fluid to be taken up by other cells for one-carbon metabolism necessary for reproduction, other cellular functions and overall physiology.

Two obvious questions are what happen's to folates after absorption and how folates contribute to reproduction? As mentioned in the Section 1.4, *C. elegans* enterocytes use absorbed nutrients to synthesise yolk and secrete as free-floating granules into pseudocoelomic space which is then transported to the oocytes in the proximal gonadal arm (57, 76, 146, 147). Then yolk material is internalized into maturing oocytes via receptor-mediated endocytosis and resides in vesicles (148, 149). During embryogenesis,

yolk granules reside in the blastomeres and *C. elegans* only use this yolk partially. During morphogenesis the leftover yolk is transferred into the intestinal cells, thus, present in larval intestines (148–151). Mutations in the genes that regulate yolk trafficking and yolk receptors are lethal suggesting that yolk is essential for embryonic development (148). The exact chemical composition of yolk is not known but it contains vitellogenin proteins and phospholipids (77, 78). Although folates are not yet reported in *C. elegans* yolk, in other organisms such as hens yolk contain 24.8 mcg folates (152). Furthermore, in several organisms including humans and mice, reduced folate levels during pregnancy is associated with infertility, NTD's and developmental delay in offspring (Section 3.6). This shows the importance of folates in embryonic development and reproduction. Folate acts as an essential co-factor in 1C metabolism and vital for purine and pyrimidine synthesis required for DNA and RNA synthesis, thereby, involved in cell division and repair (Section 3.6), thus, important for embryonic development. Previous studies have reported that FOLT-1 and bacterial folates are required to stimulate germline proliferation in isolated *C. elegans* germ cells *in vitro* (119). During reproductive life, *C. elegans* germ line undergo proliferation and meiotic development to produce gametes (153). Therefore, as folates are important for gamete production and *C. elegans* germ cells receive nutrients from the yolk, this indicates that absorbed folates are stored in yolk and transported into gonads through body cavity to support gamete production and oocyte embryonic development. Thus, observed decline in brood size of *C. elegans* with increasing folate inhibition is due to reduction in *C. elegans* germline development.

The Figure 36 with images of growth phenotype displays how SMX induced folate synthesis inhibition affected the wild-type and *gcp-2* mutants differently. The NGM plates

with *gcp-2.1* and *gcp-2.2* worms were drastically less crowded compared to wild-type and *gcp-2.3* mutants. The NGM plate with wild-type was the most crowded and contained a lot of gravid adults, eggs and L1-L2 worms. The NGM plate with *gcp-2.2* mutants was the least crowded plate with few worms and eggs which did not develop into L1 larva. Therefore, observed disparities in reproduction between *gcp-2* paralogs indicates that cGCPII plays a role in reproduction through regulating folate metabolism and each *gcp-2* paralog contributes to folate metabolism at different levels. These observed disparities in reproduction between *gcp-2.1*, *gcp-2.2* and *gcp-2.3* mutant strains indicate that cGCPII each *gcp-2* paralog contributes to folate metabolism at different levels. As *gcp-2.1* and *gcp-2.2* mutants were affected to higher extent compared to the wild-type and *gcp-2.1* mutants implies that *gcp-2.1* and *gcp-2.2* paralogs are more important in folate metabolism compared to *gcp-2.1*.

Another important observation is that both *gcp-2.1* and *gcp-2.2* showed significant reduction or total abolition of progeny production beyond 100 µg/mL SMX treatment. Both *gcp-2.1* and *gcp-2.2* may not be functional complements in folate metabolism as they failed to restore each other's role.

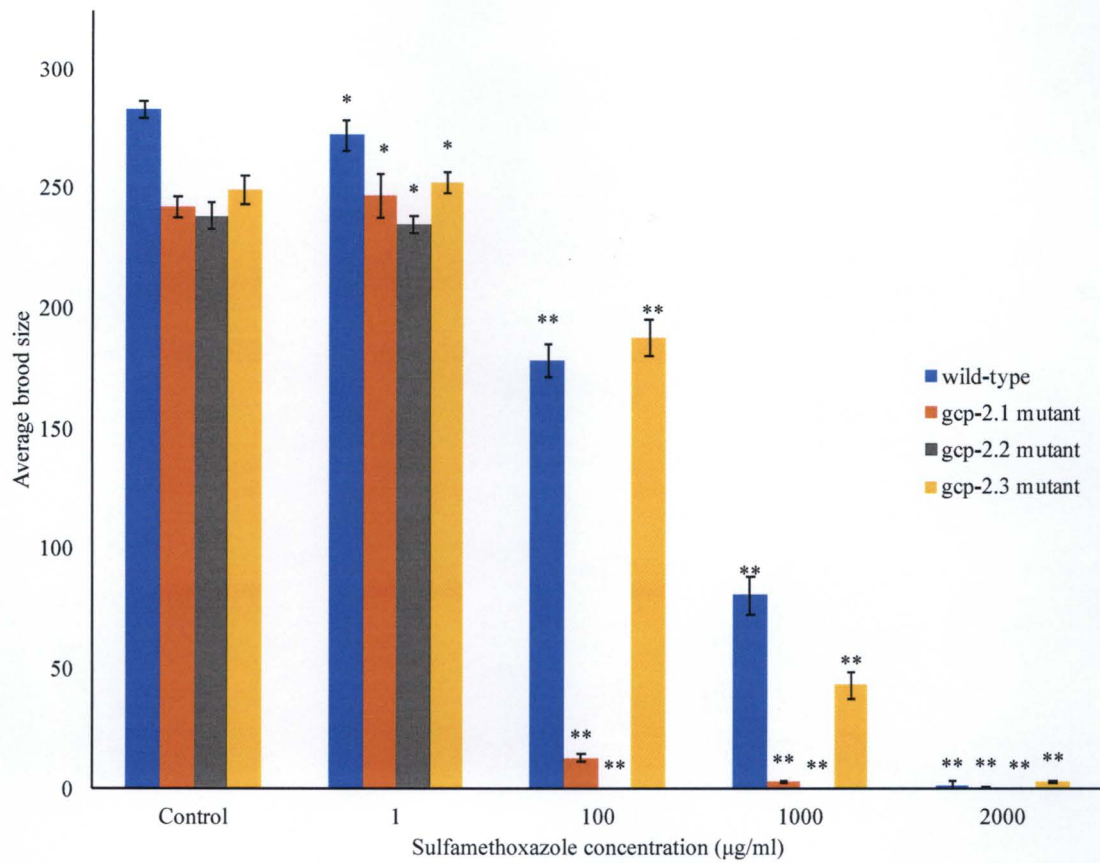


Figure 58. Comparative plot of the effect of SMX dependent folate inhibition on brood size of wild-type and *gcp-2* mutant *C. elegans*.

Statistical significance was determined using two sample T-test (* $p > 0.001$, ** $p < 0.001$).

** $p < 0.001$ considered significant. The error bars represent \pm SEM.

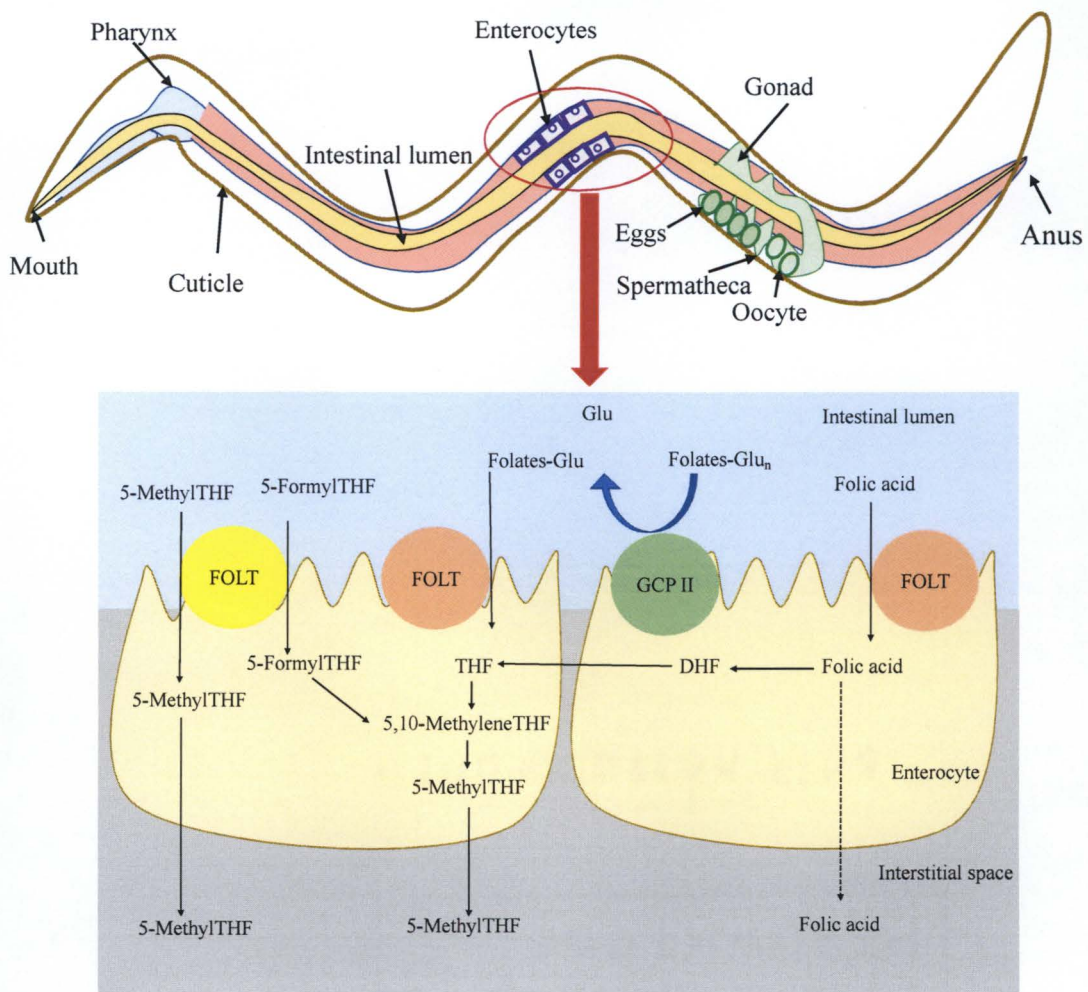


Figure 58. Hypothetical model for GCPII dependent folate absorption in *C. elegans*.

FOLT, folate transporter-1/2; Folate-Glu_n, polyglutamated folates; Folate-Glu, monoglutamated folates; THF, tetrahydrofolate; 5-Methyl-THF, monoglutamated methyl-THF; and Formyl, monoglutamated formyl-THF.

The body development of wild-type and *gcp-2.3* mutant strains were not affected by folate inhibition whereas the development of *gcp-2.1* and *gcp-2.2* mutants were affected by SMX induced folate synthesis inhibition. This suggests that cGCPII dependent folate metabolism contributes to *C. elegans* development even after hatching *i.e.* postembryonic. As mentioned in the Section 1.3.5, *C. elegans* contains only ~550 cells at the end of embryonic development or when eggs hatch but a gravid adult has 959 cells. Therefore, cells further divide at postembryonic level. This allows animals to substantially grow during the larval stages from 550 to 959 cells. Postembryonic development is stimulated through feeding by pharyngeal pumping. However, it is not clear whether pharyngeal pumping takes food from outside or from the yolk vesicles within the embryo. The postembryonic development at larval stages is due to the germ line proliferation and meiotic development (153). Yolk synthesis starts during L4 lethargus and continues through the adult life (154). However, as mentioned earlier, during morphogenesis the leftover yolk is transferred into the intestinal cells, thus, present in larval intestines. This suggests that yolk is utilized during larval stages to support germ line proliferation and meiotic development allowing worms grow *i.e.* to increase in body length.

As the SMX induced retardation in body length was only observed in *gcp-2.1* and *gcp-2.2* mutants and not in wild-type and *gcp-2.3* mutant strains show that *gcp-2.1* and *gcp-2.2* paralogs are more important in folate metabolism compared to *gcp-2.3* supporting the conclusion from reproduction data.

As discussed in results, *gcp-2.2* worms with 100 and 1000 µg/mL SMX laid eggs as shown in Figure 36, however, only few eggs hatched, and most of the eggs did not develop into L1 larva. Even in multiple attempts to obtain an age synchronized population,

these eggs did not survive after treating with bleach (no L1 were present after the bleaching process). These results suggest that there is a link between folate levels, *gcp-2.2* and the development of embryo outside the hermaphrodite. As discussed in the Section 1.3.5, when an embryo is released to the environment through vulva opening it is only 28–30 cells and at the end of embryonic development embryo is ~550 cells. Therefore, there is substantial embryonic cell division outside the hermaphrodite. Interestingly, embryo starts pharyngeal pumping at 760 min after the first cell cleavage and hatches at 800 min (80). Therefore, embryo starts feeding (either through yolk vesicles or diet) before hatching and the fact that postembryonic development is stimulated through feeding (80), indicates that observed results are due to laid embryos not getting enough folates for embryonic development to become a larva. Furthermore, as such observations were not present in wild-type, *gcp-2.1* and *gcp-2.3* mutant worms suggest that *gcp-2.2* may play a role in folate absorption within embryos. I suggest conducting an egg viability assay to strengthen these finding in the future.

Folinic acid supplementation was effective in partly reversing the effect of SMX induced folate synthesis inhibition on reproduction of wild-type worms but not in *gcp-2* mutants. This indicates that Folinic acid is one of the forms of folate that contributes for *C. elegans*' progeny production and supplementation is only effective if all *gcp-2* paralogs remain intact in the animal. This observation further suggests that role of *gcp-2* paralogs in the metabolism of different folate derivatives may be complicated.

HPLC analysis showed that *E. coli* OP50 extract consists 5-formyl-THF, 5-methyl-THF, DHF and THF (Table 6). In order to confirm which of these forms are required for

C. elegans' reproduction and growth, I suggest conducting supplementation experiment with each folate form on brood size and body length assay as demonstrated in this work.

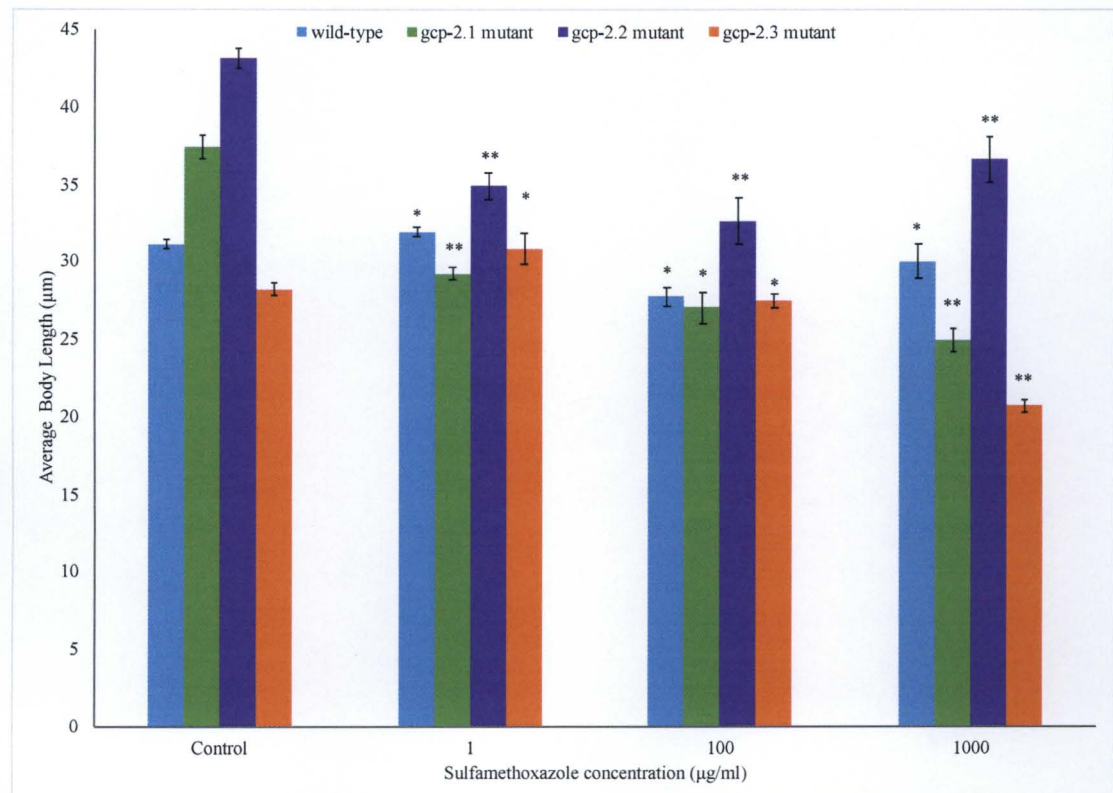


Figure 59. Comparative plot of the effect of SMX dependent folate inhibition on body length of wild-type and *gcp-2* *C. elegans* mutants.

Statistical significance was determined using two sample T-test (*p > 0.001, **p < 0.001).

**p < 0.001 considered significant. The error bars represent ± SEM.

Taken together, this chapter shows that restricting dietary folates reduces worm progeny production and hinders development differently in cGCPII mutants in a concentration dependent manner. Furthermore, cGCPII and *gcp-2* paralogs, specifically *gcp-2.1* and *gcp-2.2* paralogs, regulates folate dependent reproduction, embryonic and post-embryonic development of *C. elegans*.

Chapter 4: Conclusions and Future Perspectives

In conclusion, the work presented established that cGCPII plays essential functions in reproductive and developmental biology of *C. elegans* by mediating folate metabolism as shown in Figure 60. Furthermore, the *gcp-2.1* and *gcp-2.2* paralogs play a significant role in folate metabolism, reproduction, and post-embryonic development in *C. elegans* where as *gcp-2.3* may play a non-significant role. Furthermore, this work demonstrated, for the first time, sheds light on the relationship between GCPII and folate metabolism in *C. elegans* that has similar characteristics to the folate metabolism in humans. Thus, *C. elegans* provides a genetically tractable model that can be used to study integrative aspects of the GCPII dependent folate metabolism in the context of the whole animal level.

Further studies are needed to fully comprehend the hypothesis of the interaction between GCPII, folate metabolism and embryonic/postembryonic developmental biology of *C. elegans* at whole animal (*in vivo*) and molecular (*in vitro*) levels. Therefore, suggestions for *in vivo* future studies is to generate a double mutant of lacking *gcp-2.1* and *gcp-2.2* paralogs, generate a complete knockout lacking all three *gcp-2* paralogs and conduct drug assays using mammalian GCPII inhibitors as discussed in the Section 1.3.5. Furthermore, suggestions for *in vitro* future studies is to clone cGCPII and *gcp-2* paralogs

to functionally characterise substrate level parameters such as pH dependence (indication of tissue specific activity as different regions of the alimentary canal has specific pH levels), saturability, substrate specificity, enzymatic activity (levels of folate-hydrolyzing activity) and inhibition profile.

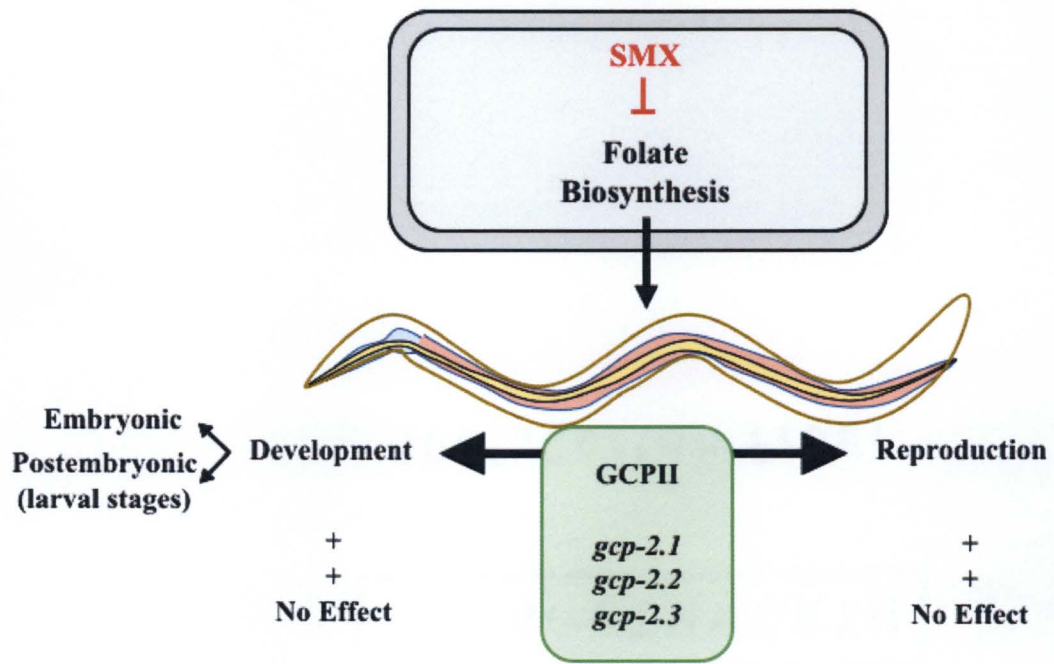


Figure 60. Graphical representation of proposed GCPII function in folate mediated reproductive and developmental biology of *C. elegans*.

Bibliography

1. Clark DP, Pazdernik NJ. 2015. Recombinant Proteins Biotechnology.
2. López-Otín C, Bond JS. 2008. Proteases: Multifunctional Enzymes in Life and Disease. *Journal of Biological Chemistry*.
3. Puente XS, Sánchez LM, Overall CM, López-Otín C. 2003. Human and mouse proteases: A comparative genomic approach. *Nature Reviews Genetics*.
4. López-Otín C. 2018. No Title. The Mammalian Degradome Database.
5. Erez E, Fass D, Bibi E. 2009. How intramembrane proteases bury hydrolytic reactions in the membrane. *Nature*.
6. Rawlings ND, Barrett AJ, Bateman A. 2012. MEROPS: The database of proteolytic enzymes, their substrates and inhibitors. *Nucleic Acids Research*.
7. Hooper NM. 1994. Families of zinc metalloproteases. *FEBS Letters*.
8. Hecht KA, Wytiaz VA, Ast T, Schuldiner M, Brodsky JL. 2013. Characterization of an M28 metalloprotease family member residing in the yeast vacuole. *FEMS Yeast Research*.
9. Vallee BL, Auld DS. 1990. Zinc Coordination, Function, and Structure of Zinc Enzymes and Other Proteins. *Biochemistry*.
10. Häse CC, Finkelstein RA. 1993. Bacterial extracellular zinc-containing metalloproteases. *Microbiological reviews*.
11. Hernick M, Fierke C. 2010. Mechanisms of Metal-Dependent Hydrolases in Metabolism *Comprehensive Natural Products II*.
12. Kilshtain AV, Warshel A. 2009. On the origin of the catalytic power of carboxypeptidase a and other metalloenzymes. *Proteins: Structure, Function and*

Bioinformatics.

13. Paul TJ, Barman A, Ozbil M, Bora RP, Zhang T, Sharma G, Hoffmann Z, Prabhakar R. 2016. Mechanisms of peptide hydrolysis by aspartyl and metalloproteases. *Physical Chemistry Chemical Physics*.
14. Chevrier B, D'Orchymont H, Schalk C, Tarnus C, Moras D. 1996. The structure of the *Aeromonas proteolytica* aminopeptidase complexed with a hydroxamate inhibitor: Involvement in catalysis of Glu151 and two zinc ions of the co-catalytic unit. *European Journal of Biochemistry*.
15. Reiland V, Gilboa R, Spungin-Bialik A, Schomburg D, Shoham Y, Blumberg S, Shoham G. 2004. Binding of inhibitory aromatic amino acids to *Streptomyces griseus* aminopeptidase. *Acta Crystallographica Section D: Biological Crystallography*.
16. Rawlings ND, Barrett AJ, Thomas PD, Huang X, Bateman A, Finn RD. 2018. The MEROPS database of proteolytic enzymes, their substrates and inhibitors in 2017 and a comparison with peptidases in the PANTHER database. *Nucleic Acids Research*.
17. Koller KJ, Coyle JT. 1984. Characterization of the interactions of N-acetyl-aspartyl-glutamate with [³H]L-glutamate receptors. *European Journal of Pharmacology*.
18. Koller K, Coyle J. 2018. The characterization of the specific binding of [³H]-N-acetylaspartylglutamate to rat brain membranes. *The Journal of Neuroscience*.
19. Horoszewicz JS, Kawinski E, Murphy GP. 1987. Monoclonal antibodies to a new antigenic marker in epithelial prostatic cells and serum of prostatic cancer patients.

Anticancer Research.

20. Ruth E. Carter, Alexis R. Feldman, Joseph T. Coyle. 1996. Prostate-specific membrane antigen is a hydrolase with substrate and pharmacologic characteristics of a neuropeptidase. *Proceedings of the National Academy of Sciences of the United States of America*.
21. Pinto JT, Suffoletto BP, Berzin TM, Qiao CH, Lin S, Tong WP, May F, Mukherjee B, Heston WDW. 1996. Prostate-specific Membrane Antigen: A Novel Folate Hydrolase in Human Prostatic Carcinoma Cells. *Clinical Cancer Research*.
22. Halsted CH, Ling EH, Luthi-Carter R, Villanueva JA, Gardner JM, Coyle JT. 1998. Folylpoly- γ -glutamate carboxypeptidase from pig jejunum: Molecular characterization and relation to glutamate carboxypeptidase II. *Journal of Biological Chemistry*.
23. McDonald AG, Boyce S, Tipton KF. 2009. ExplorEnz: The primary source of the IUBMB enzyme list. *Nucleic Acids Research*.
24. Bařinka C, Rojas C, Slusher B, Pomper M. 2012. Glutamate carboxypeptidase II in diagnosis and treatment of neurologic disorders and prostate cancer. *Current medicinal chemistry* 19:856–70.
25. Barinka C, Sacha P, Sklenar J, Man P, Bezouska K, Slusher BS, Konvalinka J. 2004. Identification of the N-glycosylation sites on glutamate carboxypeptidase II necessary for proteolytic activity. *Protein science : a publication of the Protein Society* 13:1627–1635.
26. Koodziejczyk K, Hamilton NB, Wade A, Kradtir R, Attwell D. 2009. The effect of N-acetyl-aspartyl-glutamate and N-acetyl-aspartate on white matter

oligodendrocytes. *Brain*.

27. Slusher BS, Vornov JJ, Thomas AG, Hurn PD, Harukuni I, Bhardwaj A, Traystman RJ, Robinson MB, Britton P, Lu XCM, Tortella FC, Wozniak KM, Yudkoff M, Potter BM, Jackson PF. 1999. Selective inhibition of NAALADase, which converts NAAG to glutamate, reduces ischemic brain injury. *Nature Medicine*.
28. Baslow MH. 2003. N-acetylaspartate in the vertebrate brain: Metabolism and function. *Neurochemical Research*.
29. Coyle JT. 1997. The nagging question of the function of N-acetylaspartylglutamate. *Neurobiology of Disease*.
30. Esposito Z, Belli L, Toniolo S, Sancesario G, Bianconi C, Martorana A. 2013. Amyloid β , glutamate, excitotoxicity in alzheimer's disease: Are we on the right track? *CNS Neuroscience and Therapeutics*.
31. Dong XX, Wang Y, Qin ZH. 2009. Molecular mechanisms of excitotoxicity and their relevance to pathogenesis of neurodegenerative diseases. *Acta Pharmacologica Sinica*.
32. Šácha P, Zámečník J, Bařinka C, Hlouchová K, Vícha A, Mlčochová P, Hilgert I, Eckschlager T, Konvalinka J. 2007. Expression of glutamate carboxypeptidase II in human brain. *Neuroscience*.
33. Gao Y, Xu S, Cui Z, Zhang M, Lin Y, Cai L, Wang Z, Luo X, Zheng Y, Wang Y, Luo Q, Jiang J, Neale JH, Zhong C. 2015. Mice lacking glutamate carboxypeptidase II develop normally, but are less susceptible to traumatic brain injury. *Journal of Neurochemistry*.

34. Villalpando S. 2008. Discussion: Effects of folate and vitamin B12 deficiencies during pregnancy on fetal, infant, and child development *Food and Nutrition Bulletin*.
35. Evans JC, Malhotra M, Cryan JF, O'Driscoll CM. 2016. The therapeutic and diagnostic potential of the prostate specific membrane antigen/glutamate carboxypeptidase II (PSMA/GCPII) in cancer and neurological disease. *British Journal of Pharmacology*.
36. Schmidt LH, Heitkötter B, Schulze AB, Schliemann C, Steinestel K, Trautmann M, Marra A, Hillejan L, Mohr M, Evers G, Wardelmann E, Rahbar K, Görlich D, Lenz G, Berdel WE, Hartmann W, Wiewrodt R, Huss S. 2017. Prostate specific membrane antigen (PSMA) expression in non-small cell lung cancer. *PLoS ONE* 12:1–12.
37. Rinker-Schaeffer CW, Hawkins AL, Su SL, Israeli RS, Griffin CA, Isaacs JT, Heston WDW. 1995. Localization and physical mapping of the prostate-specific membrane antigen (PSM) gene to human chromosome 11+. *Genomics*.
38. Mesters JR, Barinka C, Li W, Tsukamoto T, Majer P, Slusher BS, Konvalinka J, Hilgenfeld R. 2006. Structure of glutamate carboxypeptidase II, a drug target in neuronal damage and prostate cancer. *EMBO Journal* 25:1375–1384.
39. Pavlicek J, Ptacek J, Barinka C. 2012. Glutamate Carboxypeptidase II: An Overview of Structural Studies and Their Importance for Structure-Based Drug Design and Deciphering the Reaction Mechanism of the Enzyme. *Current Medicinal Chemistry*.
40. Gasteiger E, Hoogland C, Gattiker A, Duvaud S, Wilkins MR, Appel RD, Bairoch

- A. 2005. Protein Identification and Analysis Tool on the ExPASy Server. The Proteomics Protocols Handbook.
41. Hlouchova K, Navratil V, Tykvart J, Sacha P, Konvalinka J. 2012. GCPII Variants, Paralogs and Orthologs. *Current Medicinal Chemistry*.
42. 7.13C: Homologs, Orthologs, and Paralogs - Biology LibreTexts.
43. The Difference Between Orthologous & Paralogous Genes | Sciencing.
44. Zallot R, Harrison KJ, Kolaczowski B, Crécy-Lagard V de. 2016. Functional Annotations of Paralogs: A Blessing and a Curse. *Life* 6.
45. Helliwell CA, Chin-Atkins AN, Wilson IW, Chapple R, Dennis ES, Chaudhury A. 2007. The Arabidopsis AMP1 Gene Encodes a Putative Glutamate Carboxypeptidase. *The Plant Cell*.
46. gcp-2.1 (gene) - WormBase : Nematode Information Resource.
47. gcp-2.2 (gene) - WormBase : Nematode Information Resource.
48. gcp-2.3 (gene) - WormBase : Nematode Information Resource.
49. Jackson PF, Cole DC, Slusher BS, Stetz SL, Ross LE, Donzanti BA, Trainor DA. 1996. Design, synthesis, and biological activity of a potent inhibitor of the neuropeptidase N-acetylated α -linked acidic dipeptidase. *Journal of Medicinal Chemistry*.
50. Thomas AG, Wozniak KM, Tsukamoto T, Calvin D, Wu Y, Rojas C, Vornov J, Slusher BS. 2006. Glutamate carboxypeptidase II (NAALADase) inhibition as a novel therapeutic strategy *Advances in Experimental Medicine and Biology*.
51. Hunter P. 2008. The paradox of model organisms. The use of model organisms in research will continue despite their shortcomings. *EMBO reports*.

52. Corsi AK. 2006. A biochemist's guide to *Caenorhabditis elegans*. Analytical Biochemistry.
53. Hodgkin J. 2001. *Caenorhabditis Elegans*. Encyclopedia of Genetics 251–256.
54. *Caenorhabditis elegans* / *C. elegans* | Learn Science at Scitable.
55. Barrière A, Félix MA. 2005. High local genetic diversity and low outcrossing rate in *Caenorhabditis elegans* natural populations. Current Biology.
56. Brenner S. 1974. The genetics of *Caenorhabditis elegans*. Genetics.
57. WORMATLAS Homepage.
58. 1998. Genome sequence of the nematode *C. elegans*: A platform for investigating biology. Science.
59. Hillier LDW, Coulson A, Murray JI, Bao Z, Sulston JE, Waterston RH. 2005. Genomics in *C. elegans*: So many genes, such a little worm. Genome Research.
60. Blumenthal T, Evans D, Link CD, Guffanti A, Lawson D, Thierry-Mieg J, Thierry-Mieg D, Chiu WL, Duke K, Kiraly M, Kim SK. 2002. A global analysis of *Caenorhabditis elegans* operons. Nature.
61. WS227 - WormBaseWiki.
62. Lya IL. Expanded human gene tally reignites debate.
63. Epstein HF, Shakes DC, American Society for Cell Biology. 1995. *Caenorhabditis elegans* : modern biological analysis of an organism. Academic Press.
64. Jorgensen EM, Mango SE. 2002. The art and design of genetic screens: *Caenorhabditis elegans*. Nature Reviews Genetics.
65. Au V, Li-Leger E, Raymant G, Flibotte S, Chen G, Martin K, Fernando L, Doell C, Rosell FI, Wang S, Edgley ML, Rougvie AE, Hutter H, Moerman DG. 2019.

CRISPR/Cas9 Methodology for the Generation of Knockout Deletions in
Caenorhabditis elegans.

66. Friedland AE, Tzur YB, Esvelt KM, Colaiácovo MP, Church GM, Calarco JA. 2013. Heritable genome editing in *C. elegans* via a CRISPR-Cas9 system. *Nature Methods* 10:741–743.
67. The Nobel Prize in Physiology or Medicine 2006.
68. Zhuang JJ, Hunter CP. 2012. RNA interference in *Caenorhabditis elegans*: Uptake, mechanism, and regulation. *Parasitology*.
69. Grishok A. 2005. RNAi mechanisms in *Caenorhabditis elegans*. *FEBS Letters*.
70. Min K, Lee J. 2010. Integrative Biosciences RNA interference in *C. elegans*: History, application, and perspectives.
71. Conte D, MacNei LT, Walhout AJM, Mello CC. 2015. RNA Interference in *Caenorhabditis elegans*. *Current Protocols in Molecular Biology*.
72. *Developmental Biology-RNAi*.
73. Francis R, Waterston RH. 1991. Muscle cell attachment in *Caenorhabditis elegans*. *Journal of Cell Biology*.
74. *Wormatlas*. No Title.
75. *Wormatlas*. No Title.
76. Kimble J, Sharrock WJ. 1983. Tissue-specific synthesis of yolk proteins in *Caenorhabditis elegans*. *Developmental Biology*.
77. Watts JL, Ristow M. 2017. Lipid and carbohydrate metabolism in *Caenorhabditis elegans*. *Genetics*.
78. Van Rompay L, Borghgraef C, Beets I, Caers J, Temmerman L. 2015. New

- genetic regulators question relevance of abundant yolk protein production in *C. elegans*. *Scientific Reports* 5:16381.
79. WORMATLAS. No Title.
 80. WORMATLAS. No Title.
 81. KIPREOS ET, VAN DEN HEUVEL S. 2019. Developmental Control of the Cell Cycle: Insights from *Caenorhabditis elegans*.
 82. BYERLY L, CASSADA RC, RUSSELL RL. 1976. The life cycle of the nematode *Caenorhabditis elegans*. I. Wild-type growth and reproduction. *Developmental Biology*.
 83. CASSADA RC, RUSSELL RL. 1975. The dauerlarva, a post-embryonic developmental variant of the nematode *Caenorhabditis elegans*. *Developmental Biology*.
 84. MULLANEY BC, ASHRAFI K. 2009. *C. elegans* fat storage and metabolic regulation. *Biochimica et biophysica acta* 1791:474–8.
 85. HIRSH D, OPPENHEIM D, KLAUS M. 1976. Development of the reproductive system of *Caenorhabditis elegans*. *Developmental Biology*.
 86. PICKETT CL, DIETRICH N, CHEN J, XIONG C, KORNFELD K. 2013. Mated Progeny Production Is a Biomarker of Aging in *Caenorhabditis elegans*. *Genes|Genomes|Genetics*.
 87. WORMATLAS. No Title.
 88. KLAUS MR. 1977. Aging in the nematode *Caenorhabditis elegans*: Major biological and environmental factors influencing life span. *Mechanisms of Ageing and Development*.
 89. HONDA S, ISHII N, SUZUKI K, MATSUO M. 1993. Oxygen-dependent perturbation of

- life span and aging rate in the nematode. *Journals of Gerontology*.
90. Donald L Riddle. 1997. *C. elegans* II. 2nd edition Cold Spring Harbor Laboratory Press.
 91. Strain: N2, Genotype: *C. elegans* wild isolate. - Caenorhabditis Genetics Center (CGC) - College of Biological Sciences.
 92. Strain: RB1055, Genotype: R57.1(ok1004) X. - Caenorhabditis Genetics Center (CGC) - College of Biological Sciences.
 93. National BioResource Project (NBRP)::*C.elegans*.
 94. Strain: OP50, Genotype: *E. coli*. - Caenorhabditis Genetics Center (CGC) - College of Biological Sciences.
 95. Porta-de-la-Riva M, Fontrodona L, Villanueva A, Cerón J. 2012. Basic *Caenorhabditis elegans* Methods: Synchronization and Observation. *Journal of Visualized Experiments* e4019.
 96. Yu L, Yan X, Ye C, Zhao H, Chen X, Hu F, Li H. 2015. Bacterial respiration and growth rates affect the feeding preferences, brood size and lifespan of *Caenorhabditis elegans*. *PLoS ONE*.
 97. Solis GM, Petrascheck M. 2011. Measuring *Caenorhabditis elegans* Life Span in 96 Well Microtiter Plates. *Journal of Visualized Experiments*.
 98. Ramachandran P V, Mutlu AS, Wang MC. 2015. Label-free biomedical imaging of lipids by stimulated Raman scattering microscopy. *Current protocols in molecular biology* 109:30.3.1-17.
 99. Source BioScience. *C. elegans* RNAi Collection (Ahringer) | Source BioScience.
 100. Fire A. 1999. Addgene: L4440.

101. Hi-Speed Mini Plasmid Kit - 300 Preps – IBI Scientific.
102. Restriction Enzymes for Droplet Digital PCR (ddPCR) | NEB.
103. Primer list for full genome microarray.
104. Dudley NR, Goldstein B. 4 RNA Interference in *Caenorhabditis elegans*.
105. Virk B, Correia G, Dixon DP, Feyst I, Jia J, Oberleitner N, Briggs Z, Hodge E, Edwards R, Ward J, Gems D, Weinkove D. 2012. Excessive folate synthesis limits lifespan in the *C. elegans*: *E. coli* aging model. *BMC Biology* 10.
106. Virk B, Jia J, Maynard CA, Raimundo A, Lefebvre J, Richards SA, Chetina N, Liang Y, Helliwell N, Cipinska M, Weinkove D. 2016. Folate Acts in *E. coli* to Accelerate *C. elegans* Aging Independently of Bacterial Biosynthesis. *Cell Reports* 14:1611–1620.
107. Nembaware V, Crum K, Kelso J, Seoighe C. 2002. Impact of the presence of paralogs on sequence divergence in a set of mouse-human orthologs. *Genome research* 12:1370–6.
108. Strutz-Seebohm N, Werner M, Madsen DM, Seebohm G, Zheng Y, Walker CS, Maricq A V., Hollmann M. 2003. Functional Analysis of *Caenorhabditis elegans* Glutamate Receptor Subunits by Domain Transplantation. *Journal of Biological Chemistry*.
109. Maricq A. Analysis of Glutamate Receptor Function in *C. elegans*.
110. Mano I, Straud S, Driscoll M. 2007. *Caenorhabditis elegans* glutamate transporters influence synaptic function and behavior at sites distant from the synapse. *The Journal of biological chemistry* 282:34412–9.
111. Meeker K. 2015. Effects of GLT-1 loss on central nervous system insulin signaling

and implications for Alzheimer's disease pathogenesis.

112. Kenyon C. 2011. The first long-lived mutants: discovery of the insulin/IGF-1 pathway for ageing. *Philosophical transactions of the Royal Society of London Series B, Biological sciences* 366:9–16.
113. Prosselkov P, Polygalov D, Zhang Q, McHugh TJ, Itohara S. 2015. Cognitive Domains Function Complementation by NTNG Gene Paralogs. *bioRxiv* 034645.
114. Qin Z, Johnsen R, Yu S, Chu JS-C, Baillie DL, Chen N. 2018. Genomic Identification and Functional Characterization of Essential Genes in *Caenorhabditis elegans*. *G3 (Bethesda, Md)* 8:981–997.
115. Holmes K, Williams CM, Chapman EA, Cross MJ. 2010. Detection of siRNA induced mRNA silencing by RT-qPCR: considerations for experimental design.
116. De-Souza EA, Camara H, Salgueiro WG, Moro RP, Knittel TL, Tonon G, Pinto S, Paula A, Pinca F, Antebi A, Pasquinelli AE, Massirer KB, Mori MA. 2019. RNA interference may result in unexpected phenotypes in *Caenorhabditis elegans*. *Nucleic Acids Research* 47:3957–3969.
117. Sutphin GL, Kaeberlein M. 2009. Measuring *Caenorhabditis elegans* Life Span on Solid Media. *Journal of Visualized Experiments*.
118. Greenberg JA, Bell SJ, Guan Y, Yu Y-H. 2011. Folic Acid supplementation and pregnancy: more than just neural tube defect prevention. *Reviews in obstetrics & gynecology*.
119. Chaudhari SN, Mukherjee M, Vagasi AS, Bi G, Rahman MM, Nguyen CQ, Paul L, Selhub J, Kipreos ET. 2016. Bacterial Folates Provide an Exogenous Signal for *C. elegans* Germline Stem Cell Proliferation. *Developmental Cell* 38:33–46.

120. Gorelova V, Bastien O, De Clerck O, Lespinats S, Rébeillé F, Van Der Straeten D. 2019. Evolution of folate biosynthesis and metabolism across algae and land plant lineages. *Scientific Reports* 9:5731.
121. Paiva EP de, Costa MMA, Azevedo CA de. 2016. Folate - Analytical properties, bioavailability and stability in foods. *Scientia Chromatographica*.
122. Tamura T, Picciano MF. 2006. Folate and human reproduction. *American Journal of Clinical Nutrition*.
123. Bermingham A, Derrick JP. 2002. The folic acid biosynthesis pathway in bacteria: Evaluation of potential for antibacterial drug discovery. *BioEssays* 24:637–648.
124. Rossi M, Amaretti A, Raimondi S. 2011. Folate production by probiotic bacteria. *Nutrients*.
125. Dewick PM. 2003. The Shikimate Pathway: Aromatic Amino Acids and Phenylpropanoids *Medicinal Natural Products*.
126. Rébeillé F, Ambach L, Stove C, Van Der Straeten D, Gorelova V. 2017. Folates in Plants: Research Advances and Progress in Crop Biofortification. *Frontiers in Chemistry*.
127. Visentin M, Diop-Bove N, Zhao R, Goldman ID. 2014. The Intestinal Absorption of Folates. *Annual Review of Physiology* 76:251–274.
128. Desmoulin SK, Hou Z, Gangjee A, Matherly LH. 2012. The human proton-coupled folate transporter: Biology and therapeutic applications to cancer. *Cancer Biology and Therapy*.
129. Zhao R, Diop-Bove N, Visentin M, Goldman ID. 2011. Mechanisms of Membrane Transport of Folates into Cells and Across Epithelia. *Annual Review of Nutrition*.

130. Patanwala I, King MJ, Barrett DA, Rose J, Jackson R, Hudson M, Philo M, Dainty JR, Wright AJA, Finglas PM, Jones DE. 2014. Folic acid handling by the human gut: Implications for food fortification and supplementation. *American Journal of Clinical Nutrition*.
131. Verhoef H, Veenemans J, Mwangi MN, Prentice AM. 2017. Safety and benefits of interventions to increase folate status in malaria-endemic areas. *British Journal of Haematology*.
132. Ducker GS, Rabinowitz JD. 2017. Cell Metabolism Review One-Carbon Metabolism in Health and Disease. *Cell Metabolism*.
133. Lim U, Wang SS, Hartge P, Cozen W, Kelemen LE, Chanock S, Davis S, Blair A, Schenk M, Rothman N, Lan Q. 2007. Gene-nutrient interactions among determinants of folate and one-carbon metabolism on the risk of non-Hodgkin lymphoma: NCI-SEER case-control study. *Blood*.
134. Shuvalov O, Petukhov A, Daks A, Fedorova O, Vasileva E, Barlev NA, Shuvalov O, Petukhov A, Daks A, Fedorova O, Vasileva E, Barlev NA, Shuvalov O, Petukhov A, Daks A, Fedorova O, Vasileva E, Barlev NA. 2017. One-carbon metabolism and nucleotide biosynthesis as attractive targets for anticancer therapy. *Oncotarget*.
135. Selhub J. 2002. Folate, vitamin B12 and vitamin B6 and one carbon metabolism. *The journal of nutrition, health & aging*.
136. Lambie DG, Johnson RH. 1985. Drugs and Folate Metabolism. *Drugs*.
137. Hammoudeh DI, Zhao Y, White SW, Lee RE. 2013. Replacing sulfa drugs with novel DHPS inhibitors. *Future Medicinal Chemistry*.

138. McLean E, de Benoist B, Allen LH. 2008. Review of the magnitude of folate and vitamin B12 deficiencies worldwide. *Food and Nutrition Bulletin*.
139. McKay JA, Mathers JC. 2016. Maternal folate deficiency and metabolic dysfunction in offspring. *Proceedings of the Nutrition Society* 75:90–95.
140. Scott JM, Weir DG. 1998. Folic acid, homocysteine and one-carbon metabolism: A review of the essential biochemistry. *European Journal of Cardiovascular Prevention & Rehabilitation*.
141. Alpert JE, Fava M. 2009. Nutrition and Depression: The Role of Folate. *Nutrition Reviews* 55:145–149.
142. Duthie SJ. 1999. Folic acid deficiency and cancer: mechanisms of DNA instability. *British Medical Bulletin* 55:578–592.
143. GORDON N. 2009. Cerebral folate deficiency. *Developmental Medicine & Child Neurology* 51:180–182.
144. Williams J, Mai CT, Mulinare J, Isenburg J, Flood TJ, Ethen M, Frohnert B, Kirby RS, Centers for Disease Control and Prevention. 2015. Updated estimates of neural tube defects prevented by mandatory folic Acid fortification - United States, 1995-2011. *MMWR Morbidity and mortality weekly report*.
145. Balamurugan K, Ashokkumar B, Moussaif M, Sze JY, Said HM. 2007. Cloning and functional characterization of a folate transporter from the nematode *Caenorhabditis elegans*. *American journal of physiology Cell physiology* 293:C670-81.
146. Hall DH, Winfrey VP, Blaeuer G, Hoffman LH, Furuta T, Rose KL, Hobert O, Greenstein D. 1999. Ultrastructural Features of the Adult Hermaphrodite Gonad of

Caenorhabditis elegans: Relations between the Germ Line and Soma.

Developmental Biology 212:101–123.

147. Bosch S, Botha TL, Jordaan A, Maboeta M, Wepener V. 2018. Sublethal Effects of Ionic and Nanogold on the Nematode *Caenorhabditis elegans*. Journal of toxicology 2018:6218193.
148. Chotard L, Skorobogata O, Sylvain MA, Shrivastava S, Rocheleau CE. 2010. TBC-2 is required for embryonic yolk protein storage and larval survival during L1 diapause in *Caenorhabditis elegans*. PLoS ONE.
149. Grant B, Hirsh D. 1999. Receptor-mediated Endocytosis in the *Caenorhabditis elegans* Oocyte. Molecular Biology of the Cell 10:4311–4326.
150. Bossinger O, Schierenberg E. 1992. Cell-cell communication in the embryo of *Caenorhabditis elegans*. Developmental biology 151:401–9.
151. Bossinger O, Schierenberg E. 1996. The use of fluorescent marker dyes for studying intercellular communication in nematode embryos. The International journal of developmental biology 40:431–9.
152. The Nutritional Value of Egg Whites Versus Egg Yolks: What Do You Use? | A Healthier Michigan.
153. Hubbard EJ. 2005. Introduction to the germ line. WormBook.
154. Wormatlas. No Title.

Appendix 1: Stock Solutions

1 M Potassium phosphate Buffer (pH 6.0): 108.3 g of KH_2PO_4 , 35.6 g of K_2HPO_4 (Fisher BioReagents) was added to 1 L of sterilized Millipore water, stirred until dissolved. Stored at 4°C.

5 mg/mL Cholesterol stock: 0.5 g of cholesterol (95% Alfa Aesar) was added to 100 mL of absolute ethanol, stirred until dissolved. Stored at 4°C.

10 mg/mL Nystatin stock: 0.5 g of nystatin was added to 50 mL of 70% ethanol, stirred until dissolved. Stored at -20°C.

100 mg/mL Streptomycin stock: 1 g of streptomycin was added to 10 mL of sterilized Millipore water, stirred until dissolved and filter-sterilized. Stored at -20°C.

1 M CaCl_2 stock: 5.6 g of CaCl_2 was added to 100 mL sterilized Millipore water and stirred until dissolved. Stored at 4°C.

1 M MgSO_4 stock: 24.4 g of MgSO_4 was added to sterilized Millipore water up to 100 mL and stirred until dissolved. Stored at 4°C.

150 mM FUdR stock: 0.37 g of FUdR (Acros Organics) was added to 10 mL sterile Millipore water and stirred until dissolved. Stored at -20°C.

100 mg/mL Sulfamethoxazole Stock: 1 g of SMX (MP Biochemicals) was dissolved in 9.5 mL of sterile Millipore water with 500 μL of 5N NaOH added to aid dissolving of the compound. Filter sterilized using a 0.2 μm filter. Stored at -20°C.

50X TAE Buffer Stock: 242 g of Tris base was dissolved in 700 mL of Millipore water. Then 57.1 mL of acetic acid and 100 mL of 0.5 M EDTA was added. Adjusted the solution to a final volume of 1 L with Millipore water. Stored at room temperature. 1X

working solution was prepared as needed by diluting stock solution with X50 Millipore water.

Freezing Solution: 5.8g NaCl, 50mL 1M KH_2PO_4 (pH 6.0), 240mL glycerol was added to 710 mL Millipore water. Sterilized by autoclaving at 121°C for 45 mins. Then added 300 μL 1M MgSO_4 .

1 M Potassium Citrate pH 6.0: 20 g citric acid monohydrate, 293.5 g tri-potassium citrate monohydrate was added to Millipore water to 1 L, stirred until dissolved and sterilized by autoclaving. Stored at 4°C.

Trace Metals Solution: Trace metals solution 1.86 g disodium EDTA, 0.69 g $\text{FeSO}_4 \cdot 7 \text{H}_2\text{O}$, 0.2 g $\text{MnCl}_2 \cdot 4 \text{H}_2\text{O}$, 0.29 g $\text{ZnSO}_4 \cdot 7 \text{H}_2\text{O}$, 0.025 g $\text{CuSO}_4 \cdot 5 \text{H}_2\text{O}$, H_2O to 1 L Millipore water stirred until dissolved and sterilized by autoclaving. Stored at 4°C.

Appendix 2: Preparation of Liquid Growth Medium

S-Complete Solution: S-Complete solution was prepared by mixing sterilized 1 L S-basal, 10 mL 1 M potassium citrate pH 6, 10 mL trace metals solution, 3 mL 1 M CaCl_2 and 3 mL 1 M MgSO_4 . Stored at 4°C.

S-Basal Solution: 5.85 g NaCl, 1 g K_2HPO_4 , 6 g KH_2PO_4 and 1 mL 5 mg/mL cholesterol was added to Millipore water to 1 L, stirred until dissolved and sterilized by autoclaving. Stored at 4°C.

M-9 Buffer: M-9 Buffer was prepared by mixing 6 g Na_2HPO_4 , 3 g KH_2PO_4 , and 5 g NaCl in 1 L Millipore water, stirred until dissolved and autoclaved at 120°C for 45 min. Then added 1 mL of 1 M MgSO_4 . Stored at 4°C.

Appendix 3: RNAi Sequence Alignment Data

gcp-2.1

BLASTN 2.8.0+

Reference: Zheng Zhang, Scott Schwartz, Lukas Wagner, and Webb Miller (2000), "A greedy algorithm for aligning DNA sequences", J Comput Biol 2000; 7(1-2):203-14.

RID: 7GWRCGM0114

Query=
Length=1384

Score E
Sequences producing significant alignments:
(Bits) Value

Query_203293
1594 0.0

ALIGNMENTS
>Query_203293
Length=1630

Score = 1594 bits (863), Expect = 0.0
Identities = 971/1027 (95%), Gaps = 27/1027 (3%)
Strand=Plus/Minus

```
Query 91 AAAACCCATCAAATAACATCACGTAGAGTGTTTACAACGCAAATAACAGAGTACTGGACA 150
      |||
Sbjct 1630 AAAACCCATCAAATAACATCACGTAGAGTGTTTACAACGCAAATAACAGAGTACTGGACA 1571

Query 151 ATGGAGATTTGGTTGATTATTTCCCTCAAGCCTTTTTGGTTGGATTCAAGTCGTAAC TG 210
      |||
Sbjct 1570 ATGGAGATTTGGTTGATTATTTCCCTCAAGCCTTTTTGGTTGGATTCAAGTCGTAAC TG 1511

Query 211 TTGATCTGAATGAAGTTTTCTTTAGCATAAATTATATTATATCACTAACCGCATTCTGTA 270
      |||
Sbjct 1510 TTGATCTGAATGAAGTTTTCTTTAGCATAAATTATATTATATCACTAACCGCATTCTGTA 1451

Query 271 CTCCTGCCATTAAAGAACTCGAGTATGAATCAGAATCGCTGACTGAAAACAGGACATGTC 330
      |||
Sbjct 1450 CTCCTGCCATTAAAGAACTCGAGTATGAATCAGAATCGCTGACTGAAAACAGGACATGTC 1391

Query 331 TAGCTGAGGGATTGTGCATTGAAACGCCACGGGGGTTGATGAAGCATCTTCCGTGCTGA 390
      |||
Sbjct 1390 TAGCTGAGGGATTGTGCATTGAAACGCCACGGGGGTTGATGAAGCATCTTCCGTGCTGA 1331

Query 391 AAACATAATGTTTTTTTTAAATATGATAAAGTGGCAAACCTCTTTAATCTCTCATTGAC 450
      |||
Sbjct 1330 AAACATAATGTTTTTTTTAAATATGATAAAGTGGCAAACCTCTTTAATCTCTCATTGAC 1271
```

```

Query 451 CGCATTACAGTGTTCGGGTCGTATGGATTCTGAGAGAAGCTGTGTTGTGTA AAAATGGAT 510
          |||
Sbjct 1270 CGCATTACAGTGTTCGGGTCGTATGGATTCTGAGAGAAGCTGTGTTGTGTA AAAATGGAT 1211

Query 511 GGTTTCTTGGAAttttttGACATTGTAAGTAAATCTTGAGCACTTTTTGAGAGAAGTGC 570
          |||
Sbjct 1210 GGTTTCTTGGAAttttttGACATTGTAAGTAAATCTTGAGCACTTTTTGAGAGAAGTGC 1151

Query 571 ATACTGTGTGCGTATATCTTCGAAATCGCTTCTCGAAACATTTATTCGGAGATTGTTGT 630
          |||
Sbjct 1150 ATACTGTGTGCGTATATCTTCGAAATCGCTTCTCGAAACATTTATTCGGAGATTGTTGT 1091

Query 631 TTTCAGTTGTGGGAGATAGGTTTTGAGCATGACTGACGCAAAATGTGTGGTATTCATTGG 690
          |||
Sbjct 1090 TTTCAGTTGTGGGAGATAGGTTTTGAGCATGACTGACGCAAAATGTGTGGTATTCATTGG 1031

Query 691 GAGAATTACATCATCCGCAAACGTCTGAAAAAGTTCAGTTCATTAATCCTTAATTT 750
          |||
Sbjct 1030 GAGAATTACATCATCCGCAAACGTCTGAAAAAGTTCAGTTCATTAATCCTTAATTT 971

Query 751 TTATCAATATTCGGAAACTGAACATTTGCAATTGGAAATATTTTATATGCGGATTCAA 810
          |||
Sbjct 970 TTATCAATATTCGGAAACTGAACATTTGCAATTGGAAATATTTTATATGCGGATTCAA 911

Query 811 GATATTaaaaaaaaaa-CCTCCAGTTCCCATGTTTCCTTCAATTTATTATCAAAAANC 869
          |||
Sbjct 910 GATATTAaaaaaaaaAACCTCCAGTTCC-ATGTTT-CTTCAATTTATTATCAAAA-C 854

Query 870 TGATCNCGCNCAGTNNTAAATCTTAAAAGGTTGACCGCGTCCCGGGGAAttttttaaaa 929
          |||
Sbjct 853 TGATCAGCACAGTC-TAAATCTTAAAAGGTTGACCGCGTCCCTGGG--ATTTTTTAAAA 797

Query 930 ttttcnnaaaaaannncattttttgactttttcaaaaaaaaaaCAAACCAAGNGACA 989
          |||
Sbjct 796 TTTTCT-AGAAAATCT-CATTTTTGACTTTTTCAAAAAAAAAACAAC-AAGTGACA 740

Query 990 TANAAANCCggggggggTANNAANCNCAATTTANCCCCGGGTTTTCCAATTTNAAAN 1049
          |||
Sbjct 739 TAGAAA-CCGGGTGGT-TATTAG-CTC-AATTTTATCTC-GG-TTTCCTA-TTTT-AAT 688

Query 1050 TAAAAANNCGNAAANCTTTTATTTAACC AAATTTCCCCNTTTTAAAGGGCNTTAAAG 1109
          |||
Sbjct 687 TAGAAT--CG-AAATCTTT-ATTTTAACT-AATTTCTCACATTTT-AA-GG-CATTAAG 636

Query 1110 NCTTAAC 1116
          |||
Sbjct 635 -CTTAAC 630

```

gcp-2.2

BLASTN 2.8.0+
Reference: Zheng Zhang, Scott Schwartz, Lukas Wagner, and Webb Miller (2000), "A greedy algorithm for aligning DNA sequences", J Comput Biol 2000; 7(1-2):203-14.

RID: 7GX0JZMP114

Query=
Length=1360

Score E
 Sequences producing significant alignments:
 (Bits) Value

Query_15775
 1561 0.0

ALIGNMENTS
 >Query_15775
 Length=1165

Score = 1561 bits (812), Expect = 0.0
Identities = 858/867 (99%), Gaps = 6/867 (1%)
 Strand=Plus/Minus

Query	104	TTTGGATCAACAGCCCCATAAGCTCCAAGCATCATAATGATTGCTCACTAGAACAAACTT	163
Sbjct	1161	TTTGGATCAACAGCCCCATAAG-TCCAAGCATCATAATGATTGCTCACTAGAACAAACTT	1103
Query	164	GTCCGGTTCCTGACTTCCTTTGATATATCCATTATATTTTGAATTTTCTAAAATTCAA	223
Sbjct	1102	GTCCGGTTCCTGACTTCCTTTGATATATCCATTATATTTTGAATTTTCTAAAATTCAA	1043
Query	224	ACGCAATCTACTTATCAATTCTACAACATAACTGACCGTTCCTCGTTTTCAGCATGAAC	283
Sbjct	1042	ACGCAATCTACTTATCAATTCTACAACATAACTGACCGTTCCTCGTTTTCAGCATGAAC	983
Query	284	GGTAACACGAAGTTTCTGATTGTTTATCAAGCCAGGTCCATAACGATATGTAACATTTAA	343
Sbjct	982	GGTAACACGAAGTTTCTGATTGTTTATCAAGCCAGGTCCATAACGATATGTAACATTTAA	923
Query	344	CTTTCCTAAATGTAAACGCTGGTATTGTACAAATATACAGTTTCACTTTGAAACCTTGAA	403
Sbjct	922	CTTTCCTAAATGTAAACGCTGGTATTGTACAAATATACAGTTTCACTTTGAAACCTTGAA	863
Query	404	AATCTGCATTCACTGCATCGCCTTTCATATTCTCAAATAATATTTGTGCTGTGGCATATG	463
Sbjct	862	AATCTGCATTCACTGCATCGCCTTTCATATTCTCAAATAATATTTGTGCTGTGGCATATG	803
Query	464	TAATTGGGAGCATGGGAATGGTAGGTATTTCTTTTCATCTAACAACGTAATTTTATT	523
Sbjct	802	TAATTGGGAGCATGGGAATGGTAGGTATTTCTTTTCATCTAACAACGTAATTTTATT	743
Query	524	TCAGTTTTTCCCAAGTGTGAACAAATAAACTACATCTTGTTCACTTTCTCTTTGAAA	583
Sbjct	742	TCAGTTTTTCCCAAGTGTGAACAAATAAACTACATCTTGTTCACTTTCTCTTTGAAA	683
Query	584	AGATCTCCGATTGATGGGAACGCAGGTGTTTCGTGGATCACCTAGGCCAATGTAGACTGAT	643
Sbjct	682	AGATCTCCGATTGATGGGAACGCAGGTGTTTCGTGGATCACCTAGGCCAATGTAGACTGAT	623
Query	644	CCCATCTGGACTGTATTTGACGGCATTGTTGTCTGTGTTCCATAAGTTTCATCTAAAAAT	703
Sbjct	622	CCCATCTGGACTGTATTTGACGGCATTGTTGTCTGTGTTCCATAAGTTTCATCTAAAAAT	563
Query	704	AAAAATAGGATAAATTTAAATAATATTTTACAGCTCACTTGGCCCTGTTCCCAAACCTGG	763
Sbjct	562	AAAAATAGGATAAATTTAAATAATATTTTACAGCTCACTTGGCCCTGTTCCCAAACCTGG	503
Query	764	CTACCTGTTTTGGATCCGAATAAACAAGACATGCTTTTGCACCTTCTTTACAGCCATT	823
Sbjct	502	CTACCTGTTTTGGATCCGAATAAACAAGACATGCTTTTGCACCTTCTTTACAGCCATT	443
Query	824	GGGCAATATTCCTCGTAATTAGAACTATACCTTGCCAGAAAATATTTTATCTAAAAA	883


```

Sbjct 241 TATTCCTAGTATAAAAAAGTATTAATACAGCAGAAAACTTTTTAGGACAAAATTGTTCTCG 300
Query 412 CTAGATACAGTTCTAACTTCCGTGGTAACATAGCTCAAATGGCCGTCAAAAAAGGAGCAA 471
|||||
Sbjct 301 CTAGATACAGTTCTAACTTCCGTGGTAACATAGCTCAAATGGCCGTCAAAAAAGGAGCAA 360
Query 472 AAGCATGTCTTCTCTACTCAGACCCTATGCAAGTAGCAAGTCTTGGAACCCGGACCAAGTG 531
|||||
Sbjct 361 AAGCATGTCTTCTCTACTCAGACCCTATGCAAGTAGCAAGTCTTGGAACCCGGACCAAGTG 420
Query 532 AGTTTTTCAAATAATACAAGCAAACCTCAATCCGTTTTTTGTAATAGATAGTACATATG 591
|||||
Sbjct 421 AGTTTTTCAAATAATACAAGCAAACCTCAATCCGTTTTTTGTAATAGATAGTACATATG 480
Query 592 GAAGAACAGATAAGATGCCATCACATGCCGTTCAAAGAGGCACATGCTATGTTCAATCAG 651
|||||
Sbjct 481 GAAGAACAGATAAGATGCCATCACATGCCGTTCAAAGAGGCACATGCTATGTTCAATCAG 540
Query 652 GAGACCCAGATTGCCGGCATTCCCTTCTATAAAAAATCTCTTCAAAGAAAAATCAGAGC 711
|||||
Sbjct 541 GAGACCCAGATTGCCGGCATTCCCTTCTATAAAAAATCTCTTCAAAGAAAAATCAGAGC 600
Query 712 AAGAGGTTTTACAGATATTTAAAATTATAAAAAACGTAGTATTTTTCCAGTTGTTGGATGG 771
|||||
Sbjct 601 AAGAGGTTTTACAGATATTT-AAATTATAAAAAACGTAGTATTTTTCCAGTTGTTGGATGG 659
Query 772 aaaaaaaGATCCCAACTATTCACACTTCCCAATTCATATAGCGCAGCGCAAANTTTTA 831
|||||
Sbjct 660 -AAAAAAGATCCCAACTATTCACACTT-CCAATTCATATAGCGCAGCGCAA-TTTTA 716
Query 832 TTCGAAAAATGAAAGGGAGACGCCGTCATTGCAGANTTTTCAAGGGTGGTTTAAAAATC 891
|||||
Sbjct 717 TTCGAAAAATGAAA-GGAGACGCCGTCATTGCAGA-TTTTCAAGGTTG-TTTG-AAATC 772
Query 892 TACATTTCCNCCGAAATTACAAGTTACTttttttAGGAAACCTTGACGTCCCATACC 948
|||||
Sbjct 773 TACATTTCCACCAGAAATTACAAGTTAC-TTTTTAGGAAAACCTTGACGTCCATACC 828

```

Score = 19.9 bits (10), Expect = 1.4
Identities = 10/10 (100%), Gaps = 0/10 (0%)
Strand=Plus/Plus

```

Query 592 GAAGAACAGA 601
|||||
Sbjct 97 GAAGAACAGA 106

```

Score = 19.9 bits (10), Expect = 1.4
Identities = 10/10 (100%), Gaps = 0/10 (0%)
Strand=Plus/Plus

```

Query 208 GAAGAACAGA 217
|||||
Sbjct 481 GAAGAACAGA 490

```

Score = 19.9 bits (10), Expect = 1.4
Identities = 10/10 (100%), Gaps = 0/10 (0%)
Strand=Plus/Minus

```

Query 169 TTTTATAAAA 178
|||||
Sbjct 67 TTTTATAAAA 58

```

Score = 19.9 bits (10), Expect = 1.4
Identities = 10/10 (100%), Gaps = 0/10 (0%)
Strand=Plus/Minus

```

Query 369 GTATTAATAC 378

```

Sbjct 267 GTATTAATAC 258
|||||
Score = 19.9 bits (10), Expect = 1.4
Identities = 10/10 (100%), Gaps = 0/10 (0%)
Strand=Plus/Minus

Query 883 TTGAAAATCT 892
|||||
Sbjct 758 TTGAAAATCT 749

Score = 18.0 bits (9), Expect = 5.2
Identities = 9/9 (100%), Gaps = 0/9 (0%)
Strand=Plus/Plus

Query 26 AGCGCAGCG 34
|||||
Sbjct 699 AGCGCAGCG 707

Score = 18.0 bits (9), Expect = 5.2
Identities = 9/9 (100%), Gaps = 0/9 (0%)
Strand=Plus/Plus

Query 1009 AAAAAATGA 1017
|||||
Sbjct 721 AAAAAATGA 729

Score = 18.0 bits (9), Expect = 5.2
Identities = 9/9 (100%), Gaps = 0/9 (0%)
Strand=Plus/Plus

Query 389 TTTTtagga 397
|||||
Sbjct 801 TTTTtagga 809

Score = 18.0 bits (9), Expect = 5.2
Identities = 9/9 (100%), Gaps = 0/9 (0%)
Strand=Plus/Minus

Query 574 TAATAGATA 582
|||||
Sbjct 91 TAATAGATA 83

Score = 18.0 bits (9), Expect = 5.2
Identities = 9/9 (100%), Gaps = 0/9 (0%)
Strand=Plus/Minus

Query 1133 AAAAGTTTT 1141
|||||
Sbjct 281 AAAAGTTTT 273

Score = 18.0 bits (9), Expect = 5.2
Identities = 9/9 (100%), Gaps = 0/9 (0%)
Strand=Plus/Minus

Query 194 TATCTATTA 202
|||||
Sbjct 471 TATCTATTA 463

3.15.4 Appendix 4: Extraction Buffer Components

Extraction Buffer contains 0.1 M phosphate buffer (pH 6.1), with 2% L-ascorbic acid (w/v) (Fisher Chemicals) and 0.1% 2-mercaptoethanol (v/v) (MP Biochemicals).

L-Ascorbic Acid: This is a water-soluble antioxidant that acts as a reducing agent and thereby, helps to decrease oxidative stress (121).

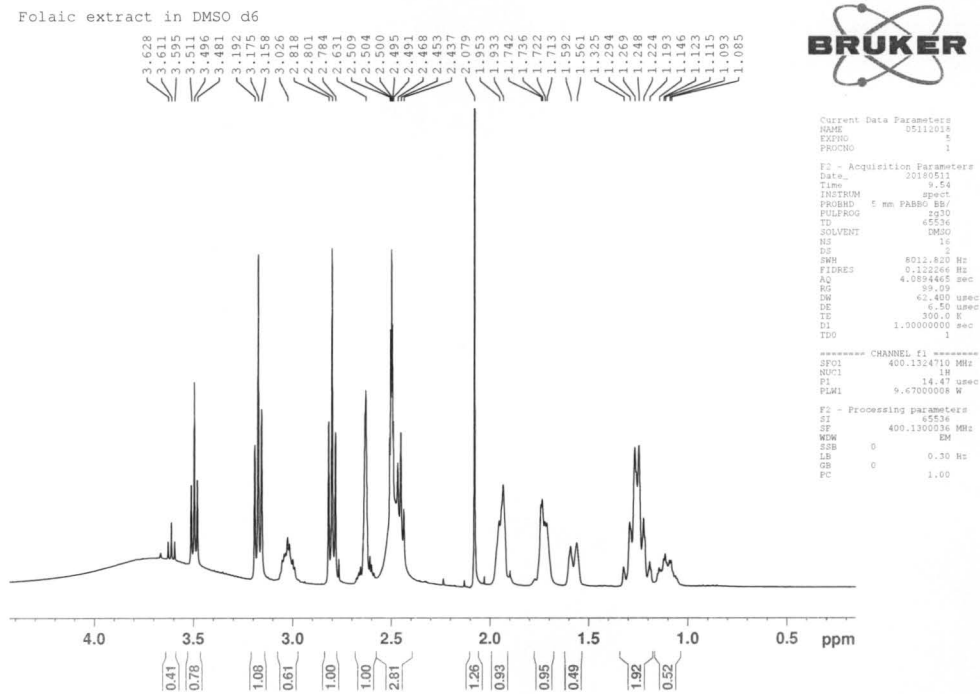
2-Mercaptoethanol: This is a water-soluble thiol derived from hydrogen sulfide and ethanol that acts as a reducing agent for disulfide bonds. Therefore, it protects sulfhydryl groups from oxidation and thereby, helps to decrease oxidative stress (121).

Phosphate Buffer: This helps folate derivatives to dissolve as folates have low solubility in water being more soluble in alkaline and saline media solutions (121).

Flushing with Nitrogen: This helps to reduce the levels of oxygen in folate extracts and standards as dissolved oxygen levels have an inverse relationship with folate stability.

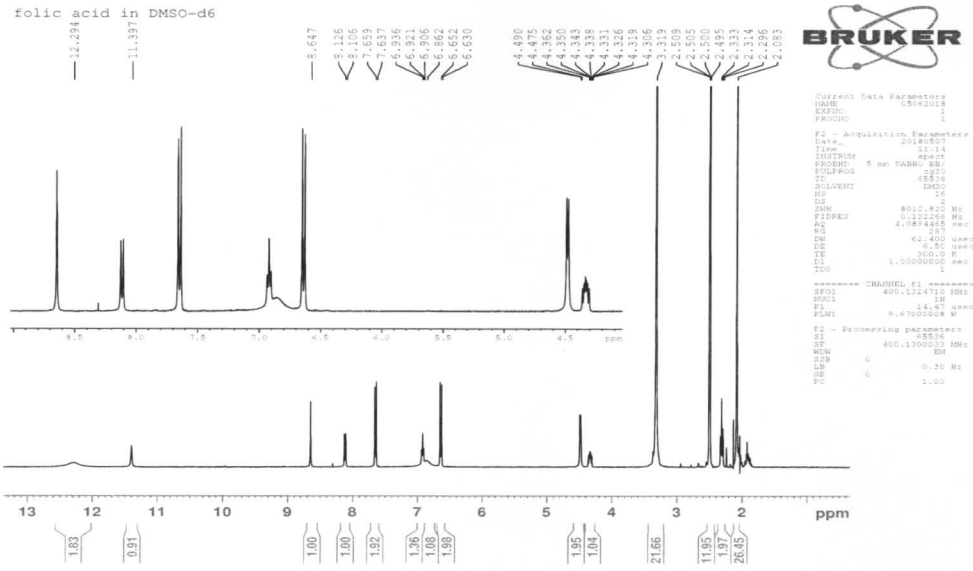
Appendix 5: NMR Spectral Parameters, Conditions and Spectra

The spectral parameters and conditions are shown in each figure.



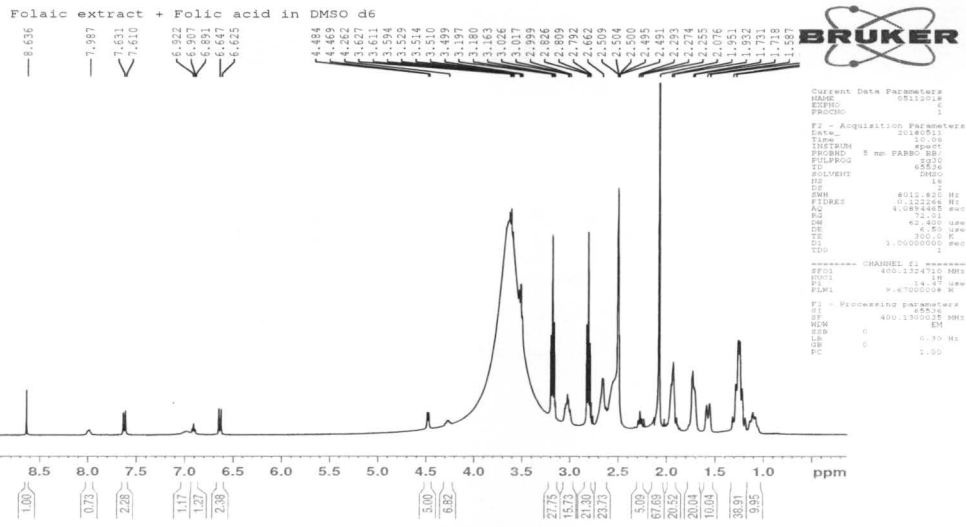
1H-NMR Analysis of *E. coli* OP50 Folate Extracts.

1 mL of *E. coli* OP50 folate extract was dissolved in DMSO.



1H-NMR Analysis of Folic Acid Standard.

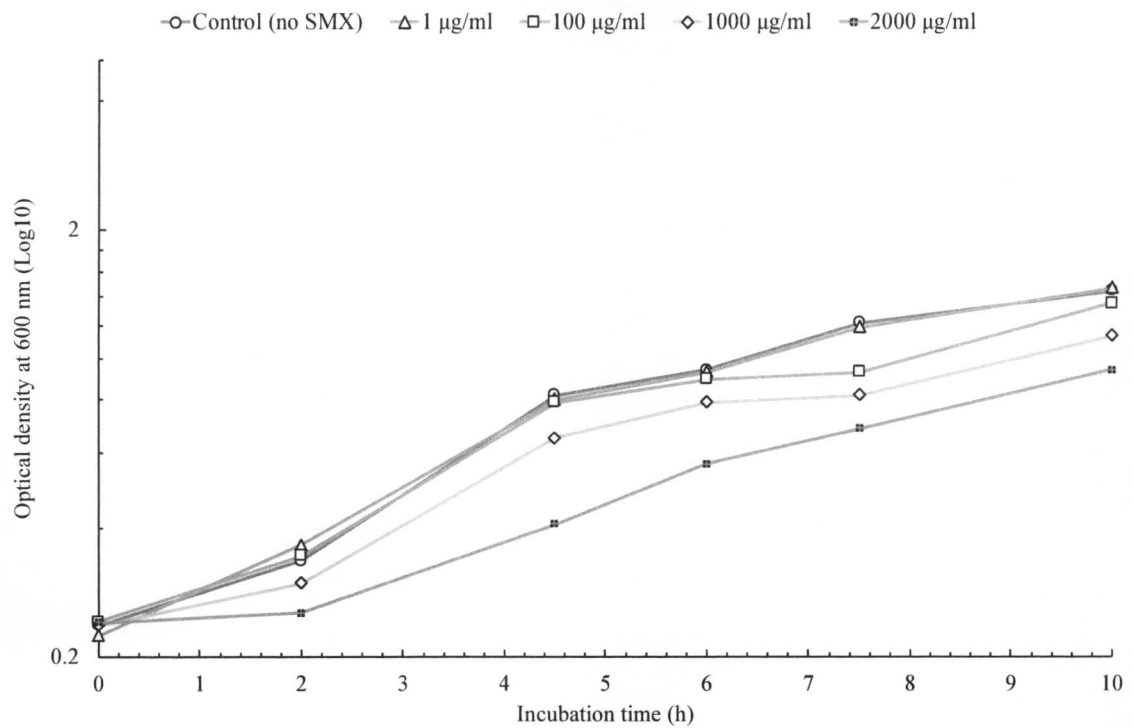
100 mg of folic acid was dissolved in 1 mL DMSO (100 mg/mL concentration)



1H-NMR Analysis of Bacterial Folate Extract and Folic Acid Standard Mixture.

1 mL of *E. coli* OP50 folate extract mixed with 1 mL of 100 mg/ml folic acid in DMSO.

Appendix 6: *E. coli* OP50 Growth Curve



Growth curve of *E. coli* OP50 treated with various concentrations of SMX.

50 µL from bacterial stock was inoculated into 100 mL Luria Bertani (LB) broth. Then the culture was incubated at 35 °C and 250 rpm using an orbital shaker. Optical density was recorded at 600 nm at regular intervals for 10 hours.